Experimental and Simulation Study of Improved Oil Recovery in Shale Formations

by

Samiha Morsy, M.Sc.

A Dissertation

in

Petroleum Engineering

Submitted to the Graduate Faculty
of Texas Tech University in
Partial Fulfillment of
the Requirements for
the Degree of

Doctor of Philosophy

Approved

Dr. James J. Sheng
Chair of Committee

Dr. Mohamed Soliman

Dr. George B. Asquith

Dr. Callum Hetherington

Dr. Habib K. Menouar

Dr. Mark Sheridan
Dean of the Graduate School

May, 2014

ACKNOWLEDGMENTS

I wish to express my great thanks to ALLAH. I also thank my husband and mother for being by my side in everything. I would like to thank my research advisors and committee member (James Shang, Mohamed Soliman, George Asquith, Callum Hetherington, and Habib Menouar) for their support and guidance during the course of this study.

Many thanks to the Petroleum Engineering department, Civil Engineering Department, and Geosciences Department at Texas Tech and Baker Hughes Company for allowing me to accomplish this work.

TABLE OF CONTENTS

ABSTRACT

Shale has ultra low permeability and cannot produce without hydraulic fracturing to improve the contact between reservoir matrix with wellbore. In addition, shale production declines very fast due to many reasons including conductivity decline over time. The techniques for improving oil production may start at an early stage by optimizing drilling and completion technologies and at a later stage where secondary and tertiary recovery methods are applied.

In this dissertation, a number of improved oil recovery technologies potentially applicable in shale are examined. The primary oil recovery is improved by optimizing stimulation fluid additives. Matrix acidizing is proposed to be a part of the propped hydraulic fracturing by injecting slugs of weak HCl solutions (less than 2 wt%) near and away from wellbore. The matrix acidizing experiments using 1-3 wt% HCl on Eagle Ford, Barnett, Mancos, and Marcellus shale formations showed a great improvement in porosity and oil recovery factors at different acid contact time, while the compressive strength and hardness of the studied rocks were lowered after the treatment due to partial mineral dissolution up to 82%. The dissertation also examines a number of stimulation fluid surfactants to alter shale wettability while fracturing on reservoir samples from Bakken Shale. One of the tested surfactant was able to improve Bakken Shale primary oil recovery factors by about 20% more compared with using of brine neutral solutions alone.

In addition, three enhanced oil recovery methods to improve waterflooding performance in shale were examined: Low Sal, alkaline, and surfactant pre-flood technologies. The three tested methods improved waterflooding oil recovery up to 30% more due to mineral dissolution and wettability alteration with shale damage effect for Mancos Shale samples when low saline solutions were used and Barnett Shale samples when higher alkaline solutions were used.

Furthermore, the dissertation investigates the potential of waterflooding in Eagle Ford Shale by building a reservoir numerical model using Eagle Ford Shale average properties and hydraulic fracturing properties of the injector and the produced wells. The simulation study confirms the experimental potential of waterflooding in Eagle Ford Shale when modeled with closer and longer factures with a recovery factor of about 18% compared with 12% from the depletion case.

LIST OF TABLES

LIST OF FIGURES

NOMENCLATURE

gpt	Gallon per thound gallons
$\mathbf{V_{sh}}$	Shale bulk volume, cm^3
d	Core sample diamter, cm
L	Core sample length, cm
$\mathbf{W_{dry}}$	Shale core sample dry weight, gram
$\mathbf{W_{sat}}$	Shale core sample saturated weight, gram
$\boldsymbol{CT_{om}}$	CT of Oil staurated shale sample, Hounsfield
$\boldsymbol{CT_{am}}$	CT of Oil staurated shale sample, Hounsfield
$\boldsymbol{CT_{a}}$	CT of air, Hounsfield
$\boldsymbol{CT_{o}}$	CT of oil, Hounsfield
HB	Brinell Hardness Number
F	load on the indenting tool, kg
D	Diameter of steel ball, mm
R.F	Recovery Factor, Fraction

LIST OF SYMBOLS

Φ Porosity, Fraction

μ_o Oil Viscosity, cp

μ_w Water Viscosity, cp

CHAPTER 1
SHALE OIL FORMATIONS

Shale formations have become one of the main sources for oil and gas in many parts of the world, especially in North America. Oil and gas shale formations vary in composition even within the same play. Shales contain roughly less than 10% organics, and less than 50% clay, and the remainder is mostly quartz or calcite. In shale reservoirs, oil is stored in matrix with ultra low permeability, with virtually all permeability concentrated in a large number of natural fractures (Fakcharoenphol *et al.* 2012). The exploitation of shales has therefore greatly benefited from the development of horizontal drilling techniques combined with hydraulic fracturing to expose significantly more reservoir rock to wellbore. In addition, the wells are stimulated with large volumes of injected water and conducted in multiple, closely spaced stages (up to 20), to shatter the shale matrix and create a permeable reservoir. The overall estimate of risked, technically recoverable shale oil and condensate for the U.S. is about 47.7 billion barrels (Table 1.1) (EIA 2013).

Table 1.1 Risked shale oil in-place and technically recoverable: seven continents

Continent	Risked Oil In-Place (B bbl)	Risked Technically Recoverable (B bbl)
North America (Ex. U.S.)	437	21.9
Australia	403	17.5
South America	1,152	59.7
Europe	1,551	88.6
Africa	882	38.1
Asia	1,375	61.1
Sub-Total	**5,799**	**286.9**
U.S.	954	47.7
TOTAL	**6,753**	**334.6**

1.1 Organization of This Dissertation

This dissertation is divided into six chapters. Chapter 1 presents a detailed literature review of shale oil formations showing the role of shale oil properties and characteristics on production and different stimulation techniques.

Chapter 2 presents a comprehensive experimental study to improve shale oil primary recovery by combining the benefits of matrix acidizing using weak HCl solutions with propped hydraulic fracturing near and away from wellbore. The study identifies the effect of matrix acidizing using low HCl acid concentrations (1-3 wt%) on shale porosity, mass loss, bulk density, crack distribution, surface wettability, hardness, and compressive strength.

Chapter 3 presents a different experimental study to improve primary oil recovery by optimizing surfactant additives in shale stimulation fluid. The research involves measurements of surfactant compatibility with formation synthetic brine, different stimulation fluids, and reservoir crude oil, and oil recovery factors using different surfactant concentrations.

Chapter 4 proposes different mechanisms to improve waterflooding secondary oil recovery. First, the study investigated the potential of Low Sal technique by studying role of water salinity on water imbibition in shale by measuring the improved oil recovery using different saline solutions. Second, Alkaline flooding was examined by studying the effect of using different NaOH alkaline solutions on shale wettability, recovery, and hardness. Last, the study investigates the potential of surfactant pre-flood to improve waterflooding oil recovery by changing shale wettability. The surfactant study covers measurements of shale contact angels and oil recovery using different neutral brine solutions and different surfactant concentrations.

Chapter 5 presents a numerical study to investigate the potential of waterflooding in Eagle Ford Shale using published Eagle Ford Shale average properties. The study shows the depletion and waterflooding base cases recovery factor results. Chapter 5 also presents different sensitivity cases to investigate the effect of fracture half-length, fracture spacing, and permeability anisotropy on oil recovery factors from Eagle Ford Shale.

1.2 Statement of Problem

Despite its enormous production potential, shale formations present a number of challenges. Shale makes about half the earth's sedimentary rock but includes a wide variety of vastly differing formations. Shale is heterogeneous in terms of its

geology, geochemistry, geomechanics and production mechanism, with the added complexity that these properties may differ from shale to shale, as well as within a single shale horizon. Nevertheless, all shale is characterized by ultra low permeability that makes production difficult compared with conventional reservoirs. Since these shale unique conditions determine the production mechanism of the various shales, knowledge of each shale characteristics is a key factor in improving shale production. In addition, every shale and shale play is different and requires a unique treatment based on local characteristics. Thus studying the main characteristics of the current main productive shales will be beneficial to improve oil recovery.

Also shale primary production declines rapidly compared with conventional reservoirs, so the hydraulic fracturing process needs to optimized in the way to produce more oil and gas from the primary stage. Since shale primary recovery factors will not exceed 5-10%, early studies of different secondary recovery methods are needed to continue production economically from shales. Waterflooding is the most cheapest and mature secondary recovery method for conventional reservoirs, but it is not mature yet in shale formations. Even the performance of waterflooding in shale is not well understood yet as shale exhibits many differences to conventional reservoirs. There are very limited studies that showed a good potential for waterflooding in certain shale formations, but since shales are different, a specific study is needed for each shale. Moreover, the expected waterflooding recovery is not expected to be high using the conventional way of waterflooding as shale has ultra low permeability that can limit waterflooding efficiency to displace oil from matrix to induced fractures. Thus, different enhanced oil recovery methods are needed to improve waterflooding performance in shales.

1.3 Objective of the Dissertation

The objective of this research is to investigate potential methods to improve oil recovery from shale. The study investigates the potential of improving shale oil recovery during the primary and secondary recovery stages. Shale oil recovery may be improved during the primary stage by optimizing the chemicals added to the stimulation fluid such as acids to improve shale porosity and permeability, and surfactants to change shale wettability. While, in the secondary recovery stage oil production may be improved by enhancing water imbibition, as water invades rock

matrix though spontaneous imbibition mechanism depending on the matrix capillary pressure. Water imbibition can be improved by adding certain chemicals to water to change rock wettability such as salts, alkaline, and surfactant. Thus, the main goal of this study is to examine the applicability of such improving mechanisms in different shales.

The research covers experimental and simulation studies on improving oil recovery in different shale formations. The experimental procedure consists of three main processes. Process 1 is composed of tests done on the effect of adding low concentrations of HCl acid to shale stimulation fluid to enhance shale porosity and permeability to improve primary oil recovery. Process 2 is composed of tests done on the effect of adjusting surfactant additives in shale stimulation fluid to improve primary oil recovery by wettability alteration. Process 3 is composed of tests done to study the effect of water salinity, alkaline, and surfactant on secondary oil recovery (waterflooding) in shale formations. The simulation process involves of a numerical study done to investigate the potential of waterflooding in Eagle Ford Shale using published shale properties.

1.4 Role of Shale Oil Properties on Shale Recovery

Shales have ultra low permeability with highly diverse mineralogy that changes from shale to shale and even within the same shale play. Many factors affect shale recovery such as mineralogy, geological complexity, mechanical properties, chemical properties, and hydraulic properties.

1.4.1 Mineralogy

Shales have highly diverse mineralogies, ranging from carbonate-rich formations dominated by calcite, dolomite, and siderite, and lesser amounts of aluminosilicates. Many shales are rich in silicates including quartz, feldspar, and clay minerals, and carbonates are a minor component (OSTS, 2012). The mineralogy of a shale, particularly its relative quartz, carbonate and clay content, significantly impacts how efficiently the induced hydraulic fracture will stimulate the shale (EIA 2013):, as illustrated by Figure 1.1.

- Shales containing higher amounts of quartz and carbonate tend to be more brittle and when hydraulically fractured they result in a vast array of small-scale induced

fractures providing well connected flow path from the matrix to the wellbore Figure1.1A.

- Shales containing higher amounts of clays tend to be ductile and when hydraulically fractured they result in a few induced fractures providing a limited flow path from the matrix to the wellbore (Figure 1.1B.)

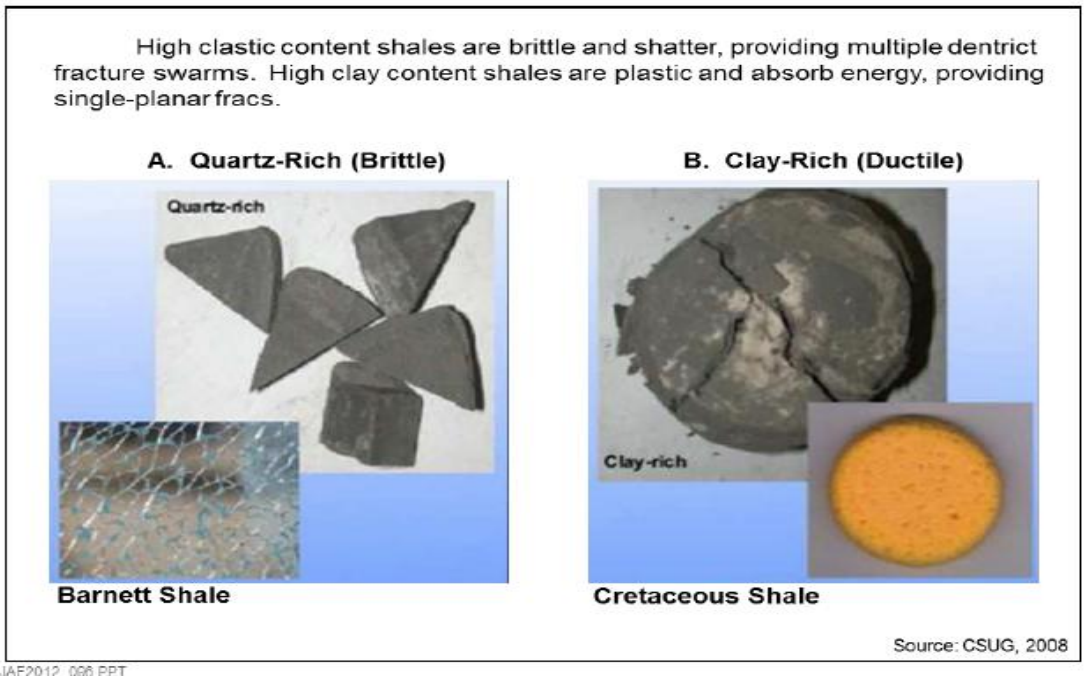

Figure 1.1 The properties of the reservoir rock greatly influence the effectiveness of hydraulic stimulations (EIA 2013)

1.4.2 Mechanical and Chemical Properties of Shale

Mechanical properties are an important component in the design of the hydraulic fracturing treatment. However, because shale mineralogy changes throughout a play, the mechanical properties may also change. Many shales are chemically and mechanically unstable which makes it difficult to produce a reasonable measurement for their mechanical properties.

Shales may be unstable and are sensitive to the physical and compositional properties of fluids (density, salinity, and ionic concentration). Shale's stability is also affected by intrinsic properties such as mineralogy, porosity, and permeability. The existence and creation of fractures may also destabilize shales upon fluid penetration. Penetrating fluid may alter shale stability by changing pore pressure or effective stress and shale strength through shale/fluid interaction. Shale with a certain

mineralogy and strength is usually at equilibrium with the reservoir conditions (temperature, in situ stress, pore pressure, etc.), but this equilibrium state may be altered when drilled or stimulated.

Chemical instability is time dependent unlike mechanical instability. Chemical instability may be eliminated by appropriate selection of drilling fluid, or any completion fluid with suitable additives that control shale/fluid interaction.

1.4.3 Fluid Transport and its impact on Waterflooding Performance

In natural fractured reservoirs such as shales, oil is stored in matrix with ultra low permeability, with virtually all permeability concentrated in a large number of natural fractures (Fakcharoenphol *et al.* 2012). Due to these fractures, oil cannot be displaced from the matrix by means of conventional waterflooding. Channeling and bypassing through the fractures would result in extremely poor recovery (Guo *et al.* 1998). Primary oil production from such fractured reservoirs in which the storage occurs in the matrix and flow happens in fractures can be divided into three stages: 1) production from the fracture network at early; 2) production from the fracture network and rock matrix at intermediate; and 3) production from the rock matrix at a later (Guo *et al.* 1998). Early production from the fracture network of shale formation declines rapidly. Most of the recovery of the intermediate and long-term stages of production depends on spontaneous imbibition of brine into the rock matrix and expulsion of oil via the fracture face.

Spontaneous imbibition can add significantly to oil recovery in fractured reservoirs with low matrix permeability depending on rock wetness quality. The rate of imbibition is mainly affected by the net effect of capillary pressure driving force and the opposing viscous resistance to flow. Because of the strong capillary forces, the smallest pore bodies, which are next to the interface, are usually invaded first. The displacement takes place at small but finite capillary numbers (Sahimi, 1995). The rate of imbibition is usually a function of porous media and fluid properties such as absolute and relative permeability, viscosity, interfacial tension, and wettability (Zhang *et al.*, 1996).

Spontaneous capillary imbibition occurs in a countercurrent manner between the matrix and fracture when the wetting and non-wetting phases flow in opposite directions. Both drainage and imbibition processes exist, simultaneously, during

countercurrent flow, although at different locations. Spontaneous imbibition in which non-wetting phase is displaced by the wetting phase occurs in both co-current and countercurrent manner in naturally fractures reservoirs (Guo *et al.* 1998). In co-current flow, the wetting and non-wetting phases flow in the same direction while the wetting phase pushes the non-wetting phase out of the matrix. In countercurrent, flow, the wetting and non-wetting phases flow in opposite directions. The petrophysical characterization of shale samples indicates the presence of high capillary forces (Sondhi *et al.* 2011), and mixed wettability systems (Elijah, 2011), which can lead to counter-current imbibition of water and hydrocarbon (Qin,2007).

During the mature stage of waterflooding in naturally fractured reservoirs, oil production can be represented by a bucket of fluid with a small hole in the bottom dripping liquid onto a conveyor belt (Guo *et al.* 1998), as is illustrated in Figure 1.2.

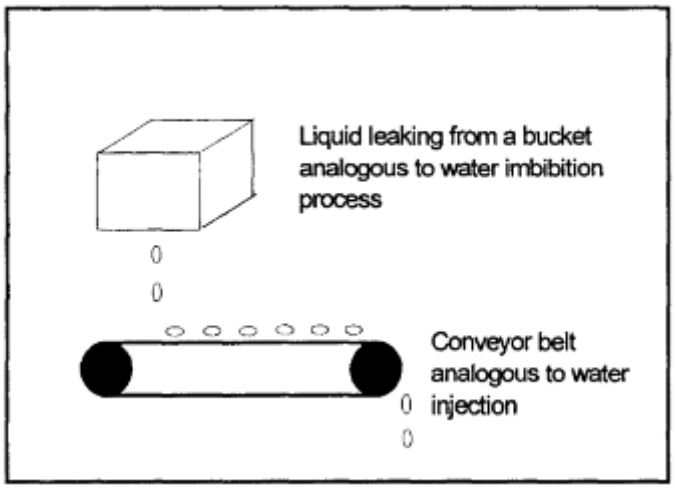

Figure 1.2 An analogue model for imbibition waterflooding in naturally fractured reservoirs with spontaneous imbibition acting as the rate-limiting step (Guo *et al.* 1998)

Liquid leaking from the bucket is analogous to oil produced from the matrix due to water imbibition dominated by capillary forces, and the conveyor belt is analogous to water flow in the fractures that produced oil to the production wellbore. Imbibition process remains the rate limiting step as there is a critical limit for water injection, in which water can displace oil from matrix to fracture without resulting in greater water production. Since the oil rate is determined by imbibition process, oil production is relatively constant and unaffected by injection rates above a certain

threshold; thus, the only result of high injection rates is increased WOR'S and reduced profitability.

Few studies have focused on the potential of waterflooding in shale formations. Fakcharoenphol *et al.* (2012) pointed out that waterflooding changes the formation in situ stress due to the increase in reservoir pressure and decrease of reservoir temperature, which enhances oil recovery of shale formations by reactivating existing natural fractures and/or creating new fractures. Similarly, Wang *et al.* (2010) showed from their experimental work done on Bakken Shale samples that there is an increase in shale permeability after forced brine coreflooding due to mineral dissolution and after spontaneous imbibition into brine due to cracking from clay swelling.

Most of the literature focused on imbibition of carbonate reservoirs (De Swaan. 1978, Cuiec *et al.* 1994, Akin *et al.* 2000, and Kantzas *et al.* 1997), while very limited studies had focused on shale reservoirs. Makhanov *et al.* (2012) showed that the imbibition could be a viable mechanism to transfer fluids from fracture to matrix in Horn River Shale and the imbibition rate along the bedding direction is higher than across the bedding direction. Iwere *et al.* (2012) presented a simulation study on Bakken Shale that shows the potential of waterflooding to recover about 6.7% oil. Takahashi and Kovscek (2009) investigated the impact of different brine formulations covering acidic (pH of 3), neutral, and alkaline (pH of 12) on siliceous shale samples. The highest oil recovery achieved during the spontaneous imbibition and forced coreflooding was from the samples with high pH brine (Alkaline) with 30% after spontaneous imbibition and 95% after the forced coreflooding. The authors related the improvement in the oil recovery from the high pH brine to the change in wettability from intermediate water-wet to strongly water-wet conditions. Wang *et al.* (2011) also studied different surfactant formulations to investigate the potential of chemical imbibition in Bakken Shale at different temperatures and brine salinities. The authors mentioned that surfactant did not imbibe effectively in Bakken cores using distilled water or low saline water, and the highest oil recovery achieved was 19% using 0.1 wt% of 58N, cationic surfactant, 0.1 wt% alkali (NaBO2.4H2O), and 30 wt% salinity at 90°C. The authors concluded that the addition of alkali improved oil recovery for all of the studied surfactants.

1.4.3.1 Effect of Water Salinity on Shale Stability and Recovery

Shales are composed of a considerable amount of clays. When fresh water contacts some clays like smectite (montmorillinite), these clays swell. Clays consist of negatively charged aluminosilicate layers kept together by cations. The characteristic property of clays to absorb water between layers results in a strong repulsive forces and clay expansion (Bleam 1993, Delville 1995, Chang *et al.* 1995, Boek *et al.* 1995, Skipper *et al.* 1995, Karaborni *et al.* 1996, Chang *et al.*1999, Young and Smith 2000, Cha´vez-Pa´ez *et al.* 2001, and Hensen *et al.* 2001). Clay swelling depends mainly on clay composition and can be caused by ion exchange and changes in salinity. The strong relationship between clay composition and swelling may be explained by the concept of cation dissociation (Foster 1955). Based on cation dissociation concept, when clay of the montmorillonite group is dispersed in water, the associated cations between the clay structure sheets tend to dissociate, prying the particles apart and leaving some of the structural units negatively charged. The negatively charged units tend to repel each other, and, if enough units are so charged, the repulsive forces are great enough to give the clay particles the appearance of swelling.

When shale is in contact with water, shale interacts with water with consequences (hydration, dehydration, fractures etc.) similar to those that occur during drilling. These consequences from shale/water interaction can significantly alter the shale's mechanical properties (Morsy *et al.* 2013a and Das *et al.* 2014) which also induce stress changes in the shale (Fakcharoenphol *et al.* 2012; Ji *et al.* 2013). The changes in shale stress may induce favorable or unfavorable fractures in the shale/water interacted zones (Ji *et al.* 2013). In a similar way, Gomez and He (2012) showed experimental results on shale/water interact where shale was exposed to fresh water and saturated salt drilling fluid. The thin-section photos (Figures 1.3 through 1.5) of the shale samples as in initial condition, exposed to fresh water, and in saturated salt drilling fluid showed clear induced fractures from shale/water interaction depending on water salinity. The thin-section of the shale sample in initial condition showed few natural micro-fractures (Figure 1.3). While, the thin-section photos of the other two samples in fresh water and saturated salt drilling fluids showed both along bedding and intersecting induced fractures with more tendency in fresh water (Figure 1.4 and 1.5). The main fractures were observed along bedding with a maximum fracture width of 250 microns in fresh water (Gomez and He 2012).

Figure 1.3 Reference shale sample without fluid exposure (Gomez and He, 2012)

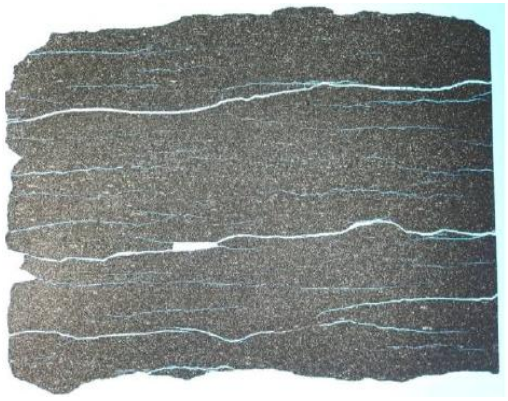

Figure 1.4 Thin section of shale sample exposed to fresh water (Gomez and He, 2012)

Figure 1.5 Thin section of shale sample exposed in saturated salt drilling fluid (Gomez and He, 2012)

In typical shale hydraulic fracturing, inhibitors like KCl or NaCl are added to the injected water to prevent clay swelling (Bennion *et al.* 1998). While in drilling wells through shale intervals, inhibitors are added in the drilling fluid (mainly water) to eliminate clay swelling that causes mud loss (Van Oort 1994, Van Oort *et al.* 1999, Van Oort *et al.* 1996, and Nolen-Hoeksema 2013). Mud loss indicates that shale permeability or flow capacity is significantly increased near wellbore. In addition, proppants are generally used to maintain the fractures open in conventional fracturing jobs (Alexander *et al.* 2011). However, slick water (fresh water with up to 5% potassium chloride by volume and almost no proppants added) is successfully practiced in fracturing shale reservoirs. It is believed that shale interacts with fresh

water in case of slickwater fracturing, and induces some secondary fractures (Ji *et al.* 2013) that started after the end of the hydraulic fracturing process based on the long-term interaction between shale and water. While changes in shale due to shale/water interaction is avoided in drilling to prevent loss of circulation and shale instability, the same changes could improve oil and gas production from shale rocks by creating more subsurface area (i.e., fracture networks for gas diffusion and communicating with wellbore) if shale/water interaction is well optimized.

Another study on Bakken Shale cores showed that there is an increase in shale permeability after spontaneous imbibition into brine due to cracking from clay swelling (Wang *et al.* 2011). Dehghanpour *et al.* (2013) measured spontaneous imbibition of aqueous (deionized water and KCl solutions of various concentrations) and oleic (kerosene and iso-octane) phases in several dry organic shale samples. They found that the imbibition rate of aqueous phases is much higher than that of oleic phases. The authors suggested that one of the causes of excess water intake was the enhancement of sample permeability through adsorption.

Recently, Ji *et al.* (2013) presented a new theory about the possibility of induced secondary fractures in shale formations due to the imbalance of chemical potential between the water in the primary fracture and water within the shale. Based on the theory, the imbalance results in a swelling pressure that if large enough, breaks the natural cementation of shale. This breaking of shale cementing material would allow secondary fractures to form along bedding planes and at right angles to the bedding planes (Gomez and He 2006). These secondary fractures can build up a network that conducts matrix to the main hydraulic fractures and improves hydrocarbon production from shales.

When shale interacts with water, shale mechanical properties can be significantly affected due to water adsorption. Das *et al.* (2014) conducted an experimental study on different shales and examined the impact of water with different salinities on shale swelling, hardness, and cation exchange capacity (CEC). The authors used shale samples from Fayetteville, Mancos, and Pierre II. The results of this study showed that Mancos Shale samples did not contain smectite clay, but it showed a higher CEC due to the presence of a mixed layer clay that exhibits some portion of smectite. The study also showed that the ratios of swelling tendency of Mancos samples in different lower salinity solutions (3 wt% KCl, 7 wt% KCl, 5 wt%

NH4Cl, and 3 wt% CaCl2) were 0.28, 0.24, 0.31, and 0.24 respectively when compared to distilled water swelling reference. In addition, the Mancos Shale samples lost about 27% of its hardness when exposed to 7 wt% KCl for 72 hrs. In a similar study, Emadi *et al.* (2013) investigated the impact of clay swelling using different saline solutions on Eagle Ford Shale reservoir samples. The authors found that the unaxial compressive strength of the samples decreased from 9,400 psi to 6,800 psi using fresh water and to 8,000 psi using 14 wt% KCl fluid.

Generally, shale reservoirs have laminated bedding in the form of heavily disk-like cores from vertical wells and small broken cores from deviated wells. In addition, shales show networks of smaller weak planes and natural fractures (Abousleiman *et al.* 2010). The formation conditions near these fractures resemble those near a borehole. Therefore, one could expect the reactive fluids to improve the flow capacity near fractures. A few operators have suggested that water adsorbed by minerals in the rock creates localized clay swelling that may serve to hold open small fractures and fissures (Hu *et al.* 2013).

1.4.3.2 Effect of NaOH on Waterflooding Performance in Shale Formations

Alkaline fluids are considered an inexpensive way of reducing interfacial tension (IFT) with natural surfactants formed in situ for enhanced oil recovery (EOR) applications (Thornton 1988). Alkali solutions react with formation oil and form natural surfactants depending on the oil acid number (Cooke *et al.* 1974). Alkali can also change rock-fluid system wettability.

In addition, alkali reacts with rock minerals and dissolves some of them with different rates depending on reservoir mineralogy, temperature, and the injected concentrations of alkali (Thornton 1988). NaOH (alkali) may dissolve many minerals in reservoir formations, including quartz, feldspars (microcline and albite), micas (muscovite and biotite), and clays (kaolinite, montmorillonite, and chlorite). Regarding the clay minerals, montmorillonite and illite are less soluble than kaolinite. Thornton (1988) studied Kern River reservoir sand interaction with different concentrations of NaOH at different temperatures. The Kern River is 84 % quartz, 15 % feldspars, and < 1% illite and montmorillonite. The author showed that the main minerals interacted with low concentrations of NaOH were silicate minerals, which dissolve in caustic solution to form silicate and aluminate ions, and precipitate to form

sodium aluminosilicate minerals. Kaolinite was found to react with NaOH solutions at concentrations greater than 0.28 wt%. There also may be oxidation of pyrite in shale formations when exposed to NaOH solutions (Ciminelli and Osseo-Asare 1995).

According to the study of Takahashi and Kovscek (2009), high pH brines may change the shale wettability of the siliceous shale from intermediate water-wet to strongly water-wet conditions. In addition, Wang *et al.* (2011) studied different surfactant formulations to investigate the potential of chemical imbibition in Bakken Shale at different temperatures and brine salinities. The authors mentioned that surfactant did not imbibe effectively in Bakken cores using distilled water or low saline water and the highest oil recovery achieved was 19% using 0.1 wt% of 58N, cationic surfactant, 0.1 wt% alkali (NaBO2.4H2O), and 30 wt% salinity at 90°C. The authors also concluded that the addition of alkali improved oil recovery by about 2-4% more for all of the studied surfactants.

1.4.3.3 Effect of Surfactant on Initial and Secondary Oil Recovery from Shale Formations

Many surfactants have been proposed to enhance initial production in shale oil and gas formations. These surfactants are injected with fracturing fluids to lower interfacial tension and alter shale wettability. Shuler *et al.* (2010) proposed use of specialized surfactant formulation combined with hydraulic fracturing treatments to enhance primary oil recovery from Bakken Shale, where faster and significant recovery was observed by spontaneous imbibition experiments made on both outcrop samples from the Texas Crème Limestone and Bakken Shale reservoir. The observed recovery factors from the Bakken Shale samples exceeded 45% using appropriate surfactant formulations compared with only 6% recovery factor when 2% KCl brine was used. Similarly, Wang *et al.* 2011 studied the potential of different surfactant formulations to imbibe into and displace oil from shale samples from the middle member of the Bakken Shale formation while minimizing clay swelling and formation damage in formation. The range of oil recovery factors measured during the study were 1.6% to 76% at high salinity (150−300 g/L or 15−30 wt %) and temperatures ranging from 23°C−120°C using brine and surfactant (0.05−0.2 wt% concentration). The most appropriate surfactants, based on their study, were ethoxylate nononic surfactant, an internal olefin sulfonate anonic surfactant, and an amine oxide cationic

surfactant as they were more stable than the other surfactants for temperatures from 105−120°C.

Another study by Xu and Fu (2012) showed that using weakly emulsifying surfactant is more efficient in solubilizing and mobilizing oil globules than a non-emulsifying surfactant in order to enhance initial production from Eagle Ford Shale formation. Paktinat *et al.* 2006 pointed out from the experimental and field case that a microemulsion accelerated post fracturing fluid cleanup in shale formations, and resulted in lowering pressure to displace injected fluids from low permeability samples and proppant packs. The authors mentioned that when 2 gpt of microemulsion was used, gas relative permeability increased and as a result water permeability decreased. The authors believed that the frac fluid effectively lowered the capillary pressure and capillary end effect associated with fractures in shales as much as 50%, thus minimizing fluid trapping and increased the flow area to the fracture (longer frac half-length).

Fernø, Haugen, and Graue (2012) presented an experimental study on carbonate reservoirs showing that surfactant prefloods helped water flooding efficiency by lowering the capillary threshold pressure for water to invade the matrix pores that makes the transport of water much easier between the matrix and the fracture (water-wet condition).

1.5 Stimulation Techniques in Shale Formations

Formation stimulation techniques have become more complex in recent years. Fracturing is not reproducible between each shale formation, so each job must be designed for the target formation and its special characteristics (thickness, lithology, rock stress characteristics, etc.) to optimize development of a complex network of fractures. There are two main types of fracturing; propped hydraulic fracturing and acidizing.

1.5.1 Hydraulic (Propped) Fracturing

Hydraulic fracturing of a horizontal well in shale formations is usually performed in stages; each stage has as many as 20 sub-stages (Figure 1.6). The typical fracturing fluid of shale formations (Figure 1.7) composes of about 98% of water and proppant and less than 2% of chemicals such as fraction reducers, iron control, scale

inhibitors, surfactants, pH adjusting agent, etc. The initial sub-stages include an acid (HCl) pre-flush to lower the compressive strength of the formation near the wellbore, remove drilling and completion damage, and enhance the micro-fractures' connectivity by removing the calcite (Fontaine *et al.* 2008). McCurdy (2011) showed that the typical acid concentration in the hydraulic fracturing fluid used for shale formations is 0.08% - 2.1% of the total fluid pumped, which is added as 15% HCl. This results in the active acid to be approximately equal to 0.012% - 0.31% of the total fluid pumped.

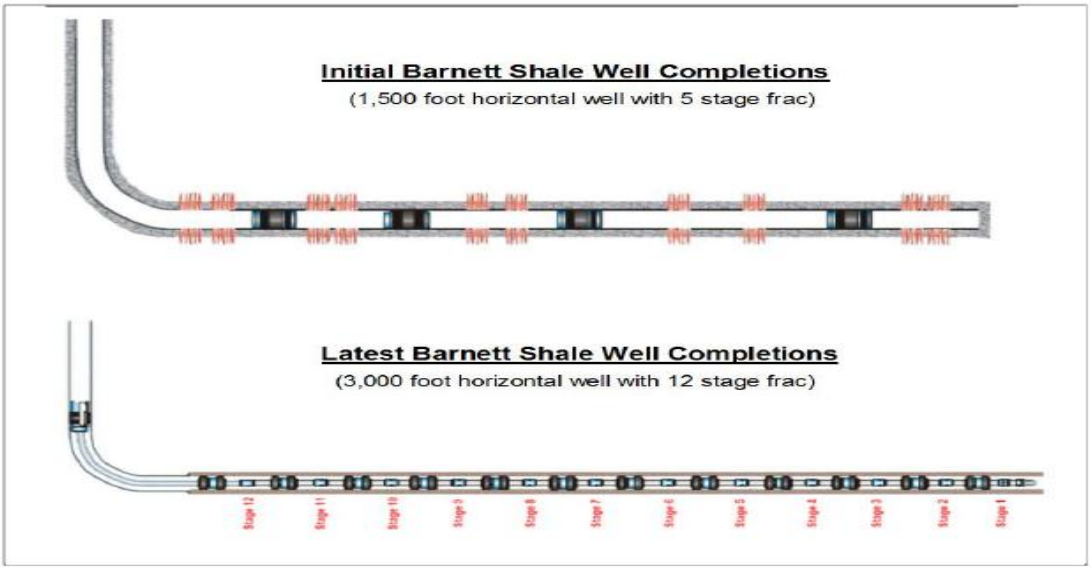

Figure 1.6 Lower damage, more effective horizontal well completions provide higher reserves per well (EIA 2013)

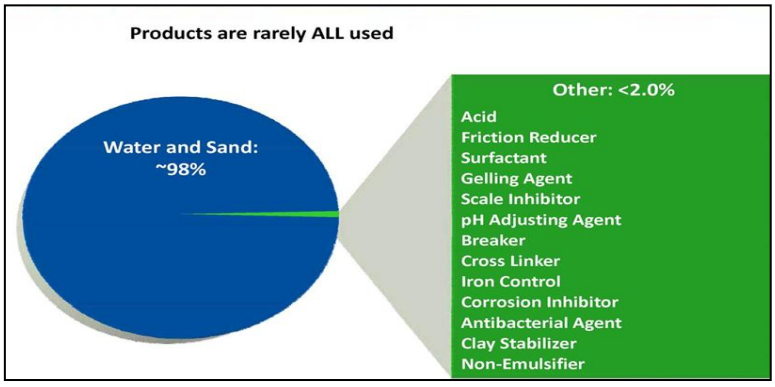

Figure 1.7 Typical fracturing fluid composition for shale formations (Fontaine *et al.* 2008)

1.5.1.1 Hydraulic Fracturing Process

The hydraulic (propped) fracturing process is typically performed in the following steps:

1. Inject a Preflush of acid to remove drilling/completion damage (no more than 2-5 ft from the wellbore).

2. Inject a large volume of fracturing fluid into a prospective producing formation at an injection rate that will place sufficient stress on the rock to cause the rock to physically split (fracture) in one or more places. This initial volume of fluid is termed the "Pad" and typically comprises 20% of total fluid volume.

3. Pump Pad fluid to create enough fracture width to accept proppant particles. Proppant is typically comprised of size-graded, rounded and nearly spherical white sand, but may also be man-made particles.

4. Proppant particles are mixed into additional fracturing fluid and the resulting slurry is pumped into the reservoir, propping open the created fracture(s) so that they will remain open and permeable after pump pressure is relieved.

5. At the end of placing the slurry, a tubular volume of clean "Flush" fluid is pumped to clear tubulars of proppant and the pumps are shut down.

6. Well pressure is then bled off to allow the fracture(s) to close on the proppant.

7. The final step in a fracturing treatment is to recover the injected fluid by flowing or lifting the well (load recovery.)

1.5.1.2 Refracturing Problem

Hydraulic fracture conductivity declines because of a variety of reasons including increasing effective stress, proppant fatigue due to stress cycling, and etc. It is important to note that a well drilled in the shale may have to be fracked several times over the course of its life to keep the well flowing, and that each fracking operation may require more water than the previous one (Vincent 2010). There has been an increase in the number of wells being refractured in shale plays, and in some

cases the wells are refractured as many as 10 times (Figure 1.8). Generally, operators do refracs for different reasons such as:

- Enlarged frac (more reservoir contact)
  - – Improved pay coverage (add pay in vertical wells)
  - – Better lateral coverage (horizontal wells)
- Increased frac conductivity
  - – Restore conductivity lost due to– frac degradation
  - – Address unpropped/poorly propped portions
- Reorientation or creating more initiation points
- Use of more suitable frac fluids
- Re-energizing natural fissures
- Other mechanisms

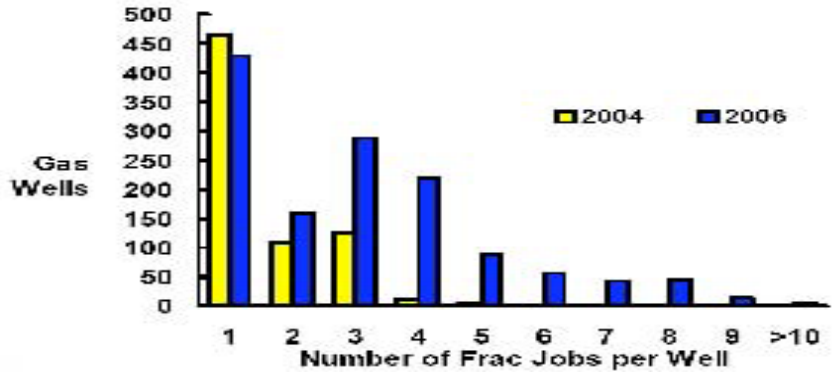

Figure 1.8 Summary of refrac jobs in gas wells (Vincent 2010)

Refracs do not always yield the desired outcomes as they might fail due to:

- Low pressure
  - – depleted wells (limited reserves in gas reservoirs)
  - – poor recovery of frac fluids
- Undesirable existing perforations
- Poor mechanical integrity
- Poor wells often make poorest refrac candidates
  - – Unless initial frac was poorly designed or implemented

1.5.1.3 Proppant Embedment

When proppant particles penetrate the walls of the fracture, the effective width of the fracture and the fracture conductivity are decreased. Proppant embedment (Figure 1.9) can reduce fracture width up to 60% with subsequent reduction of productivity from oil and gas wells. Proppant embedment is caused by stress change in the formation when formation pore pressure declines with production.

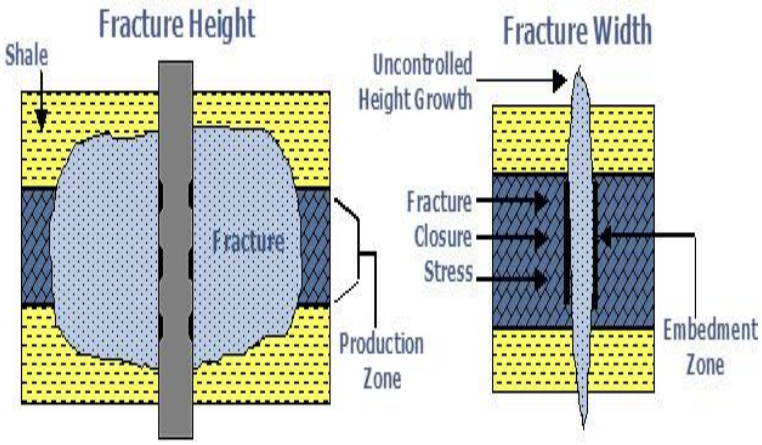

Figure 1.9 Proppant embedment configuration (Core Lab 2014)

1.5.2 Acidizing

In addition to an acid pre-flush, two more stimulation techniques employed as alternatives to propped fracturing are matrix acidizing and acid fracturing.

1.5.2.1 Matrix Acidizing

Matrix acidizing is performed at low pressures to avoid fracturing the reservoir rock when acid is pumped into the well and permeability is increased by acid dissolution of sediment and mud solids. Permeability is enhanced by enlarging the natural pores of the reservoir and stimulating flow of hydrocarbons in immediately proximity to the wellbore.

1.5.2.2 Acid Fracturing

Acid fracturing involves pumping highly pressurized acid into the well, physically fracturing the reservoir rock and dissolving sediments to improve permeability. This process forms channels through which the hydrocarbons may flow (Figure 1.10: Bale *et al.* 2010). The most common acid employed to stimulate production is hydrochloric (HCl), which is useful in removing carbonates from

reservoirs. Hydrochloric acid may be combined with hydrofluoric acid (HF), which dissolves silicate phases from the reservoir rocks (Patton *et al.* 2003). In order to protect the integrity of the already completed well, inhibitor additives are introduced to the well to prohibit the acid from breaking down the steel casing in the well. Also, a sequestering agent can be added to block the formation of gels or precipitate of iron, which can clog the reservoir pores during an acid job. After an acid job is performed, the used acid and sediments removed from the reservoir are washed out of the well in a process called backflush.

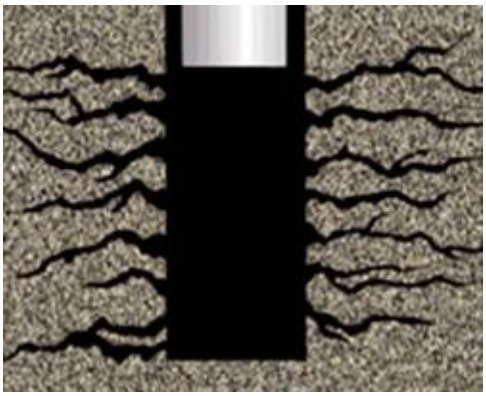

Figure 1.10 Typical acid fracturing network (Bale *et al.* 2010)

A fracture conductivity experiment done by Jiao (2004) on two different conventional reservoirs showed the great potential of acid treated fracture at lower confining pressures less than 3000 psi for reservoir 2 (Figure 1.11), while proppant treated fracture was slightly better between confining pressures of 3000- 6000 psi. However, proppant treated fracture for reservoir 1 was better than acid treated fracture at all tested confining pressure of 0-6000 psi (Figure 1.11). The difference between the two studied reservoirs shows the importance of reservoir studies to determine the proper fracturing technique to be applied.

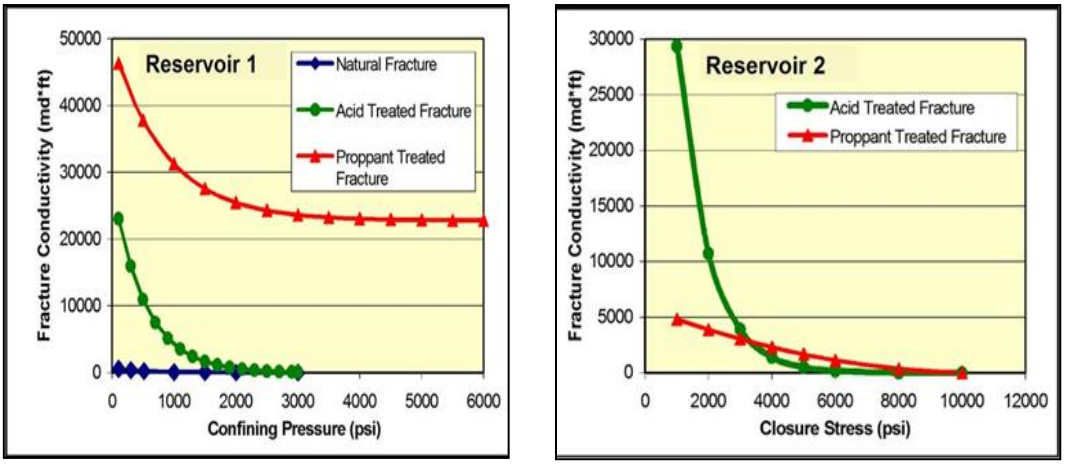

Figure 1.11 Conductivity measurements for acid and proppant treated fracture on Carbonate reservoirs after Jiao 2004

1.5.2.3 HCl Acid Reaction with Formation Minerals

HCl reacts rapidly with calcite, and to a lesser extent, dolomite, and it is predicted that the main impact of HCl on shales will vary as a function of how much calcite is dissolving, which in turn is controlled by acid strength, temperature and pressure. Calcite (calcium carbonate) reacts with HCl to produce calcium chloride, water and carbon dioxide (Eq. 1.1), while dolomite reacts with HCl to produce calcium chloride, magnesium chloride, water and carbon dioxide (Eq. 1.2). The reaction rate for calcium carbonate is rapid, while the reaction with dolomite is slower (Patton *et al.* 2003).

$$CaCO_3+2HCl \rightarrow CaCl_2+H_2O+CO_2 \quad (1.1)$$

$$CaMg(CO_3)_2+4HCl \rightarrow CaCl_2+MgCl_2+2H_2O+2CO_2 \quad (1.2)$$

The rate of dissolution depends on the speed with which acid can be delivered to the rock. This results in rapid generation of irregular shaped channels (Figure 1.12) calls “wormholes.” The acid improves production by creating bypasses around the damage rather than removing it.

HCl not only reacts with calcite and dolomite, but also with some clay minerals that could result in formation damage. Some clays react with HCl and result in iron precipitations. Minerals such as Chlorite have faster reaction rates with HCl compared to kaolinite that reacts slowly with HCl and needs higher concentrations of

HCl to precipitate iron (Simon and Andereon. 1990). Illite is stable when exposed to HCl even at 180°F (Simon and Andereon. 1990).

Figure 1.12 Mold of wormholes created by HCl in Limestone from a central conduct after Crowe *et al.* 1992

1.5.2.5 Acidizing and Matrix Acidizing Application in Shale Formations

Shale formations may have highly variable mineralogies, which makes it difficult to predict the consequences of matrix acidizing. It is also important to consider damage mechanisms when designing a matrix treatment, as dissolving calcite, quartz, or clay minerals may affect the reservoirs differently (Patton *et al.* 2003). Shales usually have natural micro-fractures, (e.g. Eagle Ford Shale (EL Shaari *et al.* 2011 and Taylor *et al.* 2012) and acid may enhance micro-fracture conductivity. A limited number of studies have quantified the effect of HCl matrix acidizing on recoverability and physical properties of shale formations (Fontaine *et al.* 2008). However, less information is known about the development of conductivity and the acid concentrations necessary to optimize conductivity, and by extension, the impact on production and rock stability.

Developing appropriate strategies for shale acidizing may significantly increase oil and gas production (Runtuwene *et al.* 2010), despite lowering Young's modulus. A successful example is the Monterey shale in California, which has a low Young's modulus (1-2 E6 psi), but, due to their silica-rich nature the shale remains highly productive (EL Shaari *et al.* 2011).

Recently, a novel stimulation technique called combination of acid fracturing with Proppant Fracturing (CAPF) has been utilized, which combines the benefits of

both acidizing and proppant fracturing in carbonate reservoirs (Bale *et al.* 2010). Acid treatment does not provide longer fracture length compared to the propped fracturing, but it does result in non-uniform acid etched fractures that keep conductivity high, so long as stable points of support "asperities" exist along the fracture length. The goal of the CAPF technique is to utilize the benefits of acid fracturing by creating etched fractures, in tandem with proppant to provide permanent conductivity in carbonate reservoirs. The study proposed this technology for heterogamous carbonate reservoirs with irregular (non-uniform) asperities that would not close when stress changes in the formation.

A similar application of combining the benefits of acidizing and propped hydraulic fracturing in unconventional shale formation shows a great improvement in gas production. One of the application of combining acidizing with propped hydraulic fracturing is the hydraulic fracturing treatment in Woodford shale formation, as acid is not only injected as a pre-flush treatment, but also is used in different sub-stages of the hydraulic-fracturing process away from wellbore (Grieser *et al.* 2007). In hydraulic fracturing treatments of Woodford shale, acid slugs (Table 1.2) are used away from wellbore to free some of the adsorbed gas by dissolving calcite and dolomite crystals (Grieser *et al.* 2007). The study used XRD analysis on a shale similar to Woodford. The Caney shale samples treated with weak HCl solution (3%), showed a great improvement in pore connectivity after 3 hours of immersion in HCl, although no deductible amounts of calcite or dolomite were detected by XRD analysis after acid treatment (Figures. 1.13 Though 1.14). The authors also mentioned that shales have many acid soluble minerals that may be dissolved in low pH fluids and result in greater production.

Table 1. 2 Pump schedule: Woodford Shale frac treatment after Grieser *et al.* 2007

Stage		Vol. gal	Fluid	Conc. lbm/gal	Proppant
1	Acid Spearhead	4,000	15% HCl acid		
2	Pad	26,400	Pad and flush		
3	Sand slug	5,000	Treated water	0.1	Premium Brown-30/70
4	Pad	26,400	Pad and flush		
5	Sand slug	5,000	Treated water	0.15	Premium Brown-30/70
6	Pad	26,400	Pad and flush		
7	Sand slug	5,000	Treated water	0.2	Premium Brown-30/70
8	Pad	26,400	Pad and flush		
9	Sand slug	5,000	Treated water	0.25	Premium Brown-30/70
10	Pad	24,400	Pad and flush		
11	Sand slug	14,240	Treated water	0.1	Premium Brown-30/70
12	Acid	7,120	26% HCl acid cut on the fly to 3%		
13	Sand slug	14,240	Treated water	0.19	Premium Brown-30/70
14	Acid	7,120	26% HCl acid cut on the fly to 3%		
15	Sand slug	14,240	Treated water	0.26	Premium Brown-30/70
16	Acid	7,120	26% HCl acid cut on the fly to 3%		
17	Sand slug	14,240	Treated water	0.37	Premium Brown-30/70
18	Acid	7,120	26% HCl acid cut on the fly to 3%		
19	Sand slug	14,240	Treated water	0.46	Premium Brown-30/70
20	Acid	7,120	26% HCl acid cut on the fly to 3%		
21	Sand slug	14,240	Treated water	0.55	Premium Brown-30/70
22	Sand slug	14,240	Treated water	0.64	Premium Brown-30/71
23	Sand slug	14,240	Treated water	0.73	Premium Brown-30/72
24	Sand slug	14,240	Treated water	0.82	Premium Brown-30/73
25	Sand slug	14,240	Treated water	0.9	Premium Brown-30/74
26	Flush	3,656	Pad and flush		

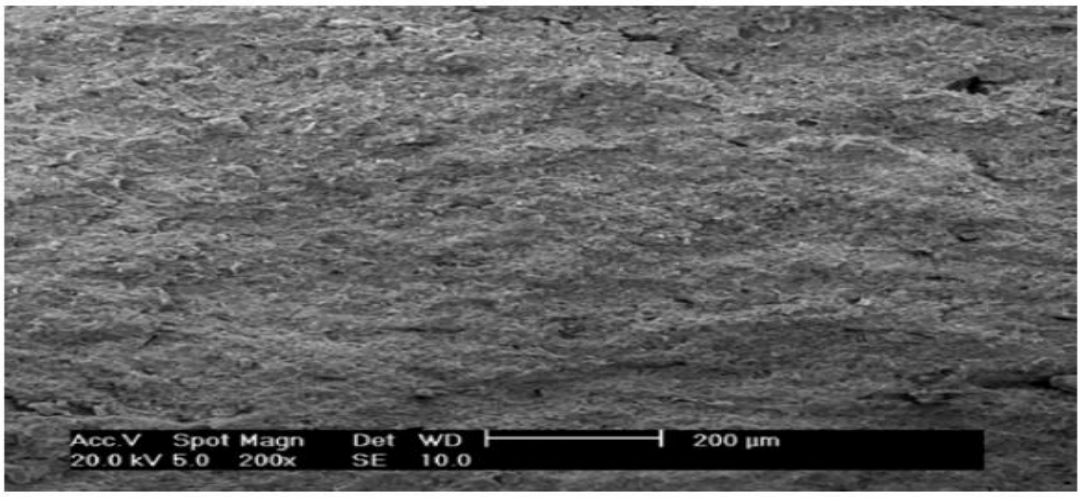

Figure 1.13 Caney Shale sample before Acid immersion with no XRD acid-soluble material, 200x after Grieser *et al.* 2007

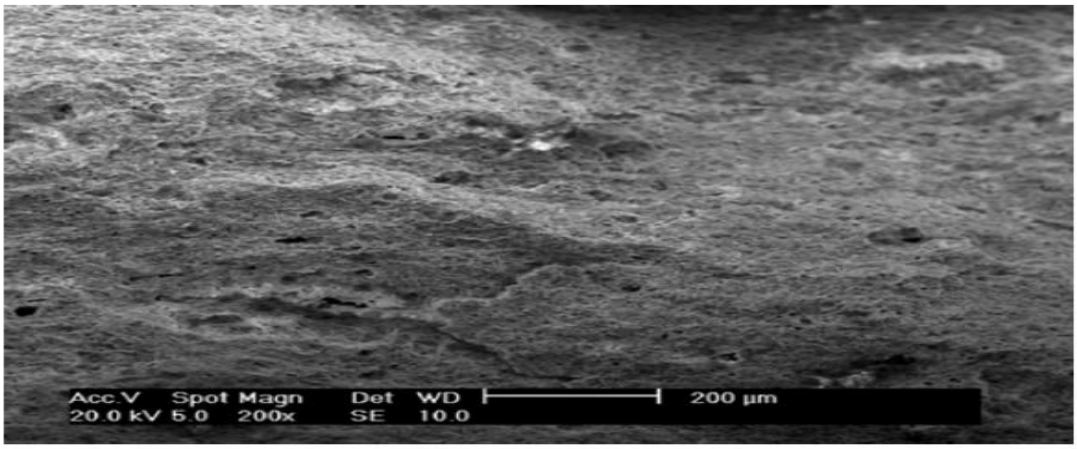

Figure 1.14 Same Caney Shale sample after 3-hr Soak in 3% HCl at 125ºF, 200x after Grieser *et al.* 2007

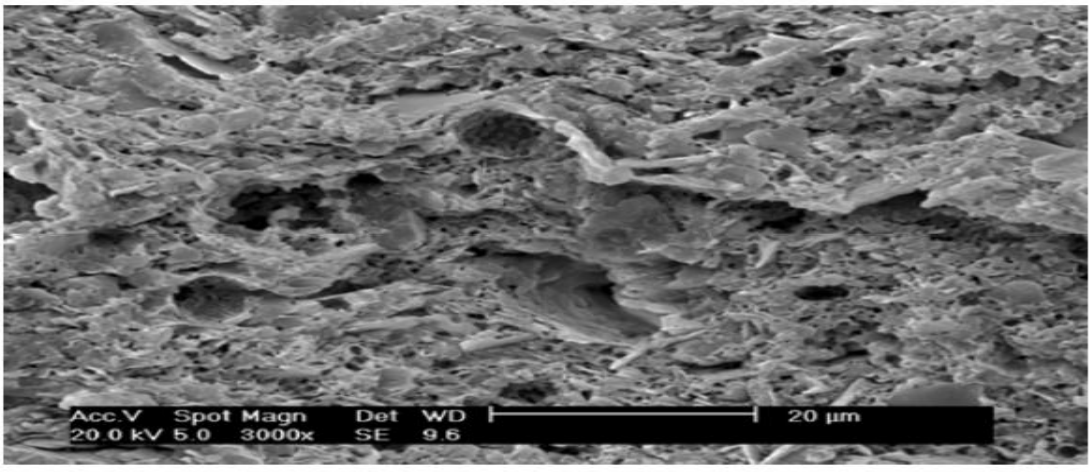

Figure 1.15 3000x closeup of acid-etched Shale that showed no detectable amount of calcite or dolomite in XRD analysis after Grieser *et al.* 2007

1.6 Shale Rocks Used in This Study

The shale samples that are covered in the present study are from Eagle Ford, Mancos, Marcellus, Barnett, and Bakken shales. The location of the studies shales among all North America shale plays are presented in Figure 1.16. The mineralogy of the studied shales are shown in Table 1.3 and Figure 1.17.

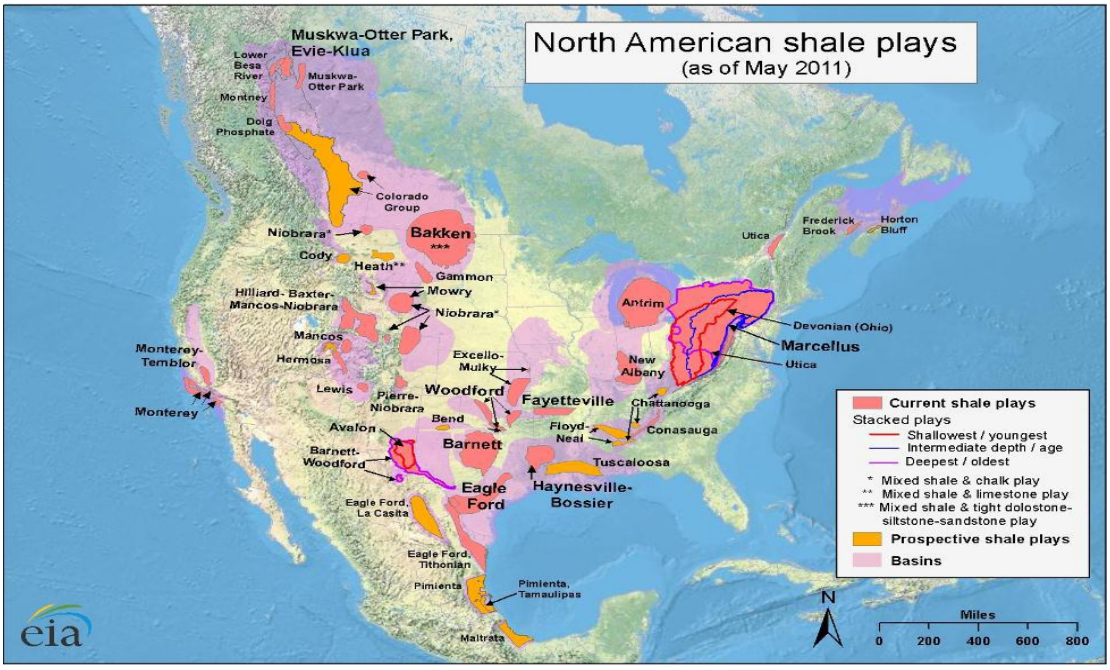

Figure 1.16 Map of North American shale plays from U.S Energy Information Administration

Table 1.3 Typical mineral abundances for studied shales

Mineral	Barnett (wt%)[a.]	Marcellus [a.]	Mancos[b]	Eagle Ford[c]	Bakken Middle[d]
	(percent)	(percent)	(percent)	(percent)	(percent)
Quartz	35-50	10-60	36-43.4	9	11
Clays, primarily illite	10-50	10-35	30.2-42.4	26	4
Calcite, dolomite, siderite	0-30	3-50	9.5-18	53	81
Feldspars	7	0-4	5.2-8.8	2	
Pyrite	5	5-13	1-2.6	4	1
Phosphate, gypsum, Apatite	trace	Trace	trace	1	
Mica	0	5-30	trace	Trace	Trace

Notes: [a]After Bruner and Smosna, 2011; [b]After *Sarker and Batzle, 2010;* [c]*Company Data,* [d]*Akrad 2011*

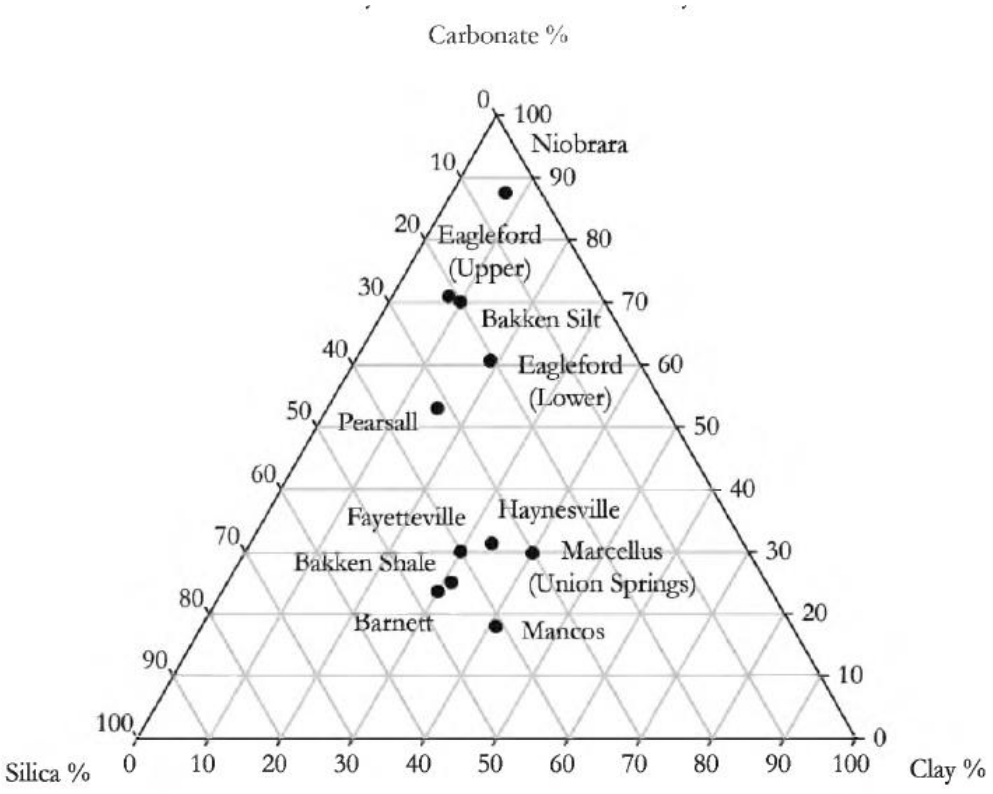

Figure 1.17 A Ternary Diagram Plotting Clay, Carbonate, and Silica Content Against Each Other for Productive Shale Plays in North America. Modified from Anderson (2012), Boyce and Carr (2009), and Bruner and Smosna (2011)

1.6.1 Mancos Shale

The Mancos oil and gas shale (Figure 1.18) was deposited in the Western Cretaceous seaway provides the source for the major shale play in the Rocky Mountains. The technically recoverable oil of Mancos Shale is estimated to about 189 million bbl. Mancos Shale is predominately steel-gray sandy shale, but includes stringers of earthy coal, impure limestones, and many thin beds of fine-grained yellow and brown sandstone, composed chiefly of sub angular and angular quartz grains cemented by lime (Torsæter *et al.* 2012). The shale varies in lithology throughout pay interval and the production is mainly controlled by the existence of natural fractures and thin sands. Total organic carbon values (TOC) were reported to range from 0.4 wt% to 3.1 wt%. The average reservoir porosity is in the range of 6-8% and clay content around 20-25% (Holt *et al.* 2012). The permeability was reported as 10 nDarcy (Sarker and Batzle 2010). Mancos formation water is very saline with 13.8-

21.2 wt % (Haszeldine *et al.* 2005). Mancos Shale is a dual-porosity, naturally fractured play, and because of its tight matrix characteristics, reservoir development depends mainly on massive natural fracturing.

Figure 1.18 Mancos Shale as fissile plates and flakes

1.6.2 Barnett Shale

The Barnett Shale play is located within the Fort Worth and Permian Basins in Texas. The Barnett Shale is a well known gas producing black shale formation, but condensate and oil are also produced by horizontal wells in certain parts of the deposits (Bruner and Smosna 2011). The Barnett Shale has many different facies including dense, organic rich, soft, thin-bedded, petroliferous, fossiliferous shale and hard, black, finely crystalline, petroliferous, fossiliferous limestone. The mineralogy of the Barnett Shale is shown in Table 1.3 and Figure 1.17. There is a set of natural fractures in the Barnett shale that strike 100–120°. Most fractures are mineralized especially close to major faults; they are believed to be wider and more common in limestone interbeds. The reservoir properties are as following: 6% porosity, 20–30% water saturation, water bound to clay minerals, no free water, 70–80% gas saturation, gas stored in interstitial pores and microfractures and adsorbed onto solid organic matter and kerogen. The adsorbed gas is as low as 20–25% or as high as 40–60%,

normally pressured to slightly overpressured (0.46–0.52 psi/ft), 3,000 to 4,000 psi formation pressure where the gradient is normal, and 4,000–8,500 ft drilling depth.

The success in the Barnett started in 1995, which established the economic potential of U.S. shale gas production and set the standard rules for shale development. A typical lateral well is about 2500 to 3000 ft.

1.6.3 Marcellus Shale

The Marcellus Shale play is currently the hottest play in the Appalachian Basin across the Eastern Part of the United States. The shale was explored prior to 2000 with very slow production rate, but when stimulated, the Marcellus saw significantly improved production rates. The Marcellus Shale is an organic-rich that was deposited in an oxygen-deficient marine environment during Middle Devonian time.

The Marcellus Shale is a well known gas producing black shale formation, but condensate and oil are also produced from horizontal wells in certain parts of the deposits (Bruner and Smosna 2011). The depth to the top of the Marcellus shale varies and can be over 9,000 feet in parts of southwestern and northeastern Pennsylvania. The gross thickness of the Marcellus shale ranges from less than 20 feet along the Lake Erie shoreline in northwestern Pennsylvania to several hundred feet in central and northeastern Pennsylvania. The net thickness of organic-rich Marcellus shale varies from less than 10 feet in western Pennsylvania along the Ohio border to over 250 feet in northeastern Pennsylvania. Matrix shale porosity is in the range of 0.5–5.0% (Myers, 2008). However, the matrix pore spaces in Marcellus are poorly connected. Permeability estimates fall between 10-6 md to 0.01 md (Myers, 2008). Sampling of soil formed on the Marcellus bedrock showed the dominant mineralogy consisted of quartz, illite, montmorillonite, muscovite, and biotite with phases of todorokite and trona appearing at depths closer to the bedrock.

1.6.4 Eagle Ford Shale

The Eagle Ford Shale gas and oil play is located within the Texas Maverick Basin. It is a Cretaceous sediment that was traditionally known as a source rock in

South and East Texas. The formation is the source rock for the Austin Chalk play. There are three zones (Figure 1.19): an oil zone; a condensate zone; and, a dry gas zone (Fan *et al.* 2011). Thickness in the productive area ranges from 40 ft to over 450 ft. Total organic content (TOC) is about 3 - 7%. Porosity range is of 6 – 11%. Pressure gradient is within 0.5 - 0.8 psi/ft. The mineralogy of the studied shale is shown in Table 1.3. The risked shale oil in-place is about 106 billion barrels with a risked technically recoverable resources of 6.3 billion barrels (EIA 2013).

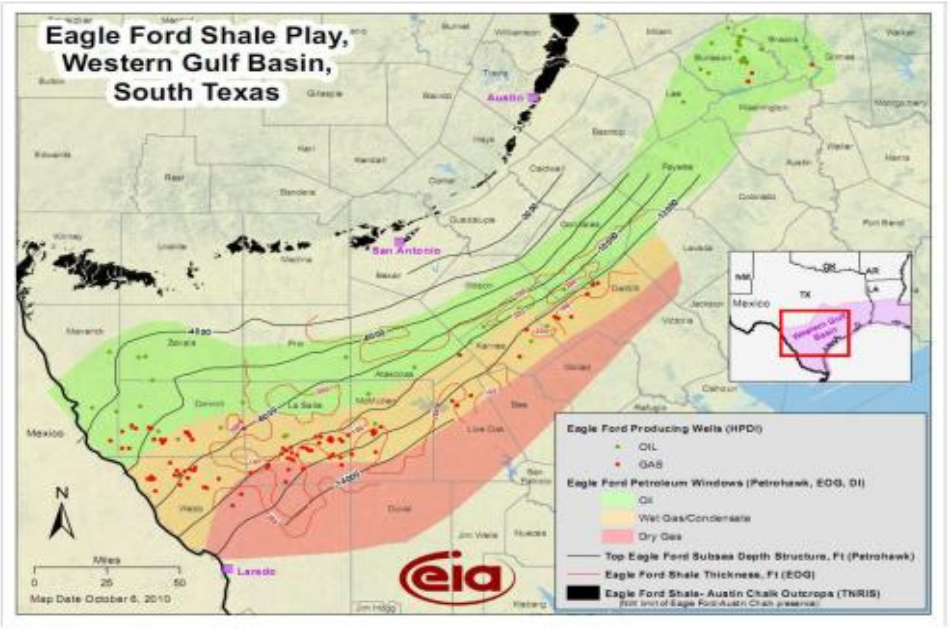

Figure 1.19 Eagle Ford Shale play (Energy Information Administration, 2011)

The Eagle Ford formation is composed of organic-rich calcareous mudstones and chalks that were deposited during the two transgressive sequences, the upper and lower Eagle Ford. The lower Eagle Ford is organically richer and produces more hydrocarbons than the upper Eagle Ford. The Eagle Ford shale is mainly a clay-rich limestone with very low quartz content. The low quartz content makes it a less brittle (more ductile) with a low Young's Modulus (YM) ranges from 1*106 to 2*106 psi (Chaudhary *et al.* 2011).

1.6.5 Bakken Shale

The Bakken is different from the other shales as it is an oil reservoir with a set of dolomite layers between two shales. The Bakken depth ranges from around 8,000 to 10,000 feet. The formation produces oil, gas, and natural gas liquids. There are

three members of the shale; lower, middle, and upper. Each member is different in its characteristics that control its reservoir quality. The middle member is sandstone that is varies in thickness, lithology, and petrophysical properties. While, both upper and lower members are consistent in lithology and considered as the petroleum source rock. Both upper and low Bakken contain high TOC content of about 11 wt%. The middle member has an average porosity of about 7% with very low permeability (0.001 m.d) (Fakcharoenphol *et al.* 2012).

Chapter 2
Matrix Acidizing While Fracturing

In this chapter, the potential of combining the benefits of propped hydraulic fracturing and matrix acidizing by introducing low concentrations of acid slugs in the hydraulic fracture treatment of shale formations is presented. The acid slugs intended to improve the micro-fracture conductivity deep in the formation and near the wellbore. This chapter presents a comprehensive experimental study to investigate the effect of low concentrations of HCl matrix acidizing on the physical, mineralogical, oil recoverability, and mechanical properties of different shale rocks.

2.1 Materials

2.1.1 Shale Core Samples

Core samples from the following shale formation were used:

- Mancos
- Barnett
- Marcellus
- Eagle Ford

Individual samples were 1.0-1.5 inch in diameter and 1-2 inches in length. Outcrop core samples of all the shales were purchased from a core lab and the well depth and location were not released. Other reservoir core samples from Eagle Ford Shale were provided by Chesapeake Oil Company.

2.1.2 Test Fluids

1. Distilled Water
2. Oil: The laboratory testing was done with Soltrol 130 oil.
   - Chemical Composition: C10- C13 Isoalkanes (100% by weight)
   - Physical Data:
   - Vapor Density (Air = 1): > 3
   - Solubility in Water: Negligible
   - Specific Gravity (H2O = 1): 0.762 at 60/60F (15.6/15.6C)

- Percent Volatile by Volume: 100
- Viscosity: 1.55 cp @ 100F (38C)

3. Hydrochloric Acid, (HCl)
   - Molar Mass 74.5513 g.mol-1
   - Appearance: Clear Colorless liquid
   - Odor: Strong repugnant

2.1.3 Salts

1. Sodium Chloride (NaCl)
   - Molar Mass 58.44g.mol-1
   - Appearance Colorless crystals
   - Odor Odorless
   - Density 2.165g cm-3
   - Melting point 801°C, 1074°K, 1474°F
   - Boiling point 1413°C, 1686°K, 2575°F
   - Solubility in water 359g L-1

2. Potassium chloride, (KCl)
   - Molar Mass 74.5513g.mol-1
   - Appearance: White Crystalline solid
   - Odor: Odorless
   - Density: 1.984g.cm-3
   - Melting point 770°C
   - Boiling point 1420°C,
   - Solubility in water 281g L-1(0°C); 344g L-1(20°C); 567g L-1(100°C)

2. 1.4 Laboratory Equipment Used

- Amott cells
- Balance
- Caliper
- Drill Press with Core Drill
- Core Trim Saw
- Vacuum Saturation Desiccators

- Vacuum Saturation Pump
- Soxhlet Extractor, Electronic Balance, Glass Pycnometer.
- Vernier Caliper, Electronic Balance, Helium Porosimeter
- Helium Gas
- Compressed Air
- Graduated cylinder
- Computed Tomography (CT) Scanner
- Rigaku Miniflex II X-ray diffractometer
- EDAX Energy-Dispersive Spectrometer (SEM-EDS)
- MTS Material Testing Machine

2.2 Effect of Acid Contact Time on Shale Porosity and Mass Loss

The objective of this experiment is to study the impact of acid contact time on overall average porosity and mass loss in order to optimize the matrix acidizing treatment during the hydraulic fracturing process. The acid contact time varies from 10 to 180 min. The experiment procedure is as following:

1. Measure the bulk volume of dry core samples before testing using a caliper. The diameter of each core was measured five times at different sections of the core and the length was measured three times. The author took the average diameter and average length at the end to calculate the bulk volume of the core as following::
   $V_{core} = (\pi d^2 L) / 4$ ……..……...…….……(Eq. 2.1)
2. Extract the formation oil from the reservoir core samples of the Eagle Ford Shale using a Soxhlet extractor apparatus, Toluene solvent and a reflux process. Figures. 2.1a and 2.1 b below show the Soxhlet extraction apparatus.

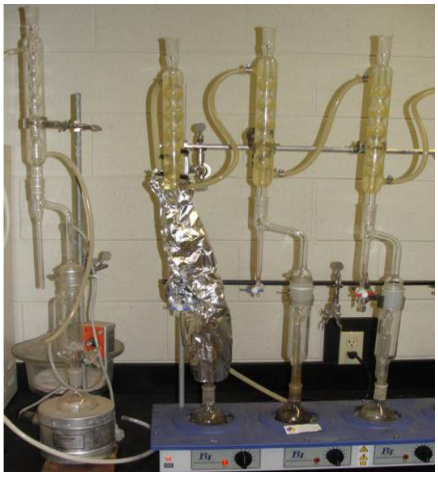

Figure 2.1a Extraction of core sample using the soxhlet extractor

Figure 2.1b Eagle Ford core plug in the soxhlet extractor

3. Dry the Eagle Ford core samples in an oven for two days at about 150°F (Figure 2.2)

Figure 2.2 Eagle Ford Shale core in an Oven being dried

4. Weigh the dry core samples twice and recorded the average weight of each samples (W_{dry}).
5. Measure the porosity for the outcrop and reservoir rock samples using Helium Porosimeter (Pre-acid porosity) as shown in **Figure 2.3**.

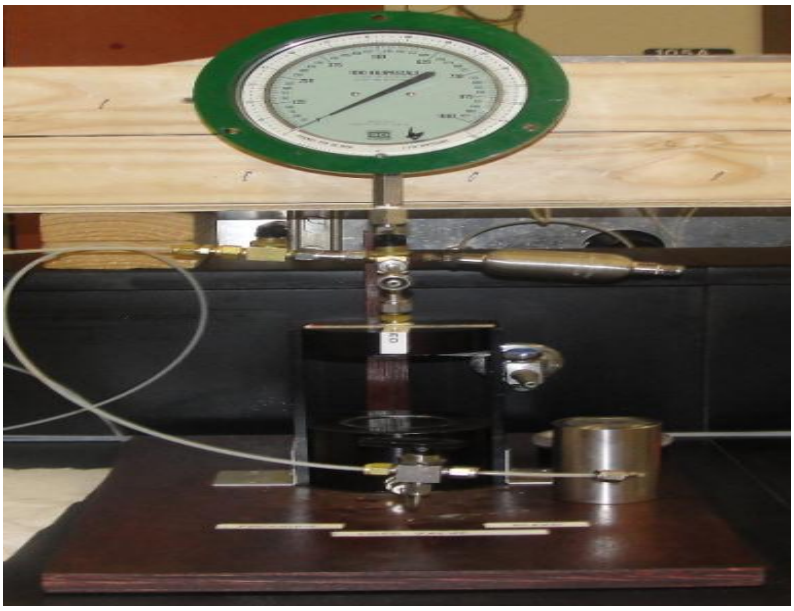

Figure 2.3 Helium porosimeter used for shale core porosity measurement

6. CT scan the dry core samples with a recorded label and alignment direction of scanning for porosity measurement.
7. Vacuum the cores using a vacuum saturation pump and a desiccator (Figures. 2.4a and 2.4b). The cores were placed in the desiccator, and placed under high vacuum for 24 hours, a hose connecting a closed valve was dipped into the Soltrol 130^{TM} oil. When the vacuum was stopped, the hose was opened and Soltrol 130^{TM} oil was ucked into the desiccator and closed the valve.

Figure 2.4a Mancos cores in a desiccator being vacuumed

Figure 2.4b Vacuum saturation apparatus

8. Put the cores in the vacuumed Desiccator to soak for about one week in Soltrol-130 oil. **Figure 2.5**.

Figure 2.5 Saturation of Mancos core with Soltrol 130^{TM} Oil

9. After saturation with soltrol 130^{TM} oil, all cores were reweighed to record the saturated weight (Wsat) and calculate the volume of Soltrol-130^{TM} oil saturated in the core using the oil density (Figures 2.6a and 2.6b).

Figure 2.6a Mancos cores after saturation and ready to be weighed

Figure 2.6b Weighing a core sample

10. CT scan the cores again after saturation with Soltrol 130™ oil in the same aligned scan direction of the first scan time when dry.
11. With the CT images of the air-saturated samples (dry) and oil–saturated samples, the porosity (Pre-acid porosity) was calculated for the second time using Eq.2.2 as following:

$$\emptyset = \frac{CT_{om} - CT_{am}}{CT_o - CT_a} \quad \text{.....(Eq.2.2)}$$

where CTN is a normalized value of the calculated x-ray absorption coefficient of a pixel (picture element) in a computed tomogram, expressed in Hounsfield units, where the CT number of air (CT_a)is −1000, measured Soltrol 130™ (CT_o) was -215. The CT numbers for the air-saturated (CT_{am}) and oil-saturated (CT_{om}) samples were measured for shale sample.

12. Dry some of the samples in the oven (will be used for acid treatment), weighted, and then exposed to different HCl acidic solutions (1, 2, and 3 wt% HCl). The acid solutions were prepared with 2% KCl for Barnett, Eagle Ford, and Marcellus samples and 30% KCl for Mancos samples to prevent any clay swelling during acidizing.
13. The samples were left in the acidic solutions at 200°F in the oven for different contact times (10, 20, 30, and 180 min) (Figure 2.7), then taken out of solution and dried in the oven to evaporate all of the acid left inside, and reweighted to calculate the mass loss due to acidizing at each contact time.

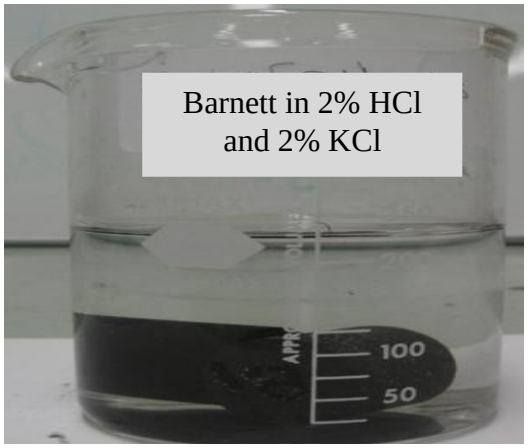

Fig 2.7 Barnett core samples in 2 wt% HCl solution

The samples were then CT scanned as dry, saturated once again with Soltrol 130^{TM} oil, and CT-scanned for a fourth time as oil saturated to calculate post-acid treatment porosity using (Eq 2.2).

Mass loss for the studied shale rock samples shows a correlation with mineralogy, insomuch that the Eagle Ford samples with higher carbonate abundance showed the greatest mass loss (Figures. 2.8 through 2.11).

The degree of carbonate dissolution in Eagle Ford systematically increases with increasing acid concentration and contact time. Eagle Ford samples lost between 1 and 12% of their mass, while their porosities increased from 1.2% to 8.7%. The non-systematic trend of mass loss between the 20 and 30 minute experiments in 2 wt% HCl is attributed to the variations in mineralogy (heterogeneity) between the tested samples at scales comparable to those identified in the compositional analyzes (Figure 2.8).

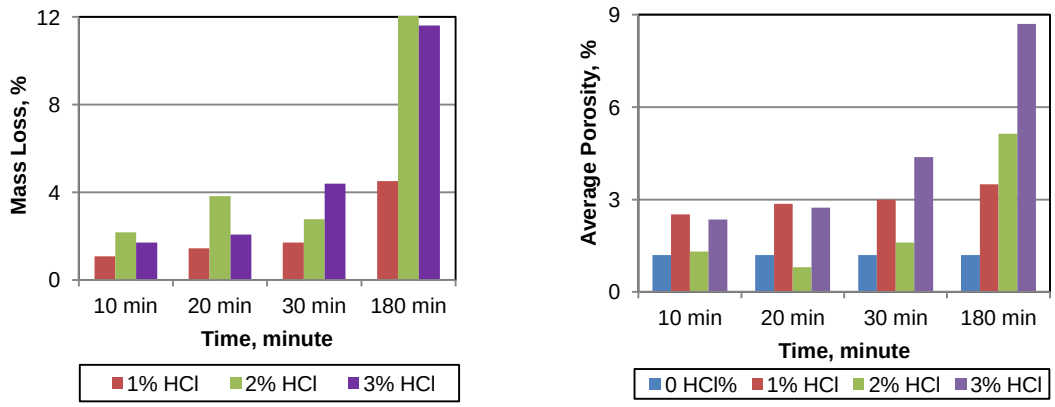

Figure 2.8 Average mass loss (left) and average porosity (right) at different HCl concentrations and different contact times for Eagle Ford samples

In the Mancos, Barnett, and Marcellus samples, the mass loss correlation with the contact time is similar to the Eagle Ford's, but all measured variables are lower (Figures 2.9 through 2.11). This is proposed to be a consequence of the much lower relative abundances of calcite (and other carbonates) in these shales. Measured porosities in post-acid treated samples do not have a linear correlation with mass loss, contact time, or acid strength. It is proposed that this is because the changes in porosity are dominated by crack development and not carbonate dissolution, which results in porosity enhancement on the scale of 3% to 19% for Mancos samples, 5.2% to 16.5% for Barnett, and 2.39% to 7.28% for Marcellus samples. Crack development after acidizing exposes greater surface area in the sample for oil to access, so the oil reaches more pores and micro-fractures, which results in higher calculated post-acid porosity values from CT-scanning.

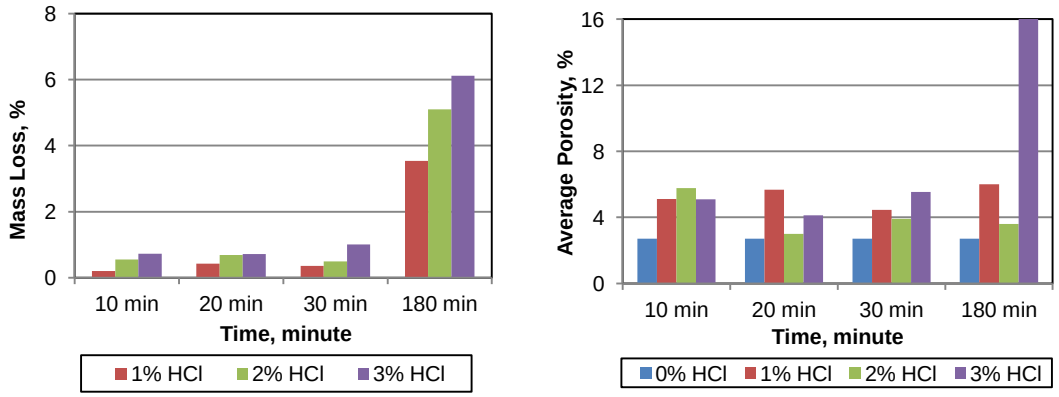

Figure 2.9 Average mass loss (left) and average porosity (right) at different HCl concentrations and different contact times for Mancos Samples

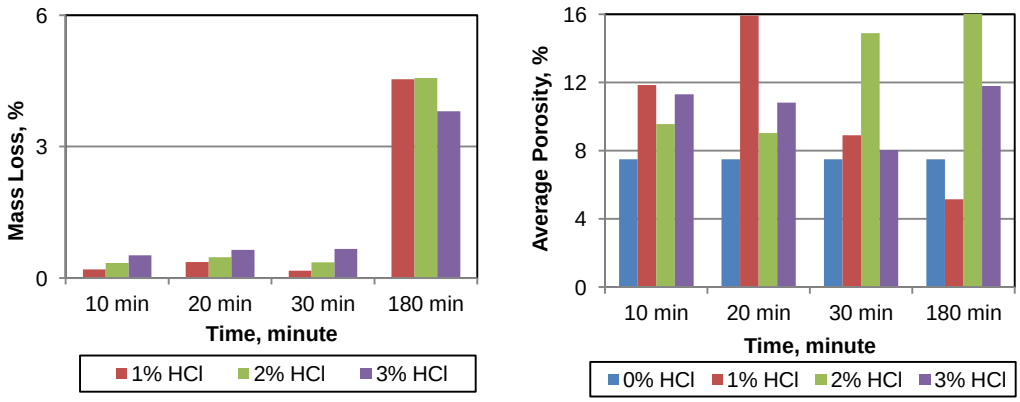

Figure 2.10 Average mass loss (left) and average porosity (right) at different HCl concentrations and different contact times for Barnett Samples

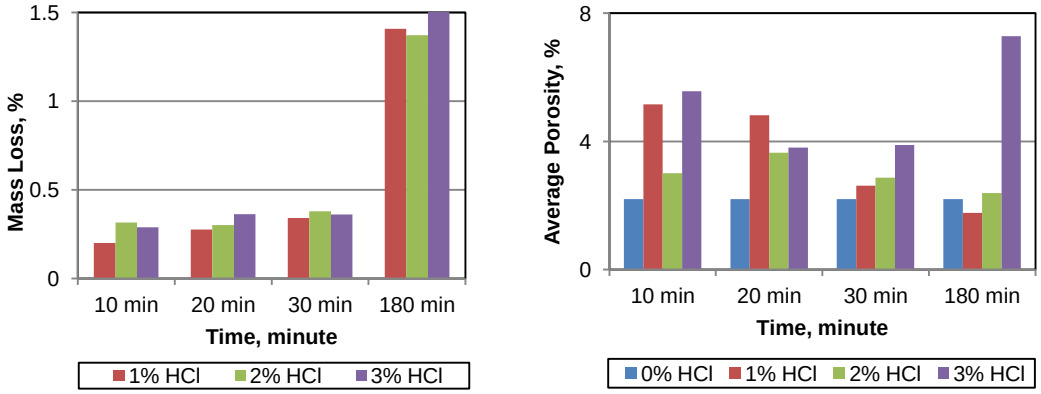

Figure 2.11 Average mass loss (left) and average porosity (right) at different HCl concentrations and different contact times for Marcellus Samples Time

2.3 Computed Tomography (CT) Scanning Analysis of Matrix Acidizing in Shale Rocks

The CT scanned images for the untreated and acid treated samples from the experiments (Section 2.2) were used to analyze the impact of HCl matrix acidizing on shale formations qualitatively and quantitatively. The qualitative technique analyzes matrix acidizing based on the visual observations for each shale rock, while the quantitative technique is based on the CT scanned measured values analysis for each rock in addition to bulk density and porosity calculations.

2.3.1 Qualitative Analysis

Different shale core samples after treatment with 3% HCl solution are shown in Figures. 2.12a and 2.12b.

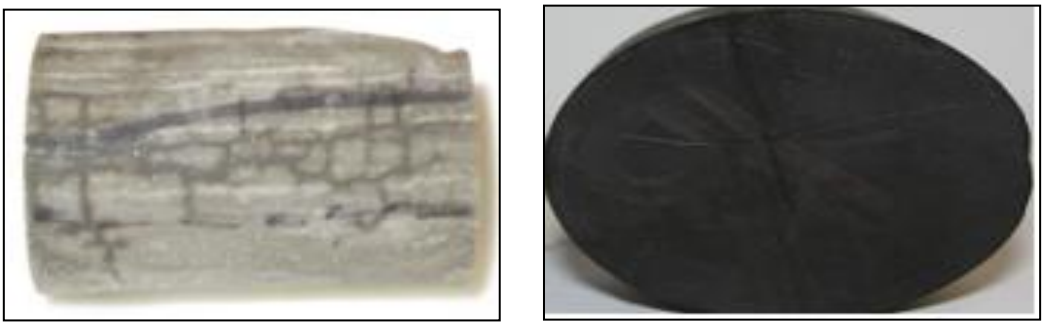

Fig 2.12a Mancos (left) and Eagle Ford (right) Shale cores after immersion in 3% HCl Solution

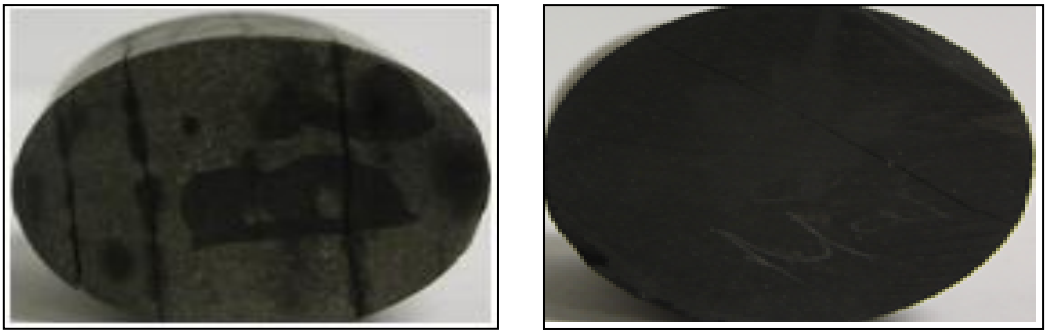

Figure 2.12b Barnett (left) and Marcellus (right) Shale Cores after immersion in 3% HCl Solution

As shown in the pictures taken for Mancos sample (Figures 2.12a and 2.12b), the acid treatment induced cracks in Mancos, Barnett, and Marcellus Shale samples when exposed to 3% HCl. In contrast, Eagle Ford samples rarely showed visible cracks when exposed to 3% HCl (Figures 2.12 and 2.12b).

Air Saturated (dry) CT scanning images were taken for the studied samples pre and post HCl treatment (Figures. 2.13 through 2.16). In addition, 3D compilations have been developed to show the acid treatment effect on the different studied shale samples (Figures. 2.17 through 2.20).

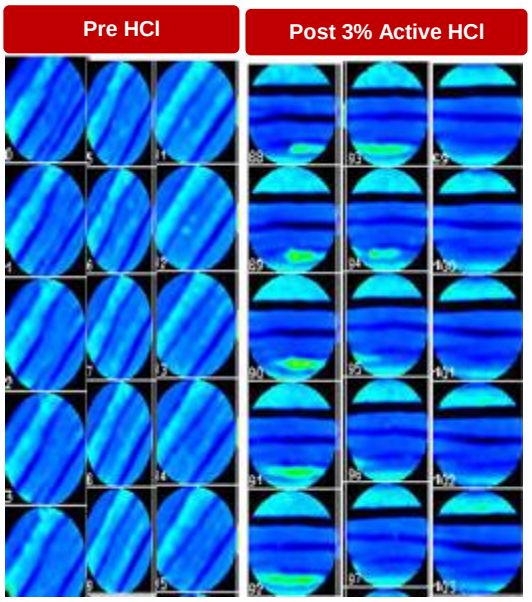

Figure 2.13 False-colored scanning computer tomography images for Barnett Shale Samples pre and post HCl.

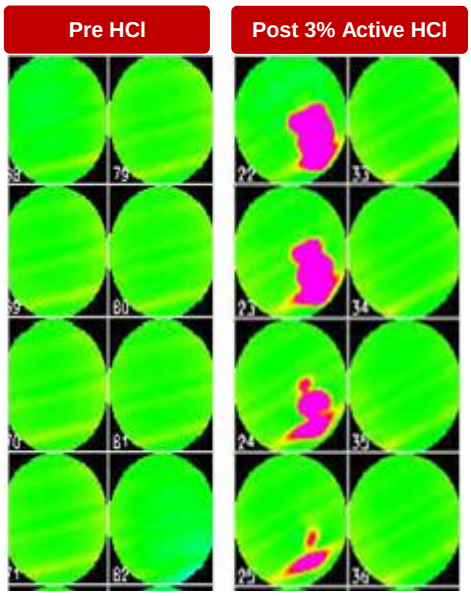

Figure 2.14 False-colored scanning computer tomography images for Marcellus Samples Shale pre and post HCl

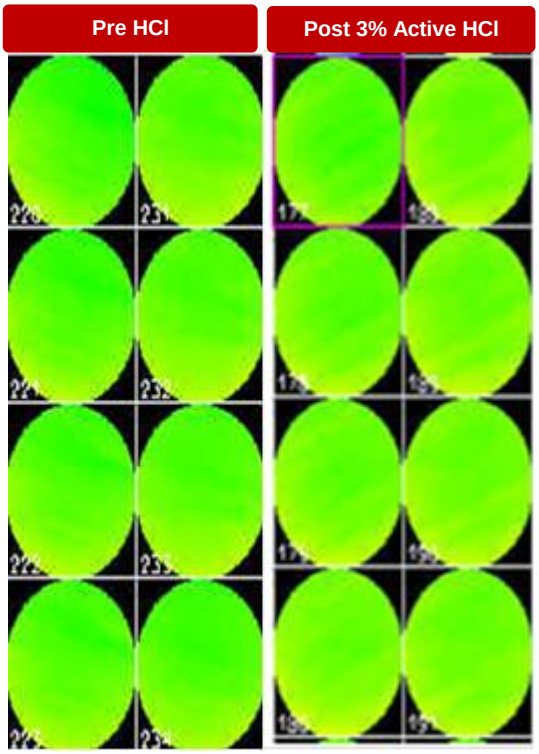

Figure 2.15 False-colored scanning computer tomography images for Eagle ford Shale Samples pre and post HCl

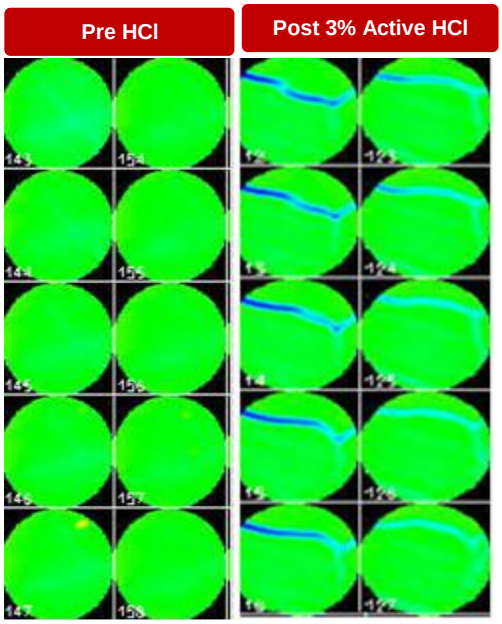

Figure 2.16 False-colored scanning computer tomography images for Mancos Samples Shale pre and post HCl

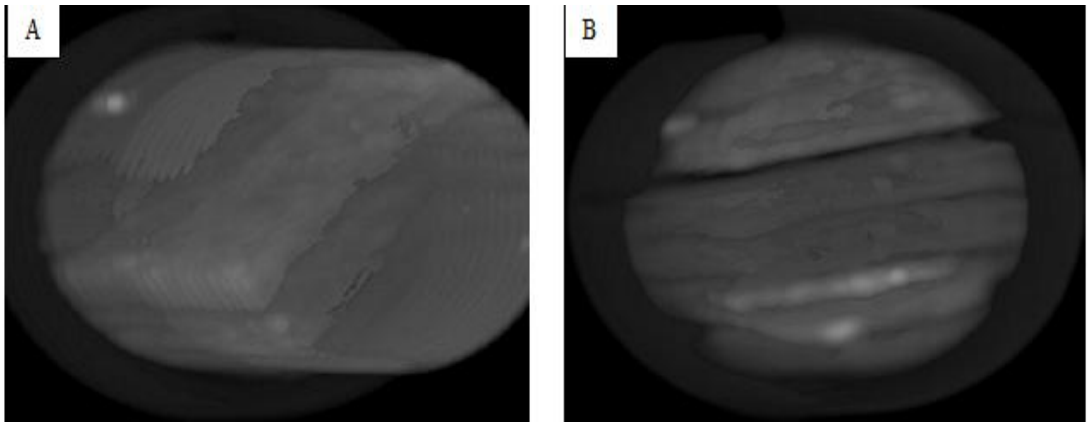

Figure 2.17 Barnett sample 3D image before and after 3% HCl; A (before HCl) and B (after HCl)

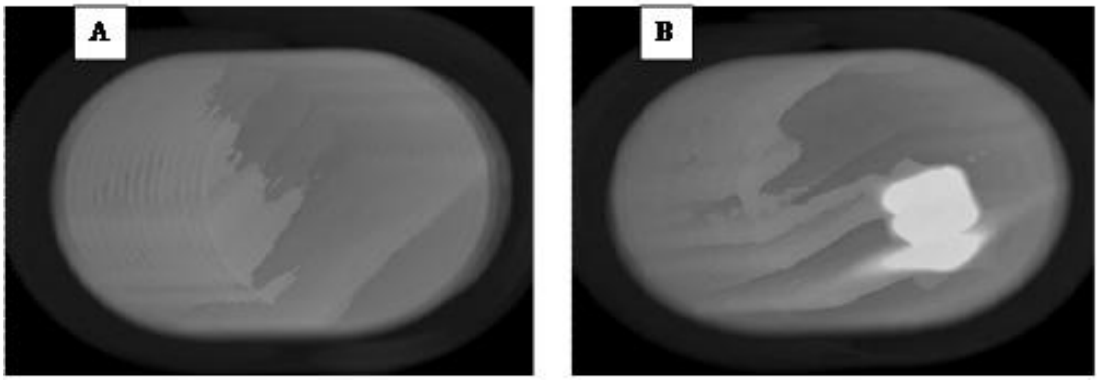

Figure 2.18 Marcellus sample 3D image before and after 3% HCl; A (before HCl) and B (after HCl)

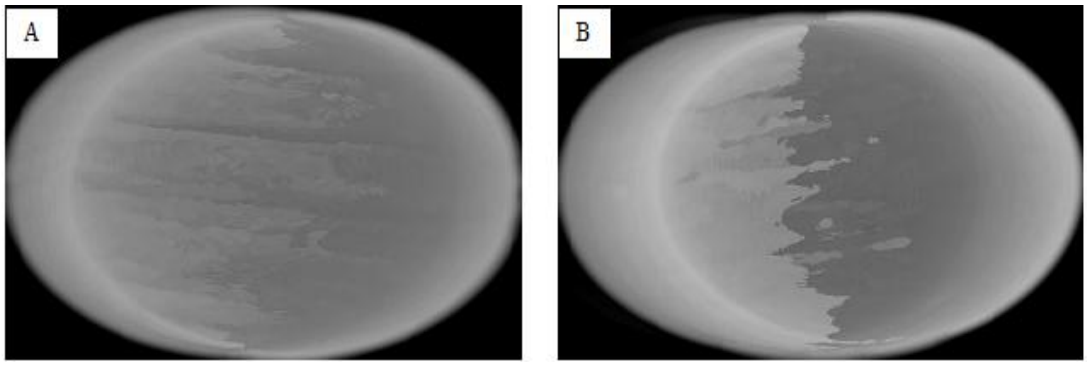

Figure 2.19 Eagle Ford sample 3D image before and after 3% HCl; A (before HCl) and B (after HCl)

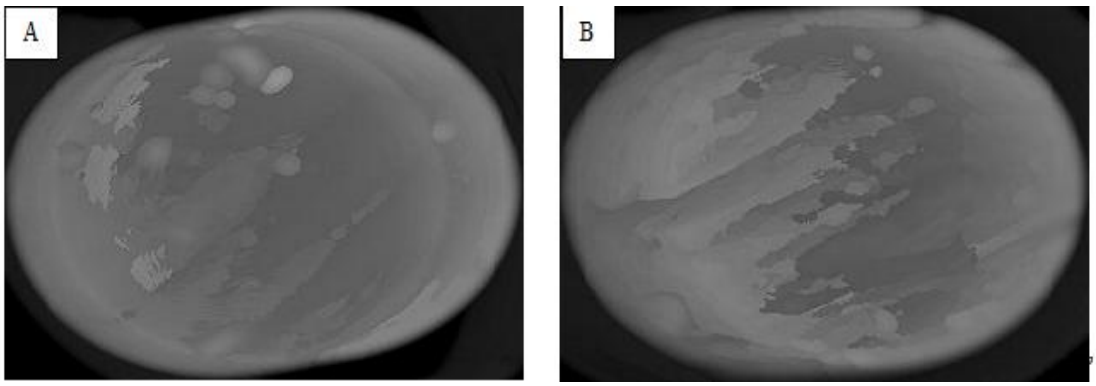

Figure 2.20 Mancos sample 3D image before and after 3% HCl; A (before HCl) and B (after HCl)

False-colored Scanning Computer Tomography images and scanning computed tomography 3D images of the four studied shales show strongly contrasting responses to acid treatment. Barnett and Marcellus Shale samples developed cracks along bedding planes in response to the presence of acidic solution; the size and number of cracks tends to increase with exposure to higher molarity acid solutions, with the greatest increase in crack density observed in Barnett samples (Figures 2.13B and 2.17B). The CT-scanning images of post-acid treated samples of Barnett and Marcellus shales also show the presence of high density material, not observed in untreated samples (white-colored in Figures 2.17B and Figure 2.18B). Based on the higher abundances of pyrite in the Marcellus and Chlorite clay minerals in the Barnett rocks (Simon and Anderson. 1990), the high-density material was interpreted to be iron oxide-hydroxide precipitation formed during clay dissolution processes (in the case of Barnett) and pyrite oxidation (in the case of Marcellus). The precipitations plugged some pores in these samples, but did not affect the recovery factors and average porosity due to the development of bedding cracks.

In the Eagle Ford, the majority of samples, regardless of acid strength, rarely show the development of visible cracks. In the Mancos samples, CT-scanning and 3D images show occasional crack development (Figures 2.16B and 2.20B). The cracks vary in length and are randomly oriented, although their abundance does increase towards the surface of the sample.

2.3.2 Quantitative Analysis

To identify the effect of HCl on the bulk density and porosity values of shales under study, a bulk density and CT number (CTN) correlation (Eq. 2.3 and Figure 2.21) was developed. It shows strong correlation between bulk density and calculated CT number (Figure 2.21).

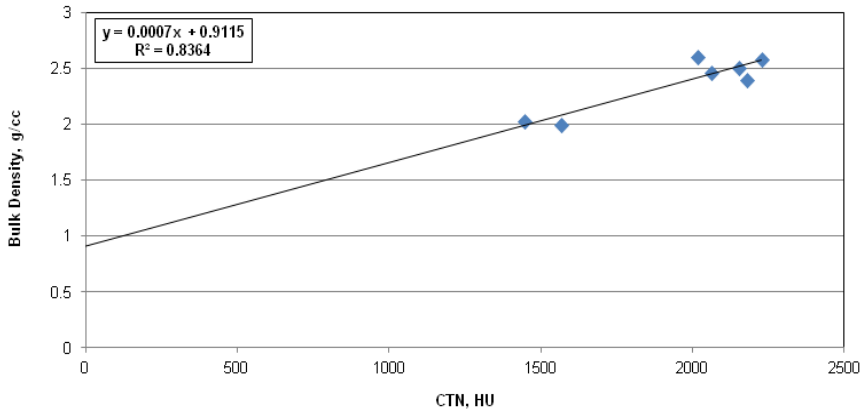

Figure 2.21 Bulk density-CTN correlation

Bulk Density =0.0007*CTN+0.9115……..……(Eq. 2.3)

CTN and bulk density histograms for Barnett, Eagle Ford, and Mancos samples show negative correlations with increasing acid molarity (Figures 2.22 through 2.33). In contrast, the measured CTN and calculated bulk density of Marcellus samples increased with the increase in HCl concentrations. This was attributed to the precipitation of higher density phases, including iron oxy-hydroxy phases during matrix acidizing treatment (Figure 2.25 Through 2.27). The range of bulk density before acidizing was 1.69-2.78 g/cc versus 1.00-2.34 g/cc after acidizing for Barnett, 2.31-2.54 g/cc versus 1.81-2.72 g/cc after acidizing for Marcellus, 2.55-

2.95 g/cc versus 2.53-2.77 g/cc after acidizing for Eagle Ford, 2.27-2.69 g/cc versus 1.8 -2.58 g/cc after acidizing for Mancos samples.

Two mechanisms enhanced shale porosity during HCl acid treatment. First, porosity was enhanced by crack development due to clay dissolution. Secondly, pre-existing natural fractures were opened further, enhancing the overall porosity by carbonate dissolution. On the other hand, porosity was reduced by pore plugging in some areas of samples due to precipitation of iron-bearing phases after chlorite and pyrite dissolution.

The CT scanning images for each sample were collected per slice, each slice is 1.25 mm in thickness. The average porosity for each CT scan slice of each sample from the pre and post acid treatment experiments was calculated using the measured CTN for samples saturated with air (dry) or Soltrol 130^{TM}. Average slice porosities for the pre-acid treated samples were 1.7-7.7% (Barnett), 0.33-5.3% (Marcellus), 0.23-6.74% (Eagle Ford), and 0.87-4.74% (Mancos) (Figures 2.22- 2.33). Post-acid treatment average slice porosities using 1-3 wt% HCl were 4.0-32.3% for (Barnett), 0.2-35.8% (Marcellus), 1.7-11% (Eagle Ford), and 1.1-35.78% (Mancos). Average porosities increased in all sample after acidizing, which is sometimes related to calcite dissolution (e.g. Eagle Ford) and in other rocks is related to cracks development after clay dissolution (e.g. Mancos, Barnett, and Marcellus).

Barnett samples showed an overall increase in the average sample post-porosity in all acidic solutions. However, at 1.0 wt% HCl the calculated average porosity per slice, for some slices, decreased. This has been attributed to iron precipitation (Figure 2.22C). In the 2.0 wt% and 3.0 wt% HCl acidic solutions, the calculated average post-porosity per slice of the Barnett samples increased significantly (Figures. 2.23C and 2.24C) due to excessive along bedding cracks development.

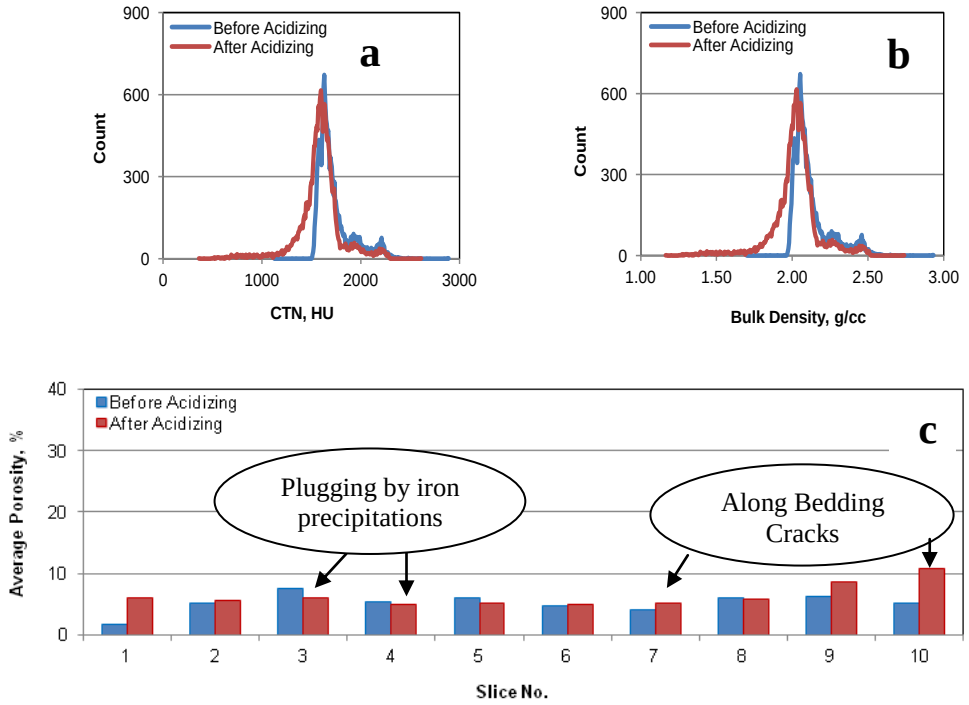

Figure 2.22 (a) Barnett sample's CTN histogram, (b) Bulk density histogram and (c) Average porosity per slice before and after 1 wt% HCl

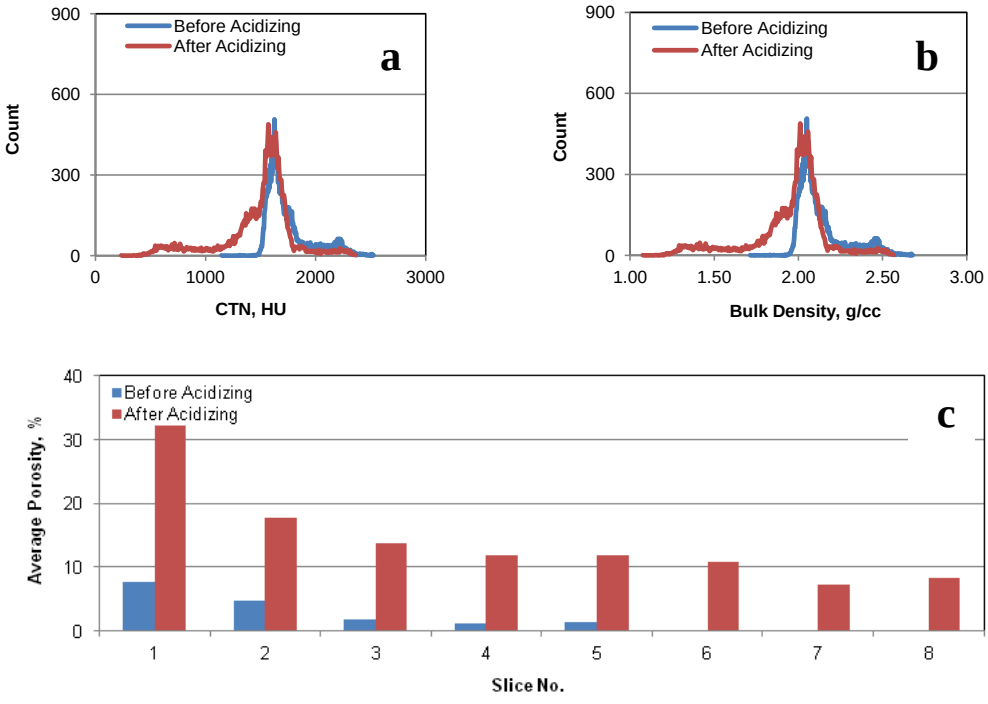

Figure 2.23 (a) Barnett sample's CTN histogram, (b) Bulk density histogram and (c) Average porosity per slice before and after 2 wt% HCl

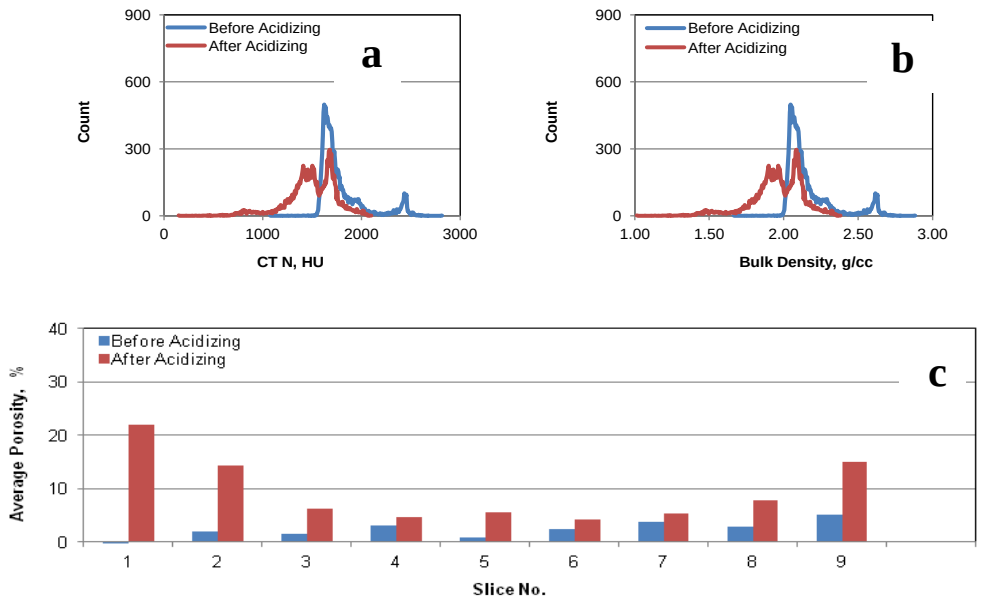

Figure 2.24 (a) Barnett sample's CTN histogram, (b) Bulk density histogram and (c) Average porosity per slice before and after 3 wt% HCl

In the Marcellus samples, the calculated average post-porosity per slice decreases in the 1.0 wt% and 2 wt% HCl experiments due to iron precipitations despite porosity enhancement at the sample surface due to along bedding cracks (Figures. 2.25C and 2.26C). In the higher acidity solution (3 wt% HCl) experiment the post-acid porosity significantly increases throughout the sample (Figure 2.27C) due to along bedding cracks that resulted from increased mineral dissolution. The increase in Marcellus porosity may correspond to the distribution of calcite rather than absolute abundance as Han, (2011) describes outcrop fractures as well as natural fractures filled with calcite and coring induced fractures of Marcellus Shale.

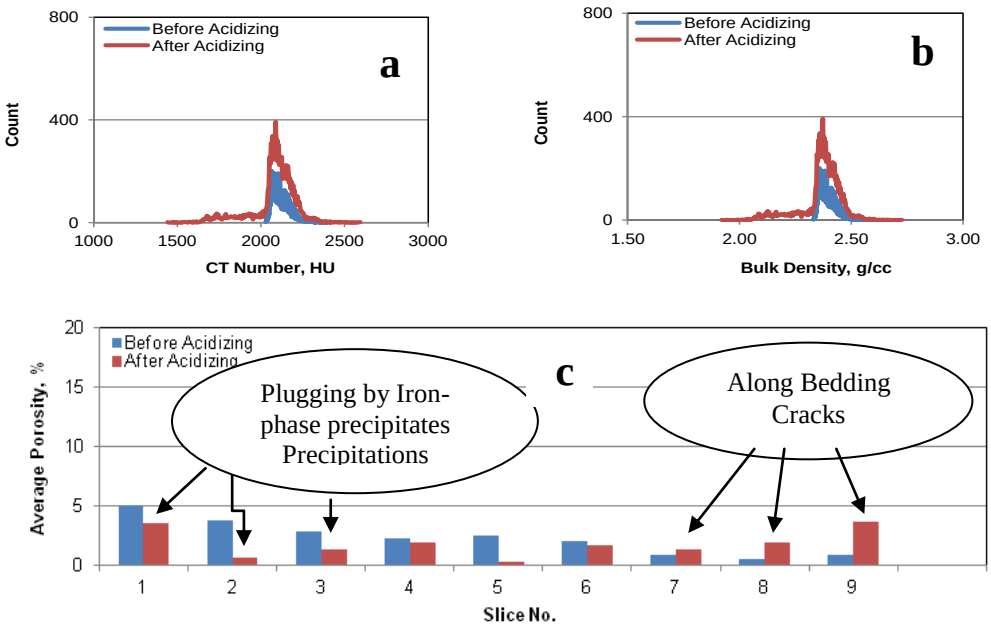

Figure 2.25 (a) Marcellus sample's CTN histogram, (b) Bulk density histogram and (c) Average porosity per slice before and after 1 wt% HCl

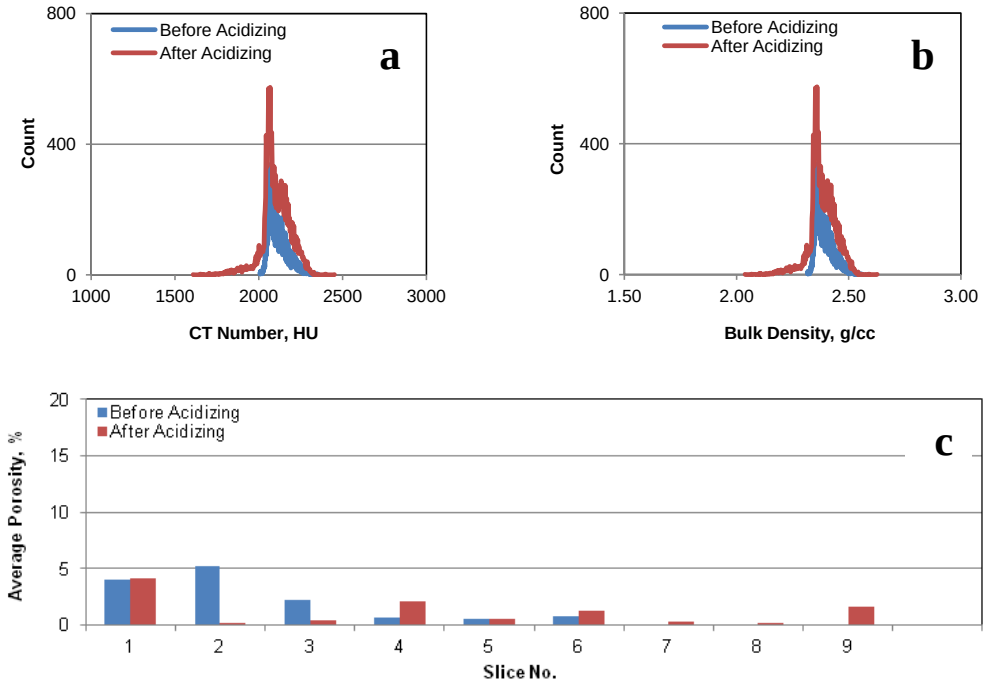

Figure 2.26 (a) Marcellus sample's CTN histogram, (b) Bulk density histogram and (c) Average porosity per slice before and after 2 wt% HCl

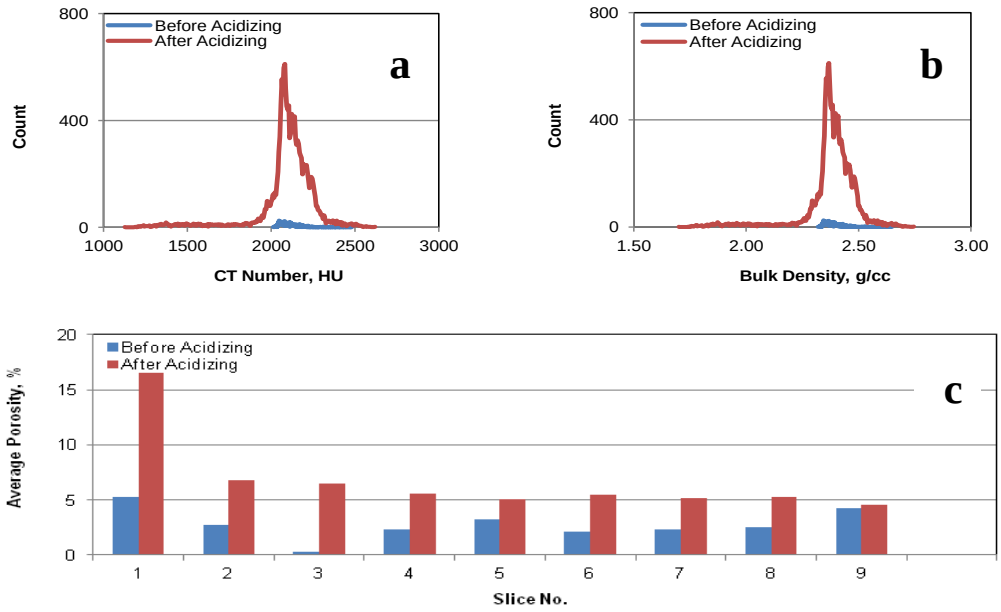

Figure 2.27 (a) Marcellus sample's CTN histogram, (b) Bulk density histogram and (c) Average porosity per slice before and after 3 wt% HCl

In the Eagle Ford samples (Figures 2.28 though 2.30), the main mechanism of porosity enhancement is secondary porosity development by calcite dissolution. No reduction in post-acid porosity was observed in the Eagle Ford Shale samples using HCl solutions up to 3 wt%.

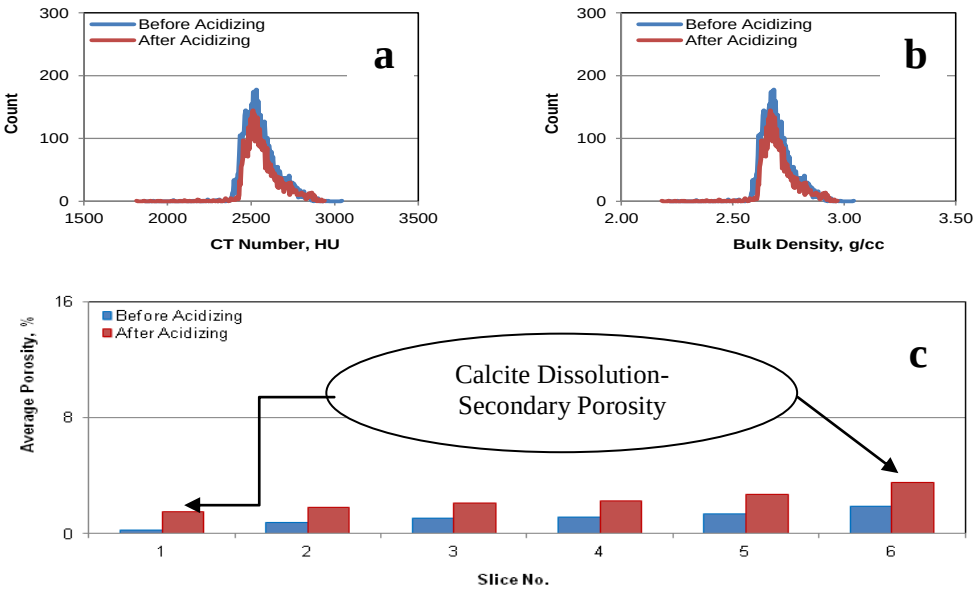

Figure 2.28 (a) Eagle Ford sample's CTN histogram, (b) Bulk density histogram and (c) Average porosity per slice before and after 1 wt% HCl

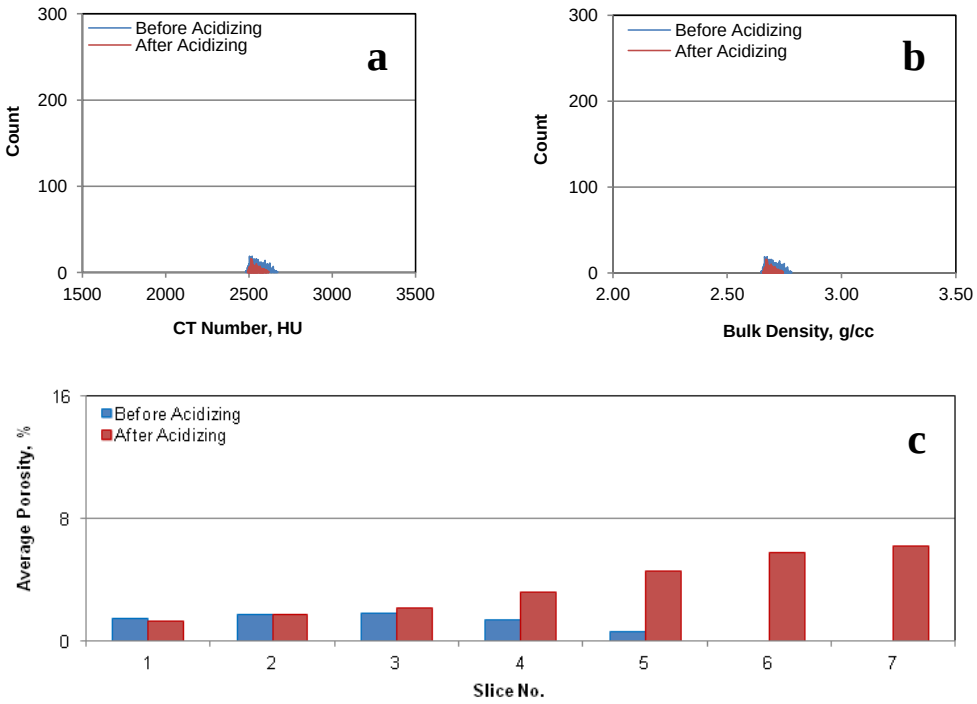

Figure 2.29 (a) Eagle Ford Ford sample's CTN histogram, (b) Bulk density histogram and (c) Average porosity per slice before and after 2 wt% HCl

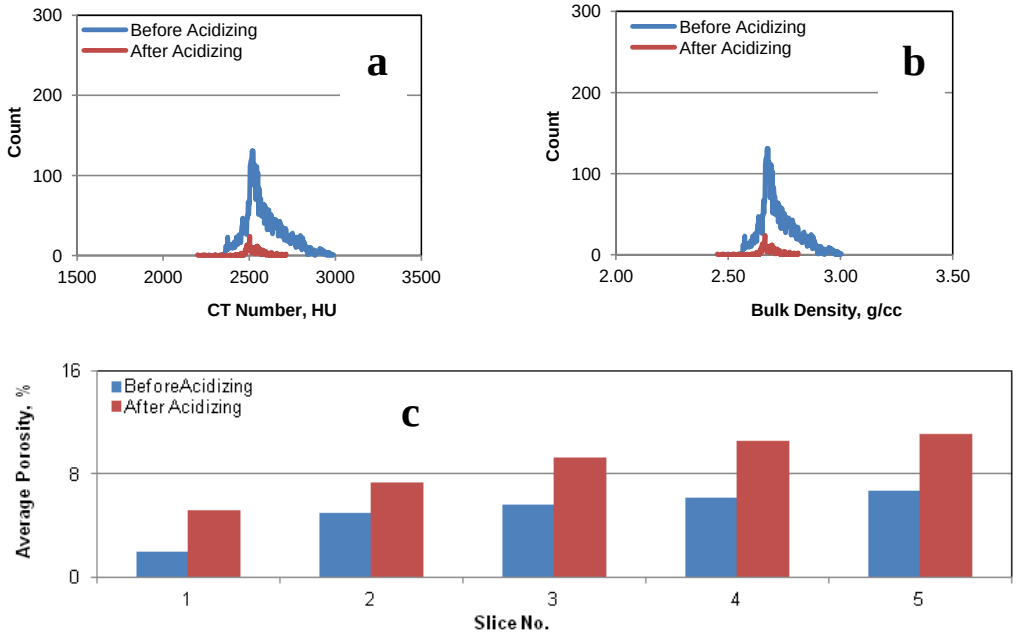

Figure 2.30 (a) Eagle Ford Ford sample's CTN histogram, (b) Bulk density histogram and (c) Average porosity per slice before and after 3 wt% HCl

Mancos samples showed post-acid treatment porosity increases (Figures 2.31 through 2.33) that correlate with the measured decrease in bulk density. Mancos post-

acid porosity improved by over 30% after treatment with 3 wt% HCl due to non-oriented crack development that formed after dissolution of clay dissolution (Figure 2.33C).

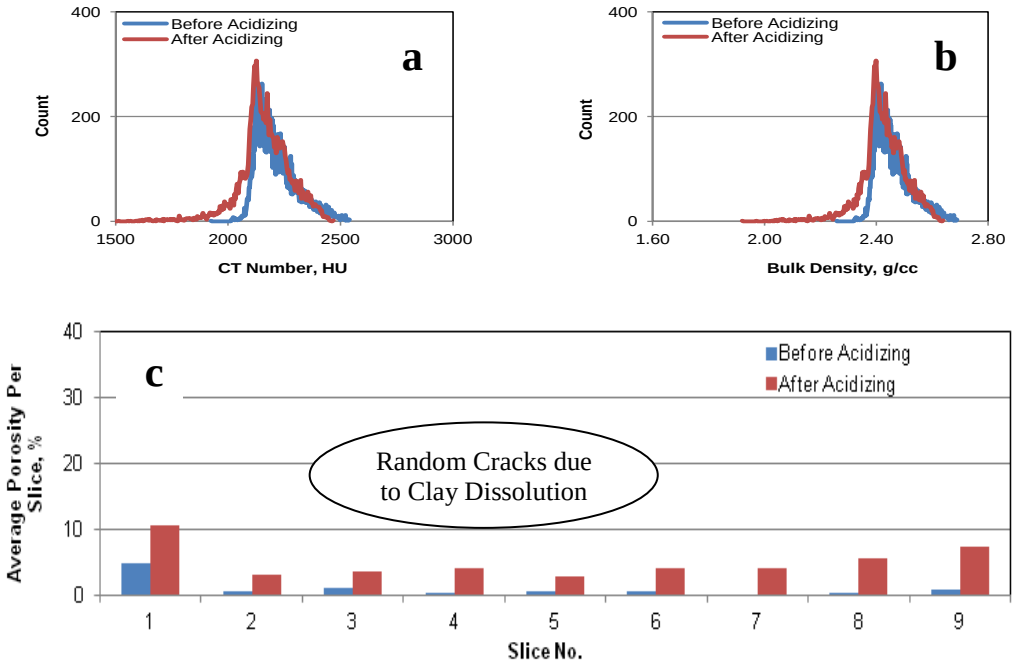

Figure 2.31 (a) Mancos Ford sample's CTN histogram, (b) Bulk density histogram and (c) Average porosity per slice before and after 1 wt% HCl

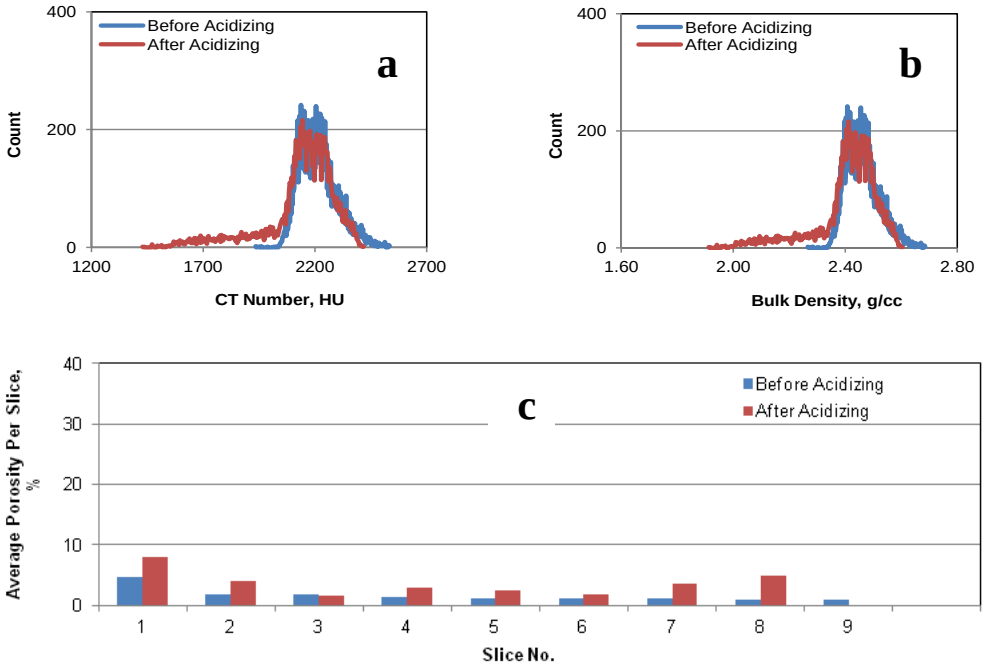

Figure 2.32 (a) Mancos Ford sample's CTN histogram, (b) Bulk density histogram and (c) Average porosity per slice before and after 2 wt% HCl

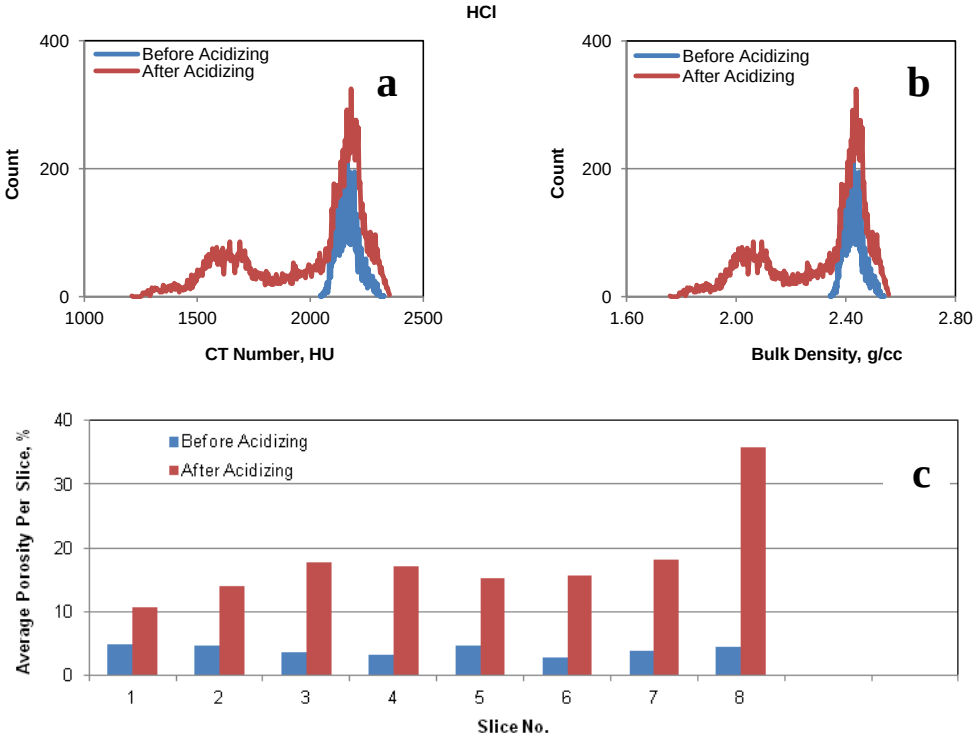

Figure 2.33 (a) Mancos Ford sample's CTN histogram, (b) Bulk density histogram and (c) Average porosity per slice before and after 3 wt% HCl

2.4 Effect of Matrix Acidizing on Shale Mineralogy

Shale mineralogy between samples varies (Chapter 1), so it is logical that the impact of different acid concentrations will be somewhat dependent on sample mineralogy. In an attempt to quantify the mineralogical impact of matrix acidizing X-ray diffraction, and Scanning Electron Microscopy (SEM) with Energy Dispersive Spectrometry (EDS) were applied to study bulk rock mineralogy and composition.

2.4.1 X-Ray Diffraction Experiments

Eagle Ford and Mancos samples exposed to 1 wt% HCl, and Barnett and Marcellus samples exposed to 3 wt% HCl were characterized using powder X-ray diffraction (XRD) methods. The analyzed samples were selected on the basis of preliminary experiments and measurements of porosity and mass loss under different HCl concentrations. Aliquots of each sample were crushed to a fine powder using a jaw crusher and tungsten carbide disc mill. Approximately 5g of sample was packed into a standard back-fill sample holder for powder X-ray diffraction. Samples were leveled by smearing the sample surface with a glass slide. A uniform sample preparation method was used for each sample to minimize differences in sample

preparation. Samples were placed in a Rigaku Miniflex II X-ray diffractometer and powder X-ray diffraction data was collected from 3° and 90° 2θ using Cu Kα radiation (λ = 1.54187 Å). Intensities were measured on a scintillation detector with graphite monochromator every 0.005° with counting times of 15 s per step. Phase identification and pattern matching of the XRD patterns was completed using PDXL proprietary software by Rigaku and the International Center for Diffraction Data PDF-2 database. Rietveld refinement was completed with the same software using structural parameters for identified phases from the PDF-2 database.

Phase identification and Rietveld refinement of X-ray diffraction patterns were used to identify the major rock-forming phases and provide semi-quantitative abundances for each sample (Table 2.1 and Figures 2.34 through 2.37).

Comparison of pre- and post-HCl treated patterns (Figures 2.34 through 2.37) shows that, in most cases, some calcite, (and occasionally dolomite) were dissolved in the samples. However, Rietveld refinement studies were unable to reconcile and quantify the changes in relative mineral proportions on the basis of the mass loss experiments.

Table 2.1 Mineralogy (Vol. %) of Untreated Samples from Rietveld Refinement of X-Ray Diffraction Patterns

	Eagle Ford	Mancos	Barnett	Marcellus
Calcite	48	4.68	-	15.7
Quartz	11.3	76	23	71
Kaolinite	13	12	-	-
Pyrite	13	-	15	3.4
Muscovite	14	6.9	38	9.6
Chlorite	-	-	24	-

For the Eagle Ford Samples, Rietveld refinement of the primary sample gives a close match to published mineralogy (Table 2.1; Borstmayer *et al.* 2011 and Fan *et al.* 2011), and a measureable decrease in the intensity of the 104 calcite peak (100% relative intensity) in the post-acid treated sample is observed (Figure 2.34). There was also a slight reduction in the relative size of peaks attributed to pyrite.

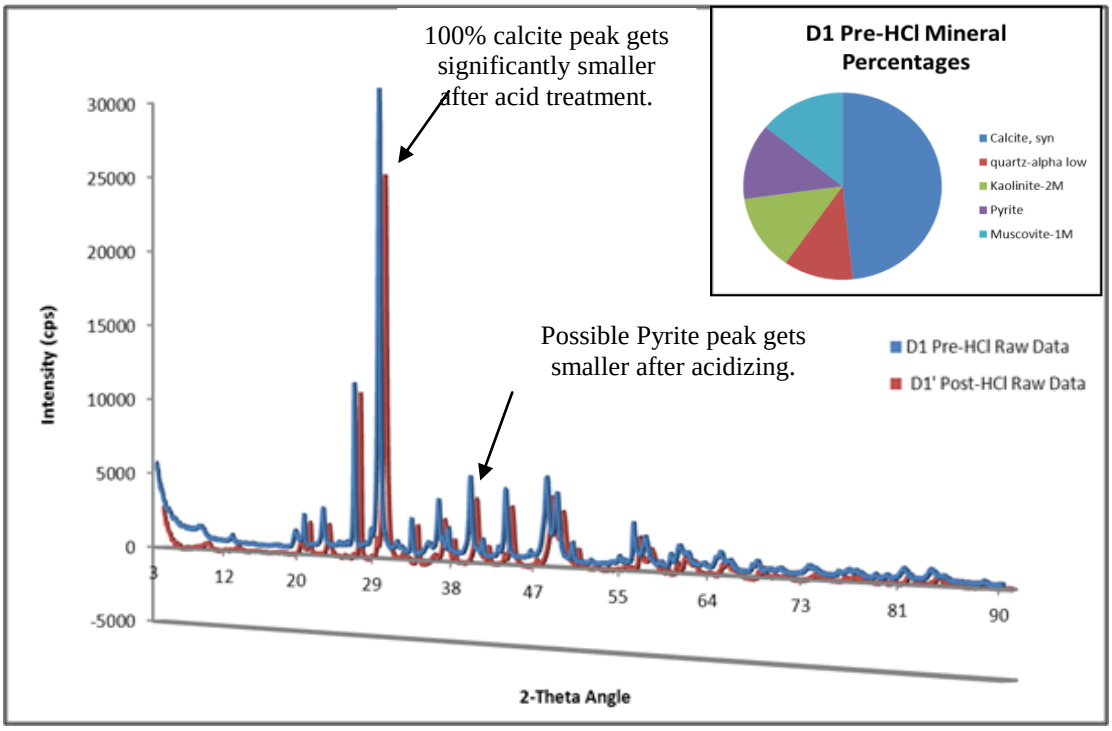

Figure 2.34 X-ray diffraction patterns for untreated and 1 wt% HCl treated Eagle Ford samples

The Mancos pre-HCl treated samples' mineralogy is also in good agreement with published values (Table 2.1; Torsæter *et al.* 2012). However, no reduction was observed in the intensity of the 104-calcite peak in the post-HCl treated sample (Figure 2.35). The results of Mancos samples match a study of Caney Shale (Grieser *et al.* 2007), which is similar to Mancos as it is rich in quartz. When treated with weak HCl solution (3%) the Mancos sample showed an increase in pore connectivity after 3 hours of acid immersion, but no detectable reduction in relative abundances of calcite or dolomite. The XRD pattern of Caney Shale demonstrated the presence of other soluble minerals in weak HCl, in addition to calcite and dolomite. The experimental observations and results of mass loss calculations on Mancos Shale suggest that there was a low dissolution rate during acidizing experiments; this differs from observations on the Eagle Ford samples. Kaolinite was recognized in the Mancos Shale X-Ray diffraction pattern (Table 2.1). Analysis of the the X-Ray diffraction pattern of the post-acid treated sample shows a slight decrease in intensity(Figure 2.35); based on expected reproducibility of the XRD experiments this is interpreted to reflect kaolinite dissolution.

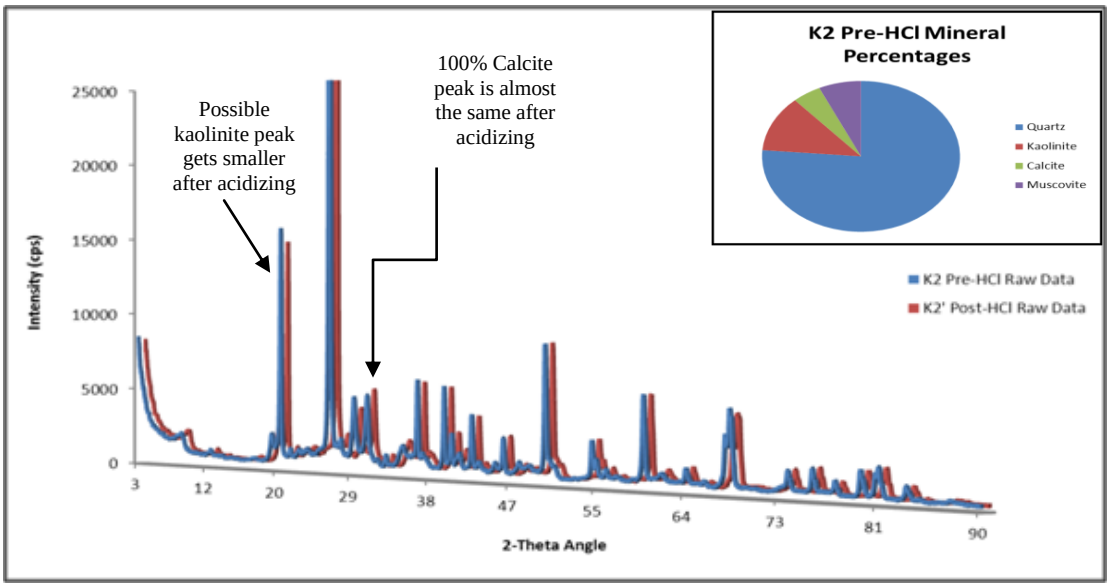

Figure 2.35 X-ray diffraction patterns for untreated and 1 wt% HCl treated Mancos samples

Calcite was not identified in Barnett samples (Figure 2.36); it is more probable that the carbonate phase present is dolomite. Effervescence was observed during the matrix acidizing experiment, which was interpreted to be the dissolution of a carbonate. Other phases identified include, chlorite, muscovite and and pyrite (Table 2.1).

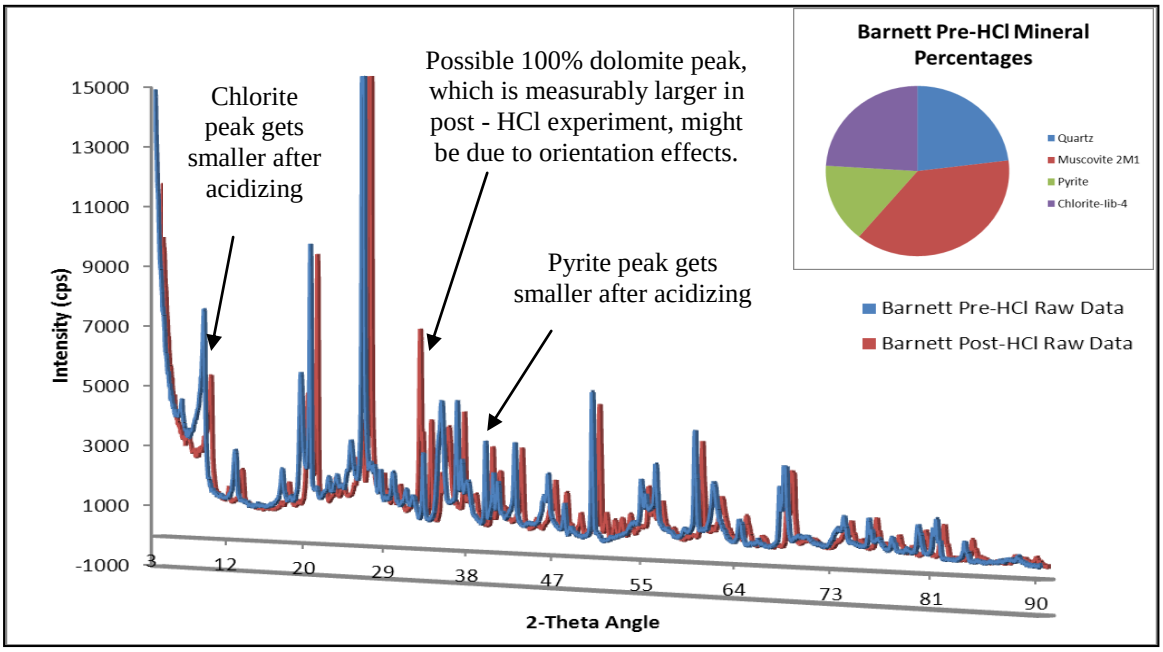

Figure 2.36 X-ray diffraction patterns for untreated and 3 wt% HCl treated Barnett samples

Rietveld refinement of XRD patterns from Marcellus samples prior to acidizing shows a good match to published mineral abundances (Table 2.1; Bruner and Smosna 2011). No measurable differences between pre and post-HCl treated samples could not be resolved (Figure 2.37), although the intensity of the 100% calcite and pyrite peaks was lower.

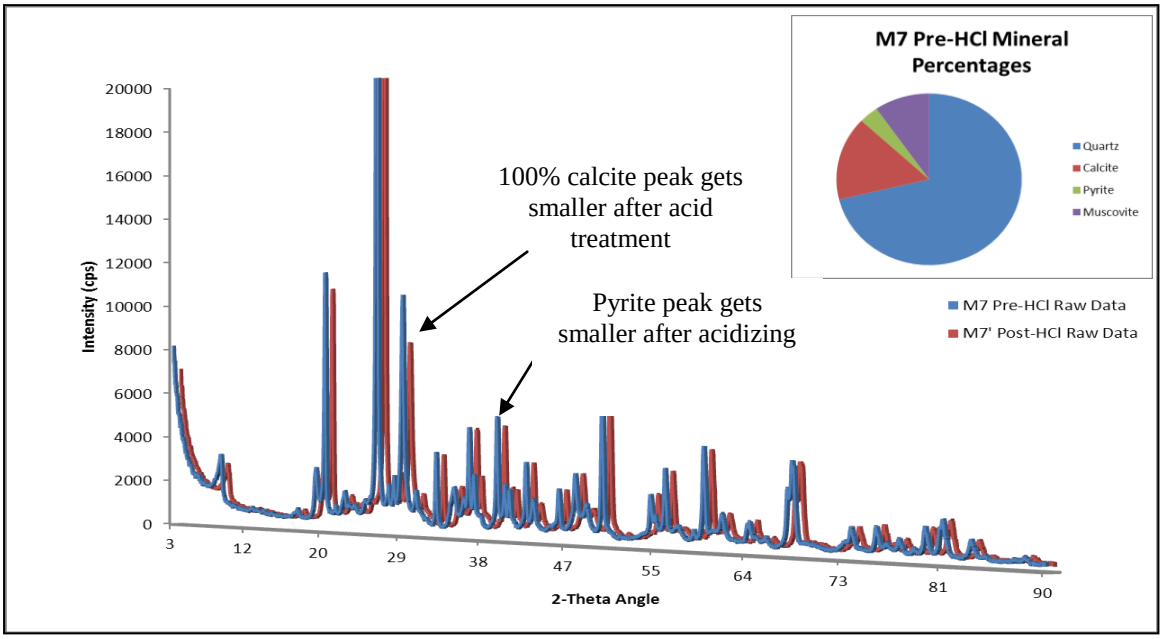

Figure 2.37 X-ray diffraction patterns for untreated and 3 wt% HCl treated Marcellus samples

2.4.2 Scanning Electron Microscopy (SEM), Energy Dispersive Spectrometry (EDS) and Bulk Rock Compositions Analysis

Bedding perpendicular thick sections of selected core plugs were prepared (primary and post-HCl treated samples) and polished using 1200 alumina grit. The thick sections were carbon coated and placed in a Hitachi S-4300SE/N field emission Scanning Electron Microscope with an EDAX Energy-Dispersive Spectrometer (SEM-EDS). Two-dimensional element distribution maps were collected for selected areas of each thick section using an electron-beam with an accelerating voltage of 15 kV and an emission current of ~56 μA. Element distribution maps were collected at a resolution of 1024 x 812 pixels over an area of ~10.5 mm^2 with a dwell time of 1200 or 1800 ms per pixel. From each area of interest a minimum of 16 frames were

collected, and the results automatically compiled to produce a single X-ray map that was corrected for beam-drift over the course of the acquisition time (approximately 8 hours).

Bulk rock compositional data for each mapped region of interest in the sample was extracted by interpreting the full spectral scan for the element distribution map. A manually fitted back-ground was constructed, and individual X-ray peaks were identified using a combination of automated peak-search and manual peak matching. A standard less quantification logarithm was applied to the total X-ray acquisition based on the peak identification and the results normalized to 100%.

The results of SEM-EDS assisted bulk rock compositional analyses show a degree of compositional heterogeneity at the sub-mm bedding scale. Eagle Ford pre-HCl sample was exceptionally rich in CaO in analyzed areas, with the low P2O5 contents. It is predicted that the Ca budget is held in carbonate, which is not quantified in this experiment after the deposition of a graphite-conducting layer (Table 2.2). However, in the post-HCl sample, the mapped area has a lower SiO2 content compared to pre-HCl treated areas mapped, demonstrating the tremendous complexity of these samples as HCl treatment should not have impacted the SiO2 abundance and distribution. The compositional analyzes and element distribution maps demonstrate that the majority of Ca is hosted by carbonate, probably calcite, with very little contribution from apatite or other calcic ferro-magnesium phases.

Table 2.2 Bulk rock compositional analyses of Eagle Ford Shale from SEM-EDS				
Eagle Ford Pre-Acid			Eagle Ford Post-Acid 1 wt.% HCl+5 wt.% NaCl	
Element	Wt %	Mol %	Wt %	Mol %
Na2O	00.33	00.33	00.46	00.46
MgO	00.82	01.26	00.92	01.40
Al2O3	09.50	05.77	09.23	05.59
SiO2	28.62	29.48	27.56	28.32
P2O5	00.90	00.39	01.01	00.44
SO3	05.43	04.20	04.95	03.82
K2O	01.54	01.01	01.59	01.04
CaO	50.02	55.20	51.25	56.43
TiO2	00.41	00.32	00.40	00.31
Cr2O3	00.10	00.04	00.16	00.06
FeO	02.34	02.01	02.35	02.02
CuO	-	-	00.14	00.11

For Mancos samples, studies of post-HCl sample show very comparable analysis, with differences between measured bulk-rock compositions within the analytical error of the instrument (Table 2.3).

Table 2.3 Bulk rock compositional analyses of Mancos Shale from SEM-EDS				
Mancos Pre-Acid			Mancos Post-Acid 1 wt.% HCl+5 wt.% NaCl	
Element	Wt %	Mol %	Wt %	Mol %
Na2O	00.78	00.80	00.82	00.85
MgO	02.93	04.61	02.85	04.52
Al2O3	13.13	08.18	13.79	08.65
SiO2	66.53	70.34	64.84	69.01
SO3	01.27	01.01	01.21	00.97
K2O	03.03	02.05	03.51	02.38
CaO	08.75	09.92	08.64	09.85
TiO2	00.55	00.44	00.65	00.52
Cr2O3	00.04	00.02	00.05	00.02
FeO	02.99	02.64	03.63	03.23

On the other hand, in the Barnett samples, there is a decrease in the Ca and P abundances that appear correlated with one another suggesting that dissolution of phosphate minerals, not carbonate (Table 2.4.)

Table 2.4 Bulk rock compositional analyses of Barnett Shale from SEM-EDS				
Barnett Pre-Acid			Barnett Post-Acid 3 wt.% HCl+5 wt.% NaCl	
Element	Wt %	Mol %	Wt %	Mol %
Na2O	00.35	00.38	00.46	00.51
MgO	02.51	04.30	02.48	04.22
Al2O3	21.46	14.50	21.60	14.55
SiO2	55.83	64.02	57.43	65.63
P2O5	01.11	00.54	00.57	00.28
SO3	06.68	05.75	06.58	05.65
K2O	05.25	03.84	05.18	03.78
CaO	01.18	01.45	00.46	00.56
TiO2	00.96	00.83	00.91	00.78
Cr2O3	00.17	00.08	00.15	00.07
FeO	04.50	04.32	04.13	03.94
NiO	-	-	00.04	00.04

Marcellus samples showed the same heterogeneity in the tested samples as the pre-HCl samples with higher CaO compared to the post-acid treated sample and less SiO2 (Table 2.5).

Table 2.5 Bulk rock compositional analyses of Marcellus Shale from SEM-EDS

Marcellus Pre-Acid			Marcellus Post-Acid 3 wt.% HCl+5 wt.% NaCl	
Element	Wt %	Mol %	Wt %	Mol %
Na2O	00.89	00.92	00.54	00.55
MgO	01.02	01.62	00.99	01.57
Al2O3	11.60	07.32	10.48	06.55
SiO2	65.47	70.06	63.30	67.11
SO3	05.88	04.73	04.93	03.93
K2O	02.28	01.55	02.19	01.48
CaO	09.25	10.61	13.40	15.22
TiO2	00.49	00.39	00.52	00.42
Cr2O3	-	-	00.07	00.03
FeO	03.12	02.79	03.28	02.91
ZnO	-	-	00.30	00.24

2.5 Effect of Matrix Acidizing on Shale Oil Recovery

Because water imbibition occur both parallel and perpendicular to bedding, samples were cut in both directions to study the effectiveness of water imbibition in both directions. The samples were 2.54-3.81 cm in diameter and 0.76-5.08 cm in length. All samples were treated with different HCl solutions (1-3 wt%) until visible evidence of reactivity (effervescence) ceased. The samples were then saturated with Soltrol 130^{TM} mineral oil, and placed in Amott cells for imbibition.

2.5.1 Effect of Matrix Acidizing on Shale Water Imbibition Across Bedding

The CT images for the samples before and after oil saturation were used to calculate average porosities. The studied samples have a range of average porosity

values: 5% for Barnett, 1.5 for Eagle Ford, 2% for Mancos, and 1.7% for Marcellus Shale samples (Figures 2.38 through 2.41).

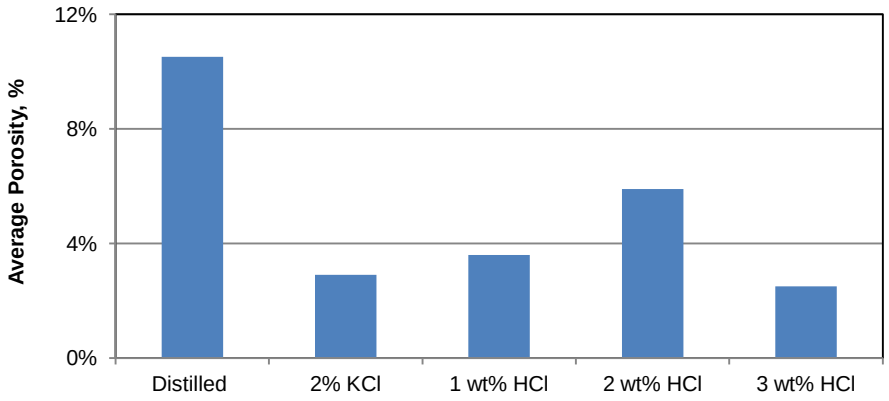

Figure 2.38 CT-scanning porosity values for the studied Barnett Shale samples before imbibition in distilled water, 2% KCl, and different HCl solutions

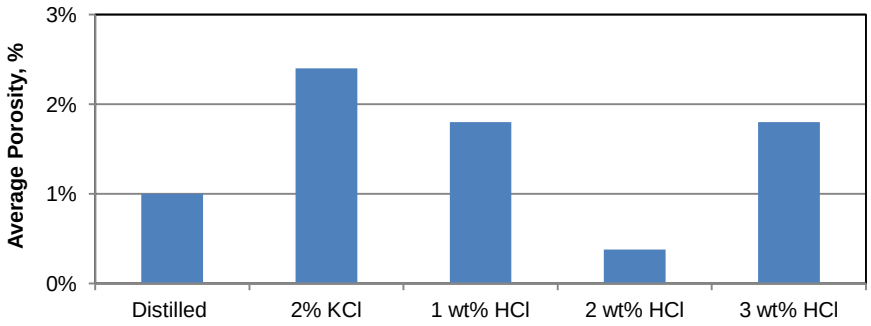

Figure 2.39 CT-scanning porosity values for the studied Eagle Ford Shale samples before imbibition in distilled water, 2% KCl, and different HCl solutions

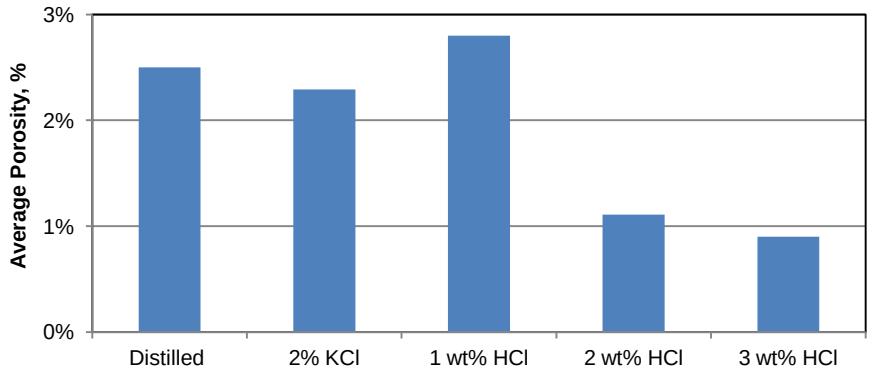

Figure 2.40 CT-scanning porosity values for the studied Mancos Shale samples before imbibition in distilled water, 2% KCl, and different HCl solutions

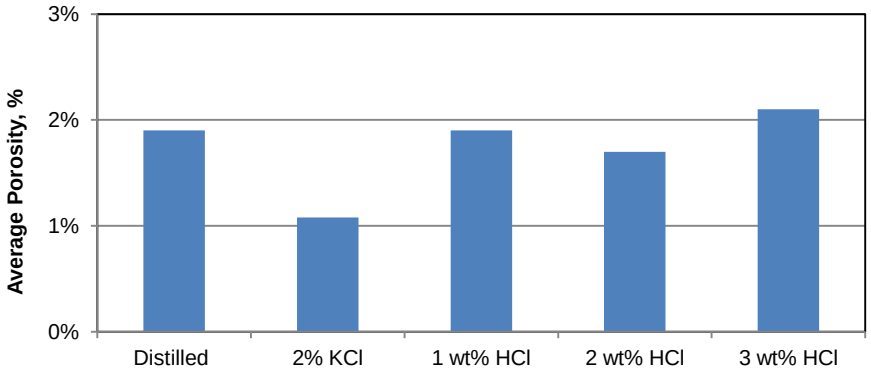

Figure 2.41 CT-scanning porosity values for the studied Marcellus Shale samples before imbibition in distilled water, 2% KCl, and different HCl solutions

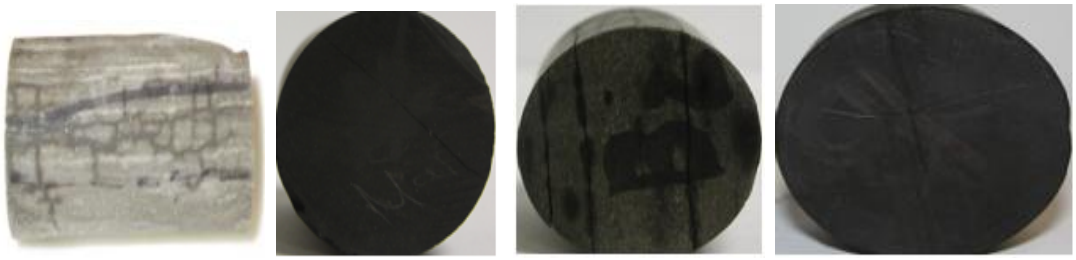

Figure 2.42 Mancos, Marcellus, Barnett, and Eagle Ford (from left to right side) Shale samples after one week in 3 wt% HCl solution

Shale samples behave differently in HCl solutions; Barnett and Marcellus developed along bedding cracks, Mancos showed non-oriented cracks throughout the sample, and Eagle Ford did not display visible cracks (Figure 2.42). Recovery factors show a systematic correlation with the strength of the acid used in the experiment (Figures 2.43 through 2.46). 3 wt% HCl solution resulted in a 53% oil recovery factor from Mancos, a 37% factor from Eagle Ford, a 24% factor from Barnett, and 4% recovery factor from Marcellus samples. Mancos, Marcellus, and Barnett Shale samples displayed less dissolution in the HCl solutions, which correlates with the lower calcite abundances (Section 2.5). Meanwhile, the Eagle Ford Shale showed significant dissolution in the HCl solutions, which correlates with the higher abundance of calcite. The calculated recovery factors for the three low pH solutions in 2 wt% or 30 wt% KCl brines increased compared with neutral brine solutions.

There was no significant difference between 1 wt% HCl and 2 wt% HCl for Barnett samples as both samples achieved almost 17% oil recovery factor with a slight acceleration in oil production from day two in 2 wt% HCl solution. It was also interesting to observe that the oil recovery factor achieved by distilled water (24%)

from Barnett sample was the same as the oil recovery from Barnett sample exposed to 3 wt% HCl in 2 wt% KCl solution. The improvement in oil recovery for Eagle Ford was mainly due to calcite dissolution, but for the other rocks since there was little observed dissolution, the main mechanism is proposed to be due to cracks development resulted from clay dissolution.

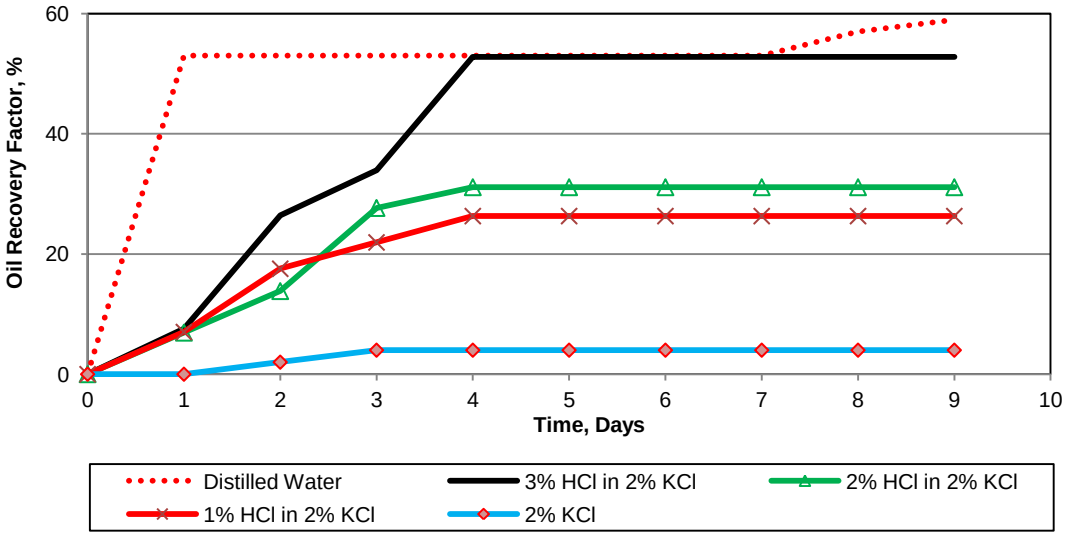

Figure 2.43 Spontaneous imbibition recovery factors of Mancos Shale (cut across bedding)

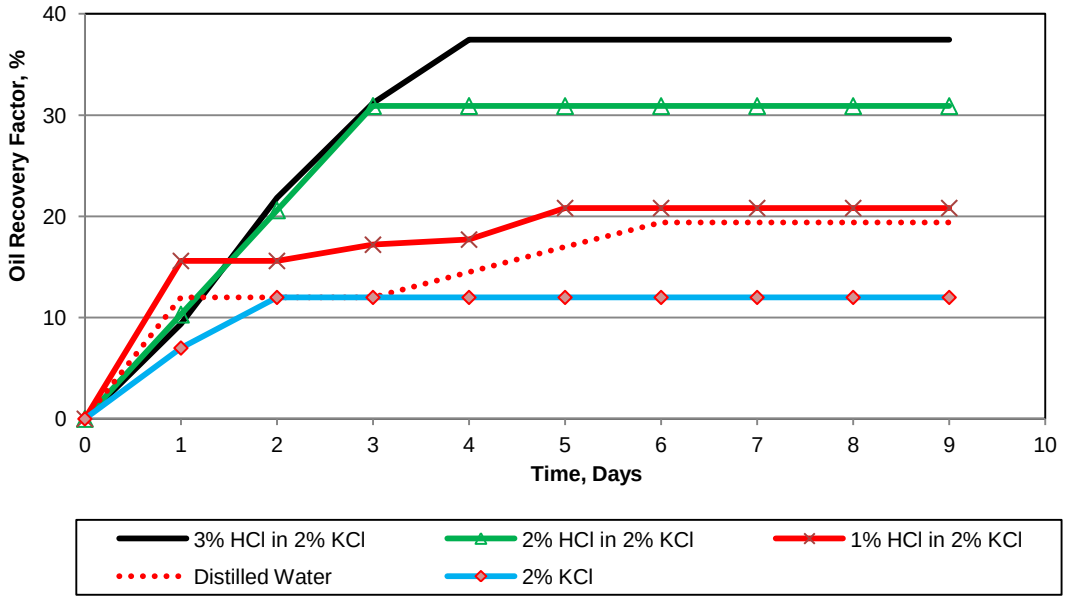

Figure 2.44 Spontaneous imbibition recovery factors of Eagle Ford Shale (cut across bedding).

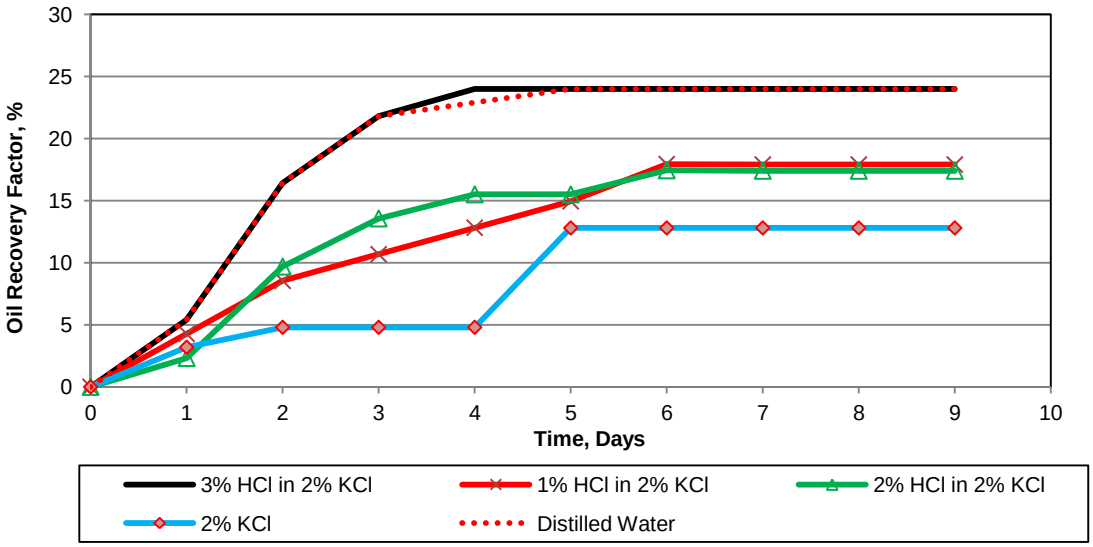

Figure 2.45 Spontaneous imbibition recovery factors of Barnett Shale (cut across bedding)

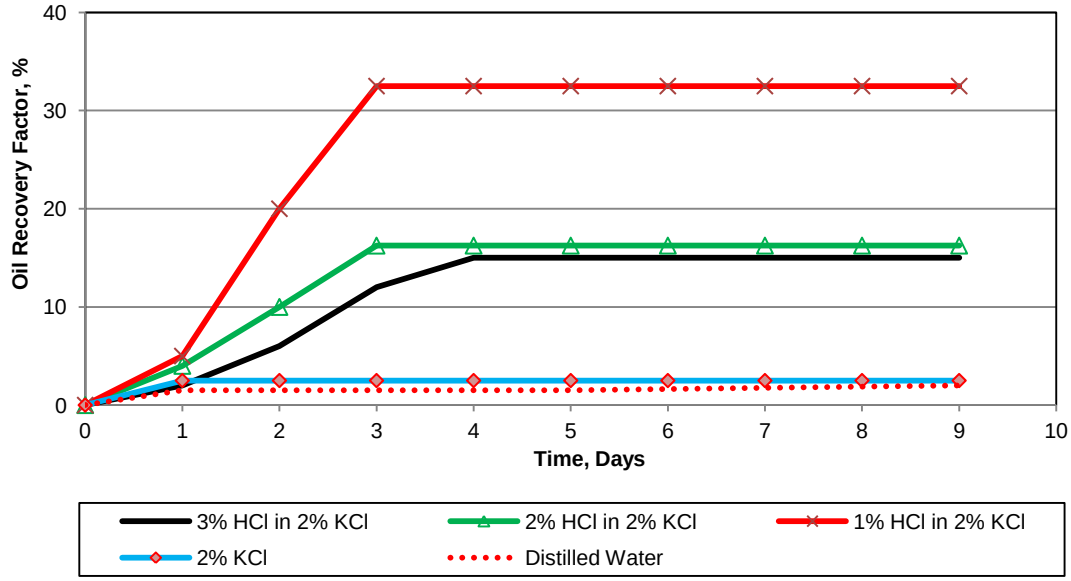

Figure 2.46 Spontaneous imbibition recovery factors of Marcellus Shale (cut across bedding)

2.5.2 Effect of Matrix Acidizing on Shale Water Imbibition along Bedding

In the previous experiments, the samples were prepared across bedding; in these experiments, the samples were prepared along bedding (Figure 2.47).

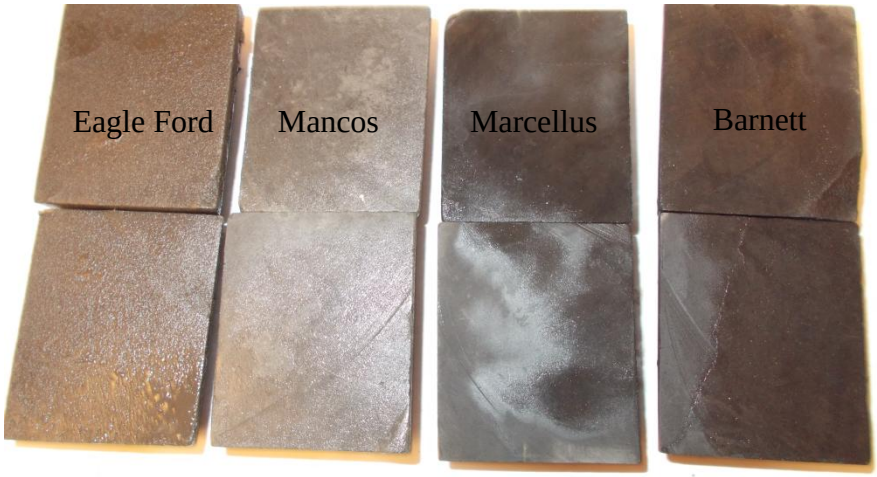

Figure 2.47 Shale samples cut along bedding before matrix acidizing

Recovery factors for samples cut across bedding are presented in Figs 2.43 through 2.46. The samples cut along bedding showed a significant improvement in spontaneous imbibition performance for all of the studied shale rocks compared to those that cut across bedding.

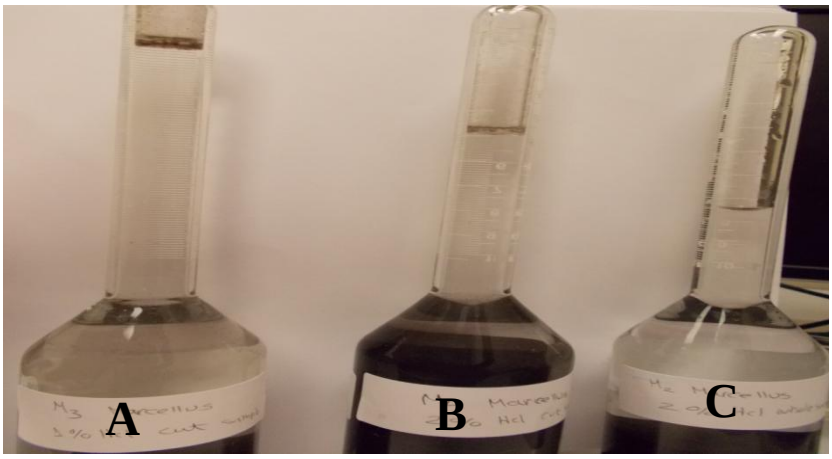

Figure 2.48 Marcellus Shale samples in spontaneous imbibition cells after treated in different HCl solutions: A) Marcellus sample cut along bedding after 1 wt% HCl treatment B) Marcellus sample cut along bedding after 2 wt% HCl treatment, and C) Marcellus sample cut across bedding after 2 wt% HCl treatment

Oil recovery factors for Eagle Ford samples were 37% when cut across bedding compared with 47% from those cut along bedding. In the Mancos, recovery factors were 36% cut across bedding compared with 53% from those cut along bedding. In Barnett samples cut across bedding recovery factors were 24% compared to 28% from samples cut along bedding cut samples. In the Marcellus samples, the

difference in preparation was most marked, with 4% recovery factors in samples cut across bedding versus 38% from along bedding cut samples (Figures 2.49 Though 2.52). The results are consistent with literature findings (Mokhtari *et al.* 2013) and CT-Scan analysis, which in the Eagle Ford Shale samples in particular showed high probability of fracture development parallel to bedding.

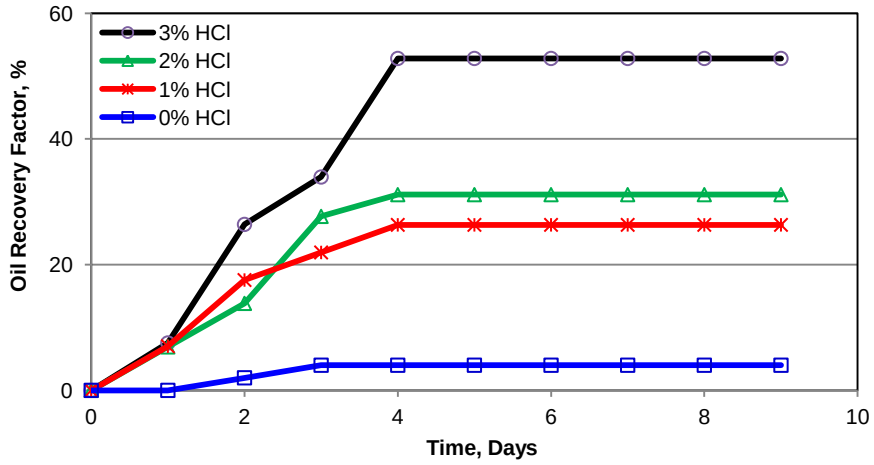

Figure 2.49 Spontaneous imbibition recovery factors (R.F) of Mancos Shale (cut along bedding)

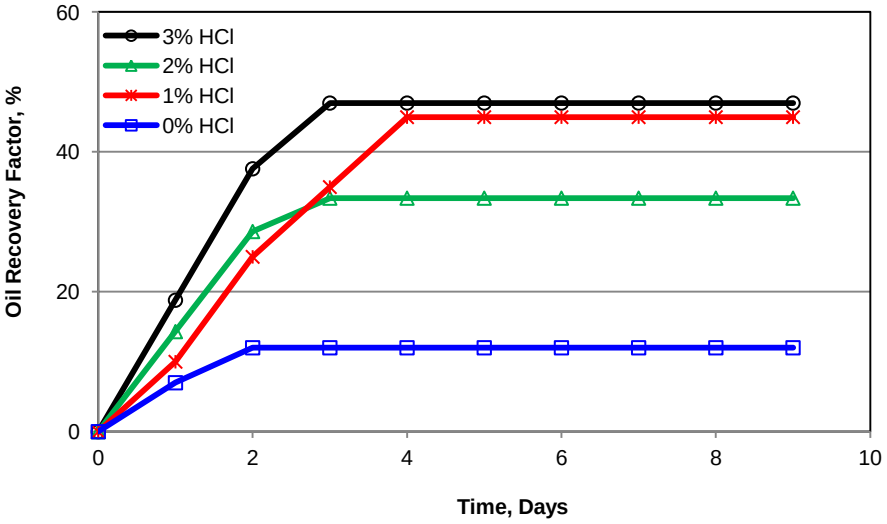

Figure 2.50 Spontaneous imbibition recovery factors (R.F) of Eagle Ford Shale (cut along bedding)

Recovery factors for the Barnett and Marcellus Shale samples that cut across bedding planes increased with increasing acid concentration (Figures 2.51& 2.52).

However, the recovery factors from the samples cut along bedding planes show an inverse trend as recovery factors decreased as acid strength increases.

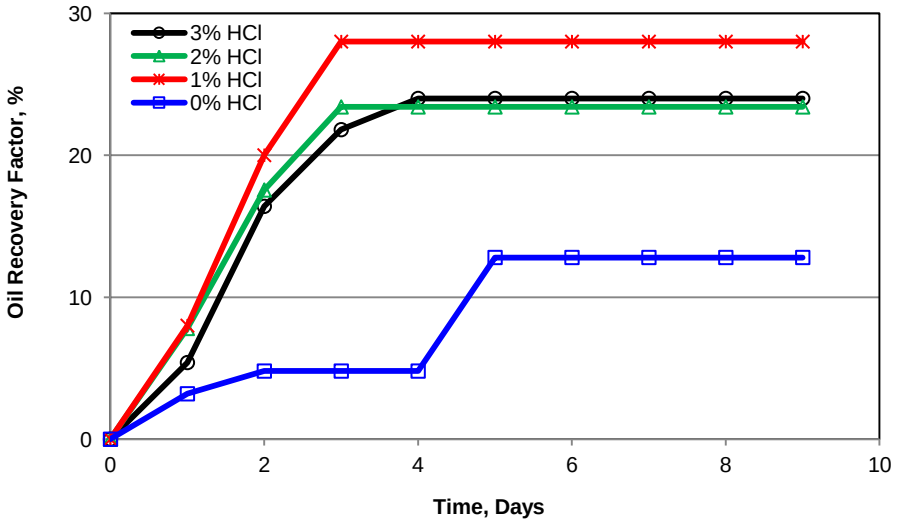

Figure 2.51 Spontaneous imbibition recovery factors (R.F) of Barnett Shale (cut along bedding)

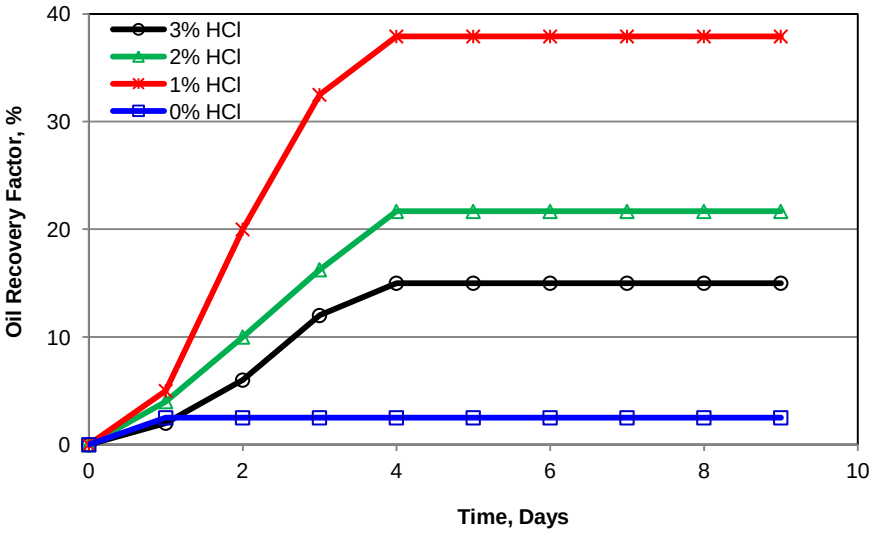

Figure 2.52 Spontaneous imbibition recovery factors (R.F) of Marcellus Shale (cut along bedding)

2.6 Effect of Matrix Acidizing on Shale Rock Wettability

There was an improvement in spontaneous imbibition oil recovery from the tested shale rocks in different HCl acidic solutions. To test the contribution from wettability alteration versus mineral dissolution an experiment to measure the contact angles of the samples was designed.

Contact angles were measured using drop shape analysis with a drop size of 8 ml. The method is to measure the angle of a sessile drop resting on a flat solid surface using a goniometer–microscope (Figure 2.53) equipped with a video camera and a suitable magnifying lens, interfaced to a computer with image-analysis software to measure the tangent value on the captured image. A suitable cold light source and a sample stage whose elevation can be controlled are also required.

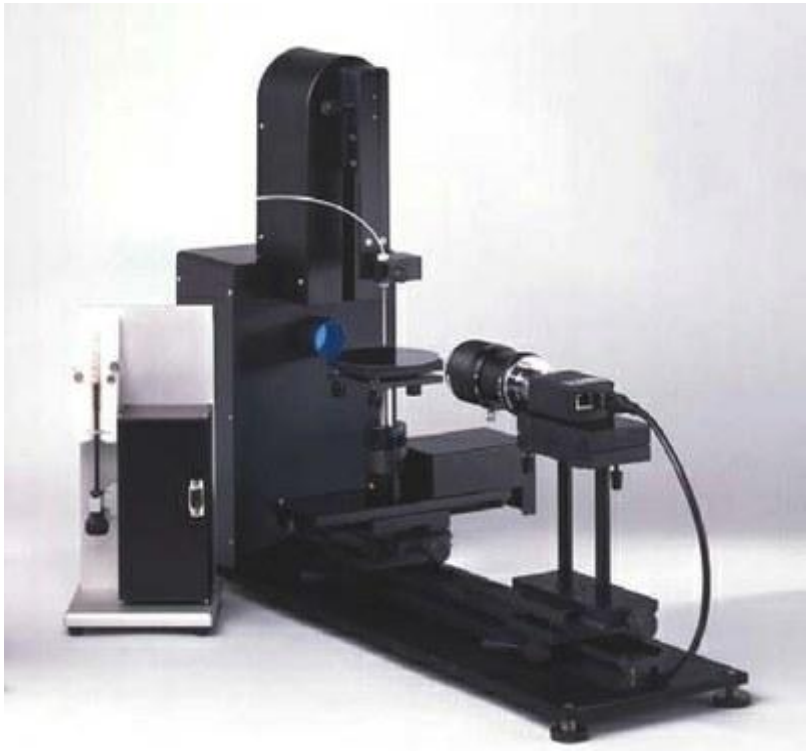

Figure 2.53 Contact angle measurement equipment

The values of the measured contact angles correlate with the oil recovery factors. Shale wettability was altered by using low pH solutions (Table 2.6). The initial contact angles of the tested shales were 12º from Mancos, 17º from Eagle Ford, and 27º from Marcellus shale samples, which is considered a water-wet rock. The final measured values for all experiments were less (0-9) compared with the initial values. This may be interpreted as reflecting the shale became strongly water-wet. In addition, the pH of the solutions increased after seven days of soaking which might be correlated with the mineral dissolution.

Table 2.6 Measured contact angles for the used shale samples soaked in different Acid solutions

Shale	Brine	Initial Contact Angle	Soaking Fluid	Initial pH at day 0	Temperature, ºF	Aging time, day	Final pH at day 7	Final Contact Angle
Mancos Shale	30 wt% KCl	12	1wt% HCl in 30wt% KCl	0.57	150ºF	7	0.85	9
	30 wt% KCl	12	2wt% HCl in 30wt% KCl	0.4	150ºF	7	0.43	7
	30 wt% KCl	12	3wt% HCL in 30wt% KCl	0.39	150ºF	7	0.1	3
Eagle Ford Shale	2wt% KCl	17	1wt% HCl in 2 wt% KCl	1.21	150F	7	5.6	2
	2wt% KCl	17	2wt% HCl in 2 wt% KCl	1.02	150F	7	5.5	0
	2wt% KCl	17	3wt% HCL in 2 wt% KCl	0.74	150F	7	5.4	0
Marcellus Shale	2wt% KCl	27	1wt% HCl in 2 wt% KCl	1.21	150ºF	7	5.6	2
	2wt% KCl	27	2wt% HCl in 2 wt% KCl	1.02	150ºF	7	5.5	0
	2wt% KCl	27	3wt% HCL in 2 wt% KCl	0.74	150ºF	7	5.4	0

2.7 Effect of Matrix Acidizing on Shale's Mechanical Properties

To test the effect of low pH solutions on shale's mechanical properties, experiments to measure the unaxial compressive strength (UCS) and rock hardness of the samples before and after matrix acidizing was designed.

2.7.1 Effect of HCl on Eagle Ford Reservoir Rock Samples Mechanical Properties

Samples for the Eagle Ford Shale reservoir measuring 1.905 cm in diameter and 3.81- 4.76 cm in length were cut across bedding. The first sample was tested

intact and the others were tested after matrix acidizing with different acid concentrations (1-3 wt) prepared with 5 wt% NaCl neutral fluid. All samples were prepared according to specifications of American Society for Testing and Materials ASTM D-2938 (Figure 2.54).

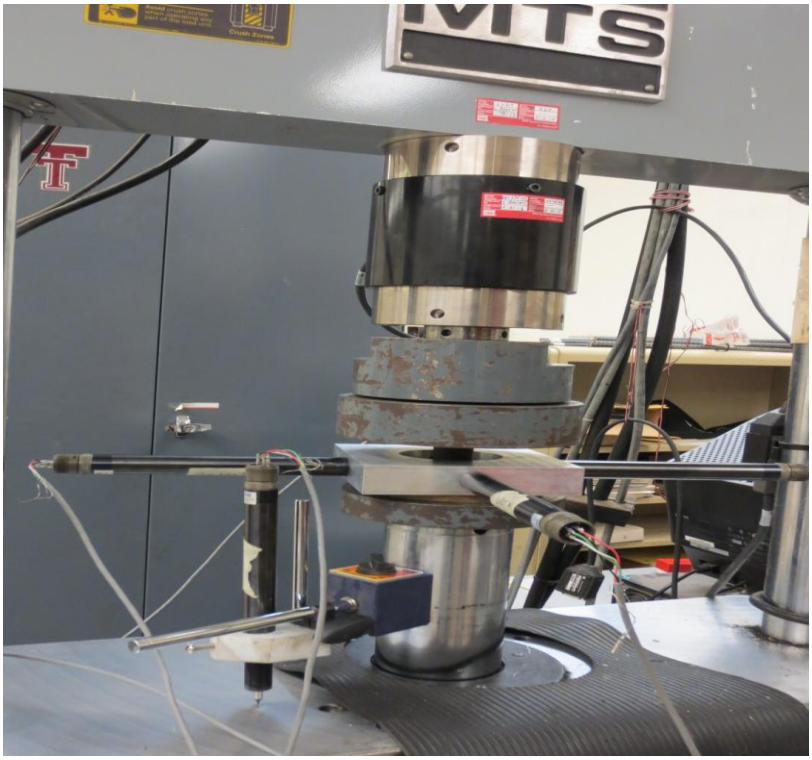

Figure 2.54 Experimental apparatus for measuring unconfined compressive strength (UCS)

A sample of Eagle Ford treated with a 5 wt% NaCl was also tested to measure hydraulic fracturing effect on Eagle Ford shale rock's strength without acid treatment. The matrix acidizing experiments were done at 200°F and ambient pressures until the effervescence of the sample ceased. The 5 wt% NaCl solution sample was also treated at 200°F for the same time duration as the matrix acidizing experiments.

For the untreated Eagle Ford reservoir sample, a single crack propagated in a diagonal manner, neither parallel nor perpendicular to bedding planes. In the 5 wt% NaCl treated sample, cracking and fracture development was a multi-stage process. Each stage of cracking for 5 wt% NaCl represented a new layer crack which may imply that NaCl affects each layer of the sample differently (Figures 2.55 and 2.56).

Jianguo *et al.*, 2006 showed that compressive strength for Arco Shale decreased after exposure to both sodium and calcium chloride solutions. The higher the water activity, the larger the reduction in shale strength. Arco Shale is dominated by clay minerals (chlorite, illite, kaolinite, smectite, and mixed layer phases) making up to 64.7% of the sample, with about 23.6% quartz, 4% feldspar, 1.2% dolomite, 2.4% pyrite and 4.1% siderite. The mineral composition of Arco

Shale differs from the Eagle Ford Shale (Table 1.3), but it is known that the identity of the clay minerals is important because that controls the ion exchange reactions that may strengthen or weaken the mechanical properties of shales.

The sample of Eagle Ford treated with 1 wt% HCl in 5 wt% NaCl neutral fluid cracked and fractured via an intermediate mechanism. Two cracks were developed that may represent two layers breaking at different stresses depending on how HCl solutions affected each layer. The sample treated with 2 wt% HCl in 5 wt% NaCl neutral fluid behaved similarly to the untreated sample with only one crack developing, whereas the sample treated with 3 wt% HCl in 5 wt% NaCl neutral fluid behaved similarly to the 5 wt% NaCl treated sample, where different cracks represent different layers breaking at different stresses (Figures 2.55 and 2.56).

In the case of the 2 wt% HCl in 5 wt% NaCl neutral fluid treated sample, it is proposed that its behavior may be the result of contrasting modal mineral abundances between the studied samples. Meanwhile, the more complex distribution and development of cracks in the 3 wt% HCl in 5 wt% NaCl neutral fluid experiment may be a consequence of heterogeneous crack and fracture distribution attributed to highly variable calcite distribution between bedding lamina. This led to localized porosity development and loss of mechanical strength as a function of differential carbonate dissolution in carbonate-richer lamina (Figures 2.55 and 2.56).

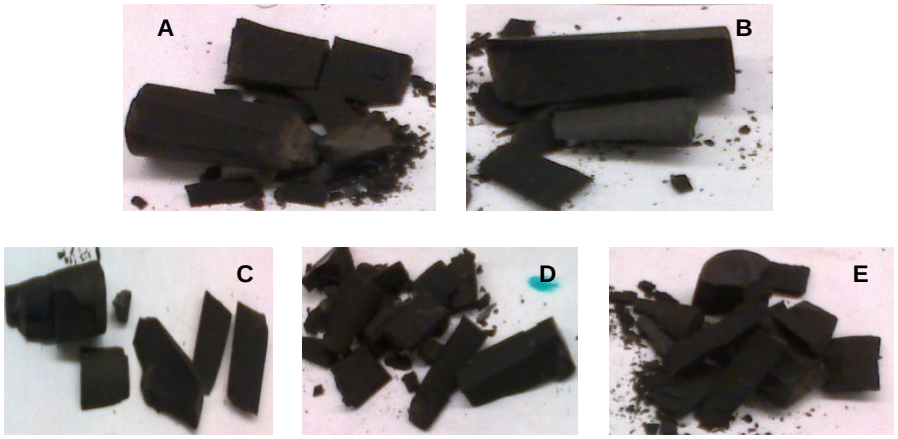

Figure 2.55 Eagle Ford samples after compressive test (A) Intact sample (B) After 5 wt.% NaCl sample (C) After 1 wt.% HCl+5 wt.% NaCl sample (D) After 2 wt.% HCl+5 wt.% NaCl sample and (E) After 3 wt.% HCl+5 wt.% NaCl sample

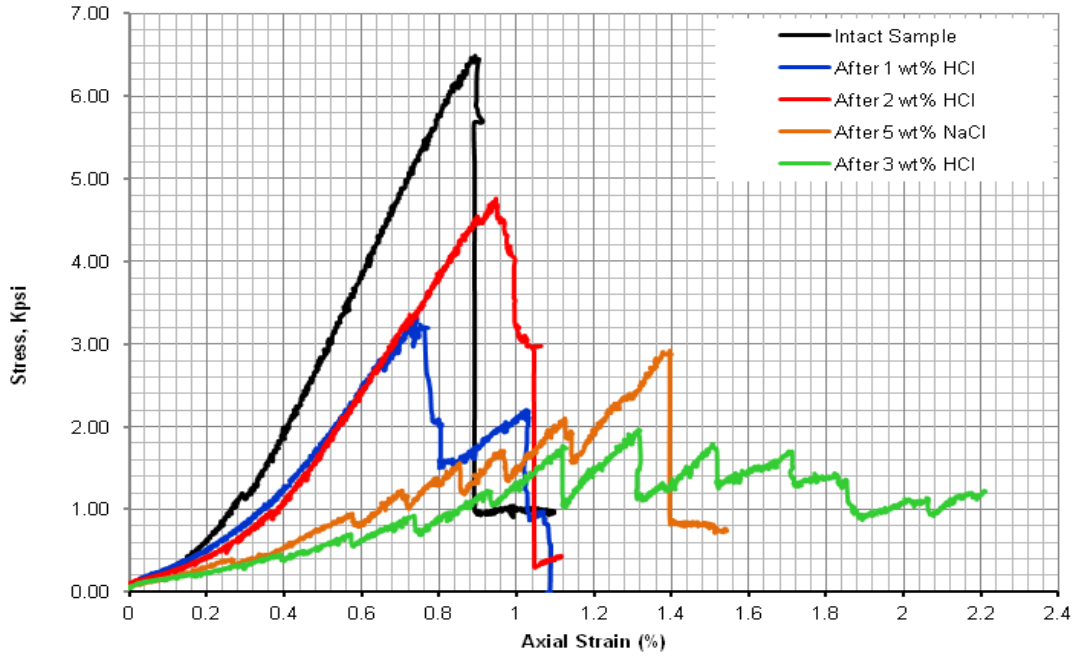

Figure 2.56 Stress-Strain Data for Reservoir Eagle Ford Rock Samples

The measured Young's Modulus and unaxial compressive strength of the intact Eagle Ford sample (0.9 E06 Psi) was in a good agreement with published data (Borstmayer *et al.* 2011 and Fan *et al.* 2011). The sample treated with only 5 wt% NaCl lost about 75% of its Young's Modulus and 55% of the unaxial compressive strength compared with the intact sample. The decrease in Young's Modulus (YM) and unaxial compressive strength (UCS) increased with increasing HCl concentrations except for the sample with 2 wt% HCl in 5 wt% NaCl neutral fluid due

to heterogeneity between the tested samples. The sample treated with 3 wt% HCl in 5 wt% NaCl neutral fluid lost about 82% of Young's Modulus and 70% of USC compared with the intact sample (Table 2.7).

Table 2.7 Mechanical data for Eagle Ford reservoir rock

	Orientation	YM (10^6 Psi)	UCS (10^3 Psi)	Confining Pressure (Psi)
Intact Sample	Perpendicular to Bedding	0.9	6.49	0
5 wt% NaCl	Perpendicular to Bedding	0.23	2.92	0
1 wt% HCl+5 wt% NaCl	Perpendicular to Bedding	0.63	3.32	0
2 wt% HCl +5 wt% NaCl	Perpendicular to Bedding	0.68	4.77	0
3 wt% HCl +5 wt% NaCl	Perpendicular to Bedding	0.16	1.96	0

2.7.2 Effect of HCl on the Mechanical Properties Eagle Ford and Mancos Outcrop Samples

The experiments in this section are made on outcrop samples from Eagle Ford and Mancos Shale formations measuring in 2.54 cm diameter and 5.5-5.7 cm in length. The Eagle Ford samples were prepared with 1-3 wt% HCl in 5% NaCl neutral fluid, and 30 wt% NaCl neutral fluid in the case of Mancos samples. A similar experimental procedure was followed as for the Eagle Ford reservoir rock (Section 2.7.1), except a confining pressure of 1000 psi was used. The Eagle Ford and Mancos samples were cut parallel and perpendicular to bedding planes.

The measured mechanical properties showed a good correlation with the acidity of the experimental solution in both orientations (parallel and perpendicular to bedding). The samples cut perpendicular to bedding showed more resistance (>30%) to fracturing compared with the samples cut parallel to bedding. The loss in UCS in the 3 wt% HCl was 60% for Mancos, and 49% for Eagle Ford when cut perpendicular to bedding and 61% in samples cut parallel to bedding. These results correlate well with the imbibition data both parallel and perpendicular to bedding (Section 2.6). This phenomenon might be interpreted as the opening of natural fractures along bedding is

easier to achieve than across bedding, which results in lower strength in along direction.

Table 2.8 Mechanical data for Eagle Ford outcrop rock samples

	Orientation	YM (10^6 Psi)	PR (%)	UCS (10^3 Psi)	Confining Pressure (Psi)
Intact Sample	Parallel to bedding	-	-	19.12	1000
1 wt.% HCl+5 wt.% NaCl	Parallel to bedding	1.11	0.12	11.84	1000
3 wt.% HCl +5 wt.% NaCl	Parallel to bedding	0.45	0.085	7.4	1000
3 wt.% HCl +5 wt.% NaCl	Perpendicular to Bedding	0.67	-	9.73	1000

Table 2.9 Mechanical Data for Mancos Outcrop Rock Samples

	Orientation	YM (10^6 Psi)	PR (%)	UCS (10^3 Psi)	Confining Pressure (Psi)
Intact Sample	Perpendicular to Bedding	1.81	-	16.8	1000
3 wt.% HCl +30 wt.% NaCl	Perpendicular to Bedding	0.76	0.26	6.64	1000

2.7.3 Effect of Matrix Acidizing on Shale Rock Hardness

Hardness is the property of a material that enables it to resist plastic deformation, usually by penetration. Hardness was measured using Brinell test method. The test is achieved by applying a known load to the surface of the tested material through a hardened steel ball of known diameter. The diameter of the resulting permanent impression in the tested metal is measured and the Brinell Hardness number is calculated. For these experiments outcrop samples from Mancos and Marcellus Shale formation were used. The test procedure is as following:

1. The indenter is pressed into the sample by an accurately controlled test force.
2. The force is maintained for a specific dwell time, normally 10 - 15 seconds.
3. After the dwell time is complete, the indenter is removed leaving a round indent in the sample.

4. The size of the indent is determined optically by measuring two diagonals of the round indent using either a portable microscope or one that is integrated with the load application device.
5. The Brinell hardness number is a function of the test force divided by the curved surface area of the indent. The indentation is considered to be spherical with a radius equal to half the diameter of the ball. The average of the two diagonals is used in the following formula to calculate the Brinell hardness (Eq. 2.4 and Figures 2.57 and 2.58):

$$HB = \frac{2F}{\pi D\,(D-\sqrt{D^2-d^2})} \quad \text{.....(Eq. 2.4)}$$

Where :

HB = Brinell Hardness Number

F = load on the indenting tool (kg)

D = diameter of steel ball (mm)

d = measure diameter at the rim of the impression (mm)

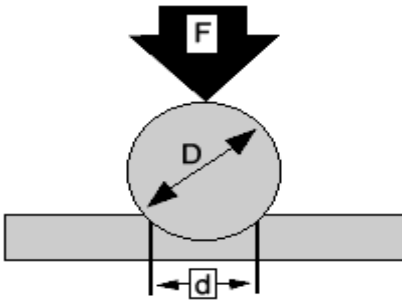

Figure 2.56 Brinell hardness test

Figure 2.58 Brinell hardness test equipment

Four values were taken at different locations of each sample and the average hardness was recorded as shown in Section 2.6, the hardness values of Mancos and Marcellus Shale samples were lower after exposure to acidic solutions, although the decrease varied depending on the acidity of the solution. Shale hardness was about 23,584 psi when the Marcellus sample exposed to 1 wt% HCl solution and much lower in 2 wt% HCl solution (4,547 psi). In the 3 wt% HCl solution, the hardness did not decrease. Instead, the measured hardness was about 30,869, which was higher than those 1 or 2 wt% HCl solutions. This only explanation for this behavior in Marcellus samples might be precipitation of iron oxy-hydroxide phases that may strengthen the sample, rather than weaken it (as discussed in Section 2.3&2.4).

Mancos Shale initial hardness was about 13,793 psi (Das *et al.* 2014) and when the Mancos sample exposed to 30 wt% NaCl neutral solution, the shale hardness was slightly affected and lowered to 11,405 psi. While, using acidic solutions the Mancos Shale hardness values were much lower to as low as 7,534 psi in 2 wt% HCl solution.

Table 2.10 Measured hardness for The used shale samples soaked in different acid solutions

Shale	soaking fluid	Conditions	Avg. BH (psi)
Mancos	Intact Sample	Initial Condition	13,793
	30% KCL solution	After soaking	11,405.6
	1wt% HCl in 30wt% KCl	After soaking	9,127.3
	2wt% HCl in 30wt% KCl	After soaking	7,534.4
Marcellus	2 wt% KCL solution	Initial Conditions	68,842.4
	1wt% HCl in 2 wt% KCl	After soaking	23,583.6
	2wt% HCl in 2 wt% KCl	After soaking	4,547.4
	3wt% HCL in 2 wt% KCl	After soaking	30,869.6

2.8 Conclusions

To improve primary oil recovery factors from shale oil formations, the potential of combining matrix acidizing and propped hydraulic fracturing was investigated. Low acid concentrations (1-3 wt%) were used for matrix acidizing

experiments; this is considered lower compared with the concentrations used for conventional reservoirs (typically 15 wt% HCl). We used lower HCl concentrations as shale rocks are ductile compared with conventional reservoirs and excessive softening could result in formation damage. The main conclusions of the matrix acidizing study may be summarized as following:

1. Shale properties may change significantly when exposed to low pH solutions and as a function of contact time and acid concentrations.
2. Porosities and recovery factors for the Eagle Ford Shale were enhanced by the opening of the natural micro-fractures after partial dissolution of calcite.
3. A two fold increase in Eagle Ford Shale porosity was observed when using 3 wt% HCl, and resulted in a three-fold increase in the recovery factors.
4. Oil recovery factors from the Eagle Ford Shale were enhanced by mineral dissolution and wettability alteration using low pH solutions.
5. Changes in porosity of Barnett, Mancos, and Marcellus Shale samples did not correlate with carbonates dissolution, but with development of cracks.
6. Iron oxide-hydroxide precipitation after pyrite oxidation in Barnett and Marcellus Shales lowered porosities in HCl experiments with concentration less than 2 wt%, but did not affect the recovery factors.
7. Low pH solutions generated cracks along bedding similar to distilled water, which accelerates the imbibition oil recovery in the Barnett Shale samples.
8. Matrix acidizing improved primary oil recovery from Mancos Shale samples up to 53% compared with 2.5% when 30 wt% KCl neutral solution was used alone.
9. Marcellus Shale samples showed very poor imbibition recovery factors (4%) using low HCl concentrations (1-3 wt%) when cut across bedding, but more

recovery was observed (38%) using the same acid concentrations but when samples were cut along bedding.

10. Water imbibition along bedding planes were higher than across bedding for all of the studied rocks, and especially for Marcellus rock samples.
11. Eagle Ford, Mancos, and Marcellus Shales' wettability was altered to strongly water-wet by using low acid concentrations.
12. 3 wt% HCl solutions lowered Mancos rock hardness by up to 34%.
13. Low concentration HCl solutions significantly affect the mechanical properties of Eagle Ford reservoir Shale samples with significant reduction in Young's Modulus ranging from 25-82% and loss of UCS of between 27 and 70%
14. The rock hardness of Marcellus Shale samples was significantly affected by low pH solutions, which resulted in 55-94% loss of its value using 2 wt% KCl neutral solution.

Chapter 3

Optimizing Surfactant Additives for Enhanced Well Simulation

This chapter presents an experimental study of Bakken Shale reservoir samples and crude oil production to exposure with synthetic formation brine. The objective of the chapter is to develop a new stimulation surfactant that enhances initial primary oil production and helps to sustain long term-production from the middle member of the Bakken Shale formation. A series of experimental procedures were applied to test surfactant compatibility with formation brine, different fracturing fluids, Bakken crude oil, and its impact on formation recovery factors from spontaneous imbibition.

3.1 Surfactant Compatibility with Formation Water

Ten surfactants were screened to identify potential surfactants for later experiments (Figure 3.1). In this test, 2% KCl, 15 wt% and 30 wt% brines were used. The Bakken formation brine as measured in field is 30 wt% and its recipe is shown in Table 3.1. The 2% KCl was used to represent fracturing base water system, 30 wt% Bakken synthetic brine was used to represent formation brine, and 15 wt% brine was used to represent the diluted formation water with fresh water after fracturing. The 15 wt% brine was prepared by the same way as 30 wt% but with half salinity values.

Table 3.1 Synthetic Bakken Shale brine

Component	15% Synthetic Brine	30% Synthetic Brine
	mg/L	
NaCl	112,500	225,000
CaCl2*2H2O	15,000	30,000
KCl	7,500	15,000
MgCl2*6H20	32,000	64,000

After vigorous mixing of the surfactant and brine, the test tubes were set aside, and allowed to sit. All of the test tubes were placed in an oven held at 190°F. The clarity of each tube was monitored and appearance noted after sitting without

agitation for one week at 190°F. Several developmental and commercially available products moved forward for additional testing. One of the formulas, "Stim-aid A," showed excellent oil recovery from imbibition tests and fluid flow-back efficiency testing. It showed no precipitation after one week at 190°F in either 15% or 30% brine using 0.1 and 0.2 wt.% concentrations (Figure 3.2). This study presents the results of only this promising formula.

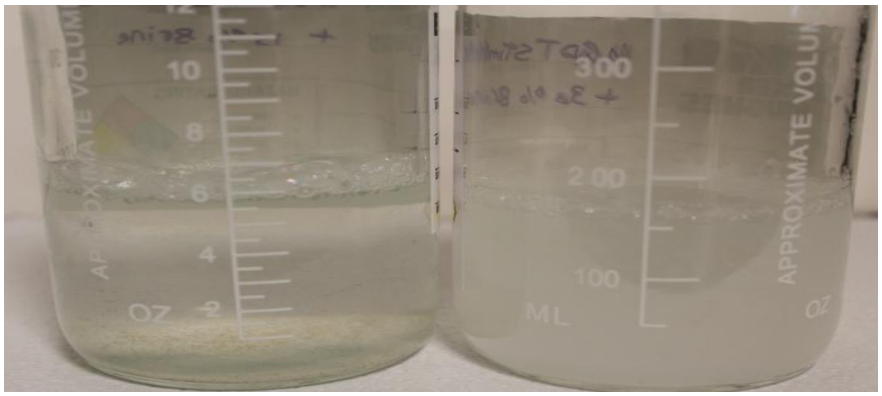

Figure 3.1 Brine compatibility test results for unsuccessful surfactants after one week in 15% and 30% brines showing fine precipitations

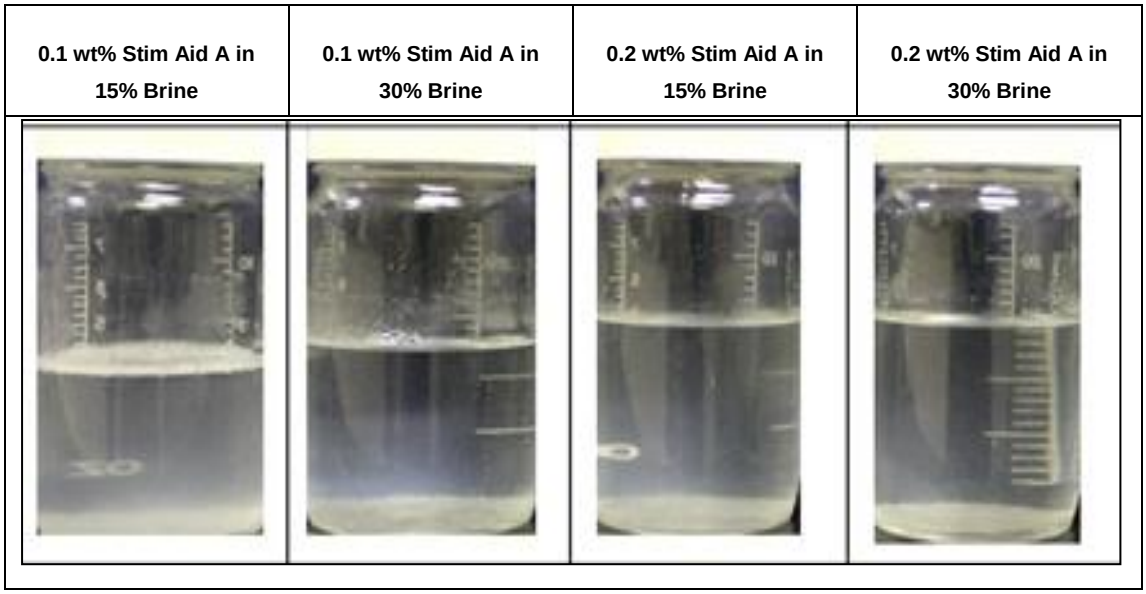

Figure 3.2 Brine compatibility test Results for Stim Aid A surfactant after one week in 15% and 30% brines

3.2 Surfactant Flowback Test

In order to retain proppant pack conductibility and avoid formation damage, surfactant is normally added to assist fracture fluid flowback. Fluid flowback tests

(Figure 3.3) were performed to check the effectiveness of the surfactant. Sand columns were packed with proppant (20/40 Ottawa sand) and the base fluid plus 0.1 wt% surfactant was added. Nitrogen gas was used to simulate production gas and flowed at a controlled rate to displace the fluid from the column. The recovered fluid volume was divided by the initial volume and a percent recovery was calculated. The test was repeated with 0.2 wt% concentration. Tap water and 2% KCl were used as base fluids.

Table 3.2 summarizes the fluid recovery test results of Stim-aid A in tap water and 2% KCl at concentrations of 0.1 and 0.2 wt.%. Both indicate suitable performance in aiding fluid flowback with 1 wt.% Stim-aid A; however, increasing to 2 wt.% only slightly improved fluid recovery from the sand pack.

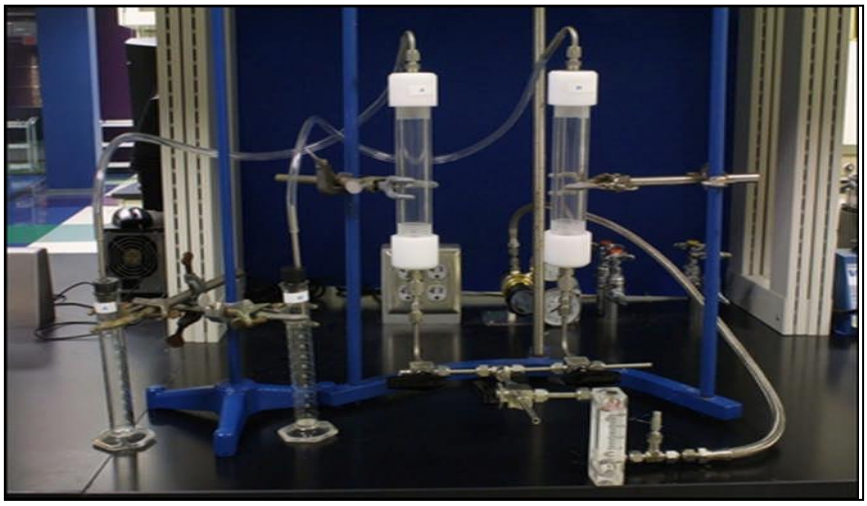

Figure 3.3 Flowback instrument setup

Table 3.3 Flowback recovery factors for the tested concentrations

Stim Aid A (wt.%)	Fluid Recovery in Tap Water (%)	Fluid Recovery in 2% KCl (%)
0.1	88	87
0.2	90.2	89.7

3.3 Emulsion Tendency Test

A crosslinked fracture fluid typically used in Bakken operations was broken to water-like consistency. The broken gel was combined with Stim-aid A (0.1 or 0.2 wt%) and used in fracture fluid/crude oil emulsion tendency testing. Noted was the percentage of breakout (calculated in Eq. 3.1), fluid interface stiffness, and oil on the container wall after 5, 15, and 30 minutes in a water bath at 180°F.

$$\text{breakout (\%)} = \frac{\text{volume of frac fluids separated} \times 100}{\text{total volume}} \quad \text{.....(Eq.3.1)}$$

Table 3.4 Emulsion tendency summary of broken fracture fluid with Stim Aid A

Time		Stim Aid A conc. (wt%)	
		0.1 wt%	0.2 wt%
5 min	Breakout %	100%	90%
	Stiff Interface	no	No
	Oil on Wall	no	No
15 min	Breakout %	100%	92%
	Stiff Interface	no	No
	Oil on Wall	no	No
30 min	Breakout %	100%	96%
	Stiff Interface	no	No
	Oil on Wall	no	No

A slight emulsion was observed when mixing broken crosslinked fluids containing 0.2 wt% of Stim-aid A with crude oil (Figure 3.4).

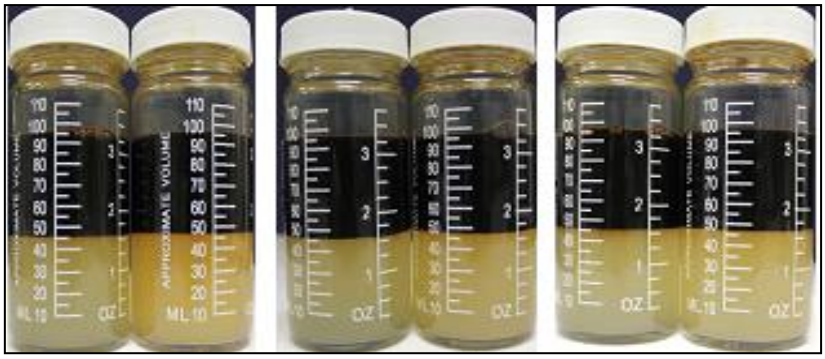

Figure 3.4 Emulsion tendency test results in guar neutral frac fluid with Bakken oil after 5, 15, and 30 min (left: base fluid, right: 0.2 wt% of Stim Aid A

The emulsion test was also done using 0.2 or 0.4 wt% Stim-aid A in 15% or 30% synthetic brines and Bakken crude oil. No emulsion formed with 0.2 wt% in 15% or 30% brine (Figure 3.5).

Figure 3.5 Emulsion tendency test Results of 0.2 wt% of Stim Aid A in 15% and 30% brines with Bakken oil after 30 min (left: 15% brine, right: 30% brine)

Slight emulsion was formed with 0.4 wt% of Stim-aid A in 15% brine only, while no emulsion formed in 30% brine (Figure 3.5). The emulsion may have contributed to the lower oil recovery results observed in imbibition tests with 0.4 wt% of Stim-aid A in 15% brine (in the spontaneous imbibition section).

Figure 3.6 Emulsion tendency test results of 0.4 wt% of Stim Aid A. in 15% and 30% brines with Bakken oil after 5 and 30 min (left: 15% brine, right: 30% brine).

It was observed that 0.05 wt% nonemulsifier was enough to prevent an emulsion from forming in the 0.4 wt% Stim-aid A/15% brine solution (Figure 3.7).

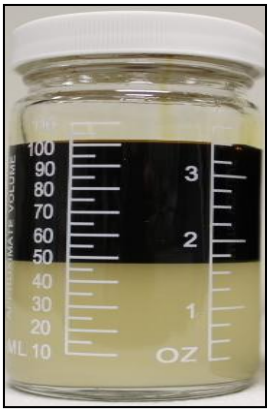

Figure 3.7 Emulsion tendency test result: 0.4 wt% of Stim-aid A in 15% Brine including 0.05 wt% non-emulsifier with Bakken oil after 30 min

3.4 Surfactant Compatibility with Crosslinked Fracturing Fluid

Compatibility of Stim-aid A with several fracturing fluids was tested using a Grace M5600 rheometer. The crosslinked fluid was tested at a constant shear rate of 100 sec-1 with an API standard shear ramp at 72°F initially, at elevated temperature (e.g. 200°F and higher) after five minutes, and then every 30 minutes for 3 hours with API standard shear ramp. The loading of 0.2 wt.% Stim-aid A was used in fracture

fluids compatibility tests. Figures 3.8and 3.9 indicate that adding 0.2 wt.% of Stim-aid A did not affect the viscosity performance of guar- or cellulose-based fracture fluids.

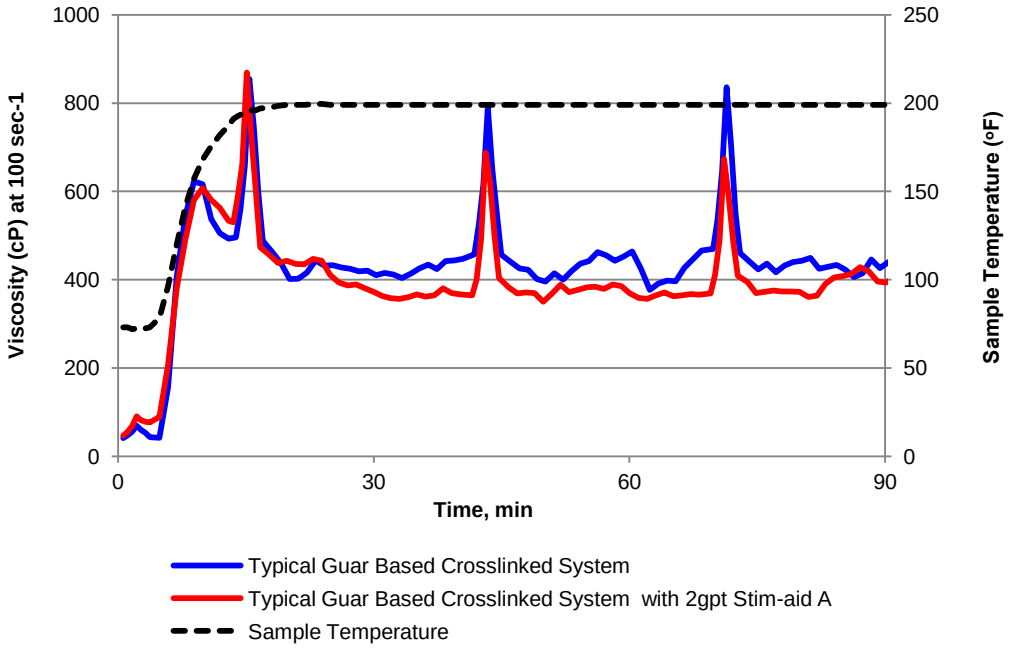

Figure 3.8 Stim-aid A compatibility with guar-based crosslinked fracturing fluid system at 200°F

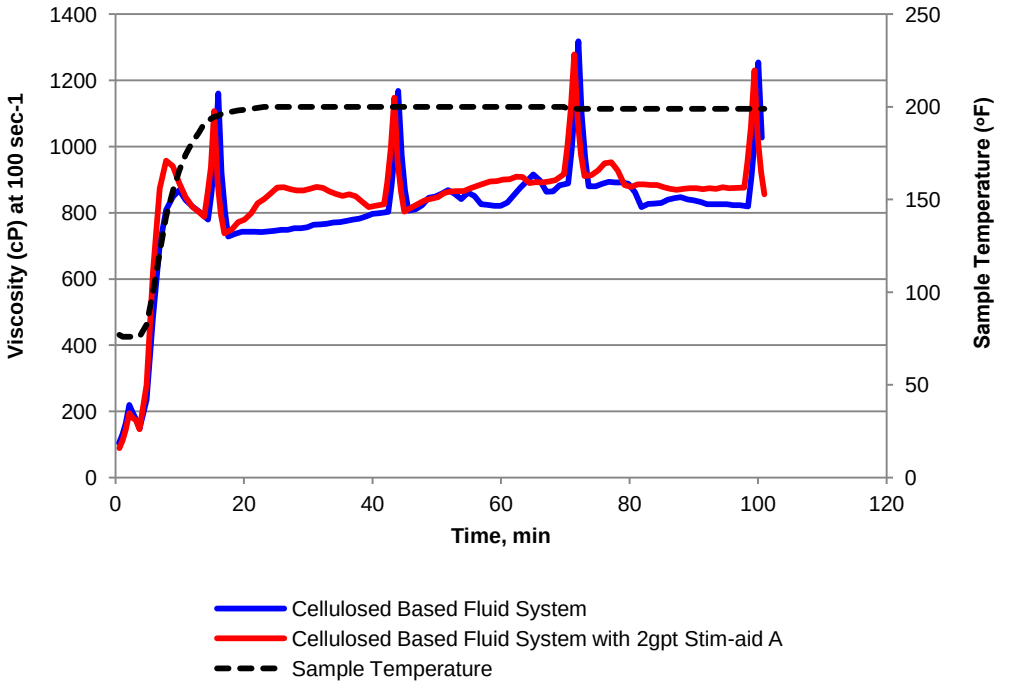

Figure 3.9 Stim-aid A compatibility with cellulose based fracturing fluid system at 200°F

3.5 Visual Assessment of Wettability

Visual wetting preference was assessed on disaggregated sand and marble. (Stim aid A) surfactant was compared to a known water-wetting surfactant and an oil-wetting surfactant using 15% and 30% brine solutions. In order to show significant color contrast, high loading of surfactants were used in the study. Figure 3.10 and 3.11 show the resulting color of 40/60 white sand and marble sand after they are exposed to surfactant followed by red dyed kerosene solution. Slightly yellow colors in white sand and white colors in marble sand mean surfactants have strong water-wetting characteristics while red color in both white sand and marble sand means surfactants tend to oil-wet the grain surfaces. The results indicated all test formulations have strong water wetting characteristics to both 40/60 white sand and marble sand.

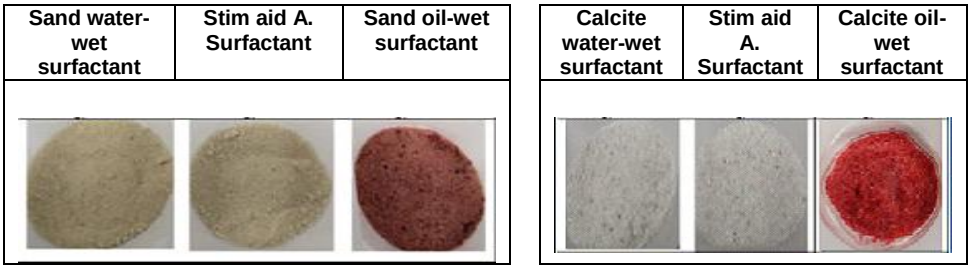

Figure 3.10 Stim Aid A. surfactant ability to alter 40/60 white sand (left) and calcite (right) wettability towards water-wet using 15% synthetic brine

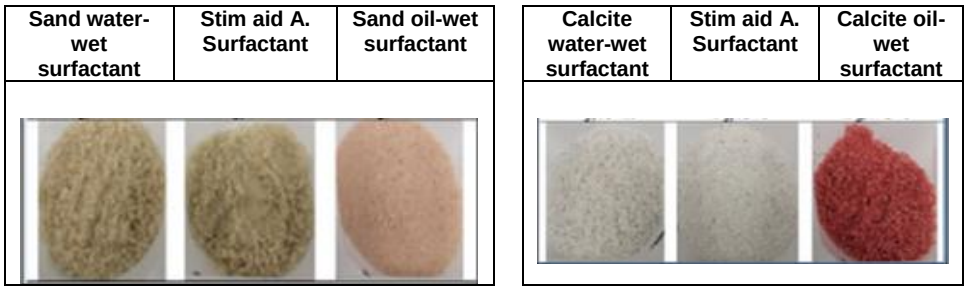

Figure 3.11 Stim Aid A. surfactant ability to alter 40/60 white sand (left) and calcite (right) wettability towards water-wet using 30% synthetic brine

3.6 Oil Recovery

The effect of surfactant and/or surfactant loading in brine on oil production was assessed by spontaneous water imbibition. Using Amott cells, crude oil aged Bakken cores were immersed in brine. The Amott cell has a calibrated stem in which

oil, as brine imbibed into the sample, migrated to the top for collection. Collected volumes were monitored and recorded. In spontaneous imbibition tests, the specific gravity of Bakken crude oil tested was 0.815 (42°API). The oil was quite light, making it favorable for use in the surfactant recovery process.

Bakken reservoir cores were from a depth of approximately 10,000 feet. The permeability to nitrogen was less than 0.05 md and porosity averaged 10%. To expedite testing, the plug samples were cut into smaller pieces. The pore volume was determined for each piece. All Bakken samples were pressure saturated (Figure 3.12) with Bakken crude oil and aged at 190°F for 2 weeks prior to use in the Amott cells. The collective pore volume of the chips in each cell was recorded.

Each Amott cell was filled with brine alone or brine plus surfactant, and placed in a 190°F oven. Spontaneous water imbibition yielded effluent oil as noted in the stem of the cells (Figure 3.13).

Figure 3.12 Coreflooding system used to saturate Bakken Shale sores prior to water imbibition

Figure 3.13 Shale cores after 24 hours soaking in the surfactant solutions

In 15% brine solutions, the highest oil recovery (32%) was achieved using 0.2 wt% of Stim-aid A (Figure 3.14). Compared to the baseline of 15% brine alone, significantly more oil was recovered with 0.2 wt% Stim-aid A solution. Also tested were 0.1 wt% and 0.4 wt.% Stim-aid A in 15% brine. Although oil recovery was improved over brine alone, these loadings were less efficient than 0.2 wt%. The loading of 0.1 wt% Stim-aid A may not have been sufficient to alter the shale wetting preference and lower the interfacial tension. While 0.4 wt% Stim-aid A was efficient in altering the wettability, it formed an emulsion as evidenced by crude oil still sticking to the Bakken Shale surface even after vigorously shaking (Figure 3.15).

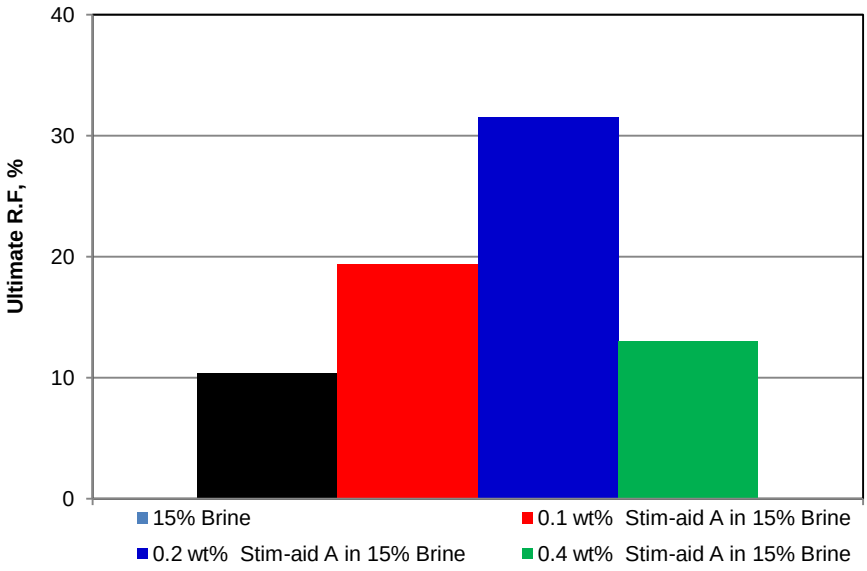

Figure 3.14 Oil recovery From Bakken Shale cores, Stim Aid A surfactant concentrations in 15% brine

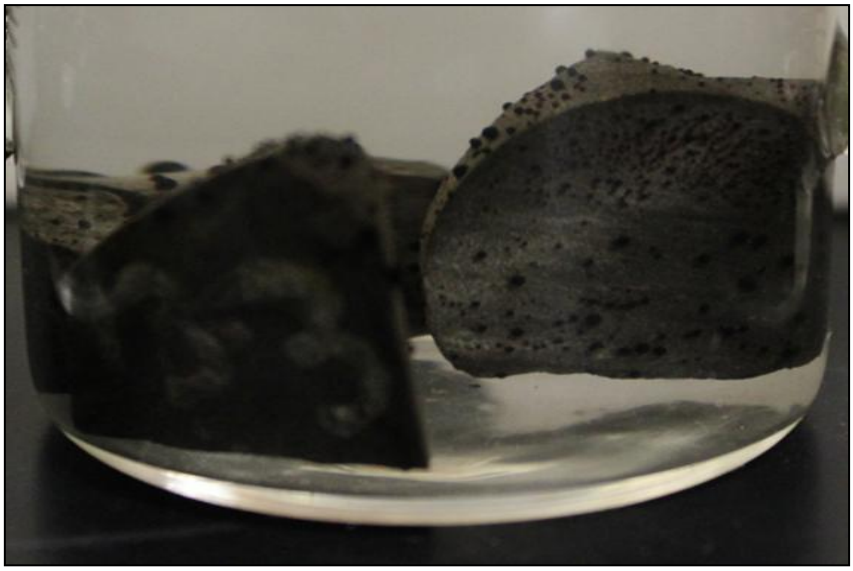

Figure 3.15 Bakken core samples in Amott imbibition cells immersed in 0.4 wt% of Stim Aid A in 15% brine

In 30% brine, 0.2 wt% of Stim-aid A again provides the highest oil recovery of 22%, an additional 13% more oil recovered than the baseline of 30% brine alone (Figure 3.16). When 30% brine was used, 0.4 wt% of Stim-aid A provides similar oil recovery as 0.2 wt% Stim-aid A.

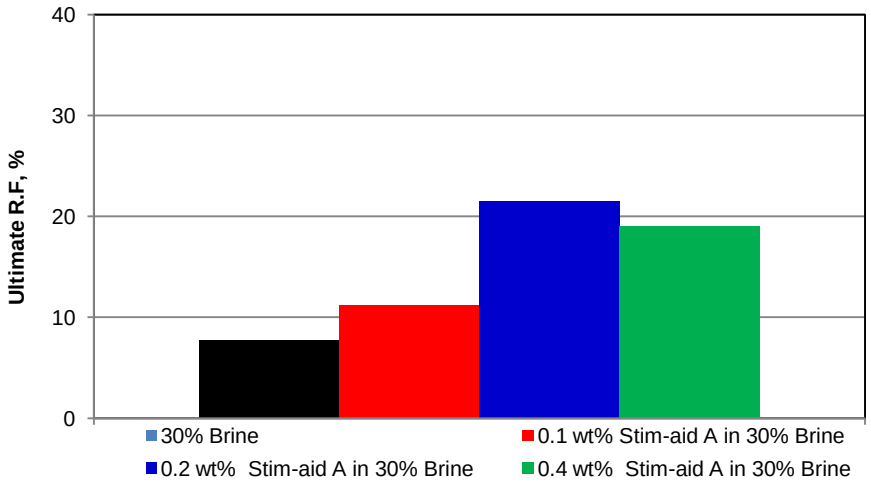

Figure 3.16 Oil recoveries from Bakken Shale cores of various Stim Aid A surfactant concentrations in 30% brine

3.7 Conclusions

Chapter 3 presented another mechanism to improve primary oil recovery by optimizing surfactant additives in well stimulation fluid. This study was done on Bakken reservoir rock samples, crude oil, and synthetic formation water. The study was initiated to enhance primary oil recovery by changing fracture surface wettability. Different surfactants were pre-screened in this study (but details not presented) to see if they are compatible with formation water, oil, and different fracture fluids used for Bakken Shale. Only one surfactant (Stim aid A.) out of the tested commercial surfactants was fully compatible with Bakken Shale, and used after for spontaneous imbibition experiment to see its ability to alter Bakken wettability and improve oil recovery. The study conclusions are as following:

1. Stim aid A. formulations were fully compatible with formation brine, crude oil, and the proposed fracture fluids
2. Stim Aid A. surfactant was able to change calcite and sand samples to strongly water wet conditions
3. For weakly emulsified Stim aid A., fast and significant oil recovery by spontaneous imbibition is observed from native Bakken core material.

Chapter 4

Potential of Low Salinity (Low Sal), Alkaline, and Surfactant Preflood in Shale Formations

Primary oil recovery factors from shale formations are very low compared to conventional reservoirs. This is exacerbated by rapid declines in early production; necessitating secondary recovery methods may be implemented to maintain oil production. Waterflooding is the cheapest technology to apply in most of oil reservoirs; it is a mature secondary recovery method for conventional reservoirs. However, it has not been fully studied and understood in shale oil reservoirs.

Water imbibition is the main mechanism of waterflooding in shale formation and enhancing it will benefit the waterflooding performance. To understand and improve waterflooding performance in shale formations, this chapter presents an experimental study to understand the effect of different water formulations to improve water imbibition in shales. The chapter investigates three mechanisms to enhance waterflooding recovery from shale rocks using water with different salinities, alkalinities , and surfactant solutions.

4.1 Potential of Low Salinity (Low Sal) in Shale Formations

It is well established that rocks containing water-reactive clays may swell in the presence of fresh water. In a conventional formation, this swelling may cause wellbore stability problems or damage the formation by reducing its permeability. However, the effect of water and its composition on shales may be different.

The lower the salinity, the greater the clay swelling effect which may result in clay expansion and cause fracturing, which can be a vital mechanism in improving oil recovery of from shales (Wang *et al.* 2010). Wettability alteration may also contribute to the improvement of shale oil recovery when exposed to lower salinity solutions (Ramez *et al.* 2013). This section will investigate the effect of water salinity on shale stability, wettability, and recovery in laboratory experiments.

4.1.1 Effect of Water Salinity on Barnett, Eagle Ford, and Marcellus Shale Stability and Recovery

Reservoir core samples from Eagle Ford Shale and outcrop samples from Barnett, Marcellus, and Mancos Shale formations were used. The samples were 2.54 to 3.81 cm in diameter and 0.762 to 5.08 cm in length. The experiments procedure is as following:

1. Extract formation oil from the Eagle Ford Shale reservoir samples, a Soxhlet extractor apparatus, toluene solvent and a reflux process were used.
2. Weigh the dry shale samples twice and record the average weight of each sample
3. CT scan the shale samples dry with a recorded label and alignment direction of scanning
4. Vacuum the shale samples using a vacuum saturation pump and a desiccator
5. Put the cores in the vacuumed Desiccator to soak for about one week in Soltrol 130^{TM} oil
6. After saturation with Soltrol 130^{TM} oil, all cores were removed. Samples were reweighted to calculate the volume of Soltrol 130^{TM} oil saturated in the core
7. CT scan the cores again after saturation with oil in the same aligned scan direction of the first scan time when dry
8. With the CT images of the air-saturated samples (dry) and oil–saturated samples, the porosity was calculated.
9. Place the samples in labeled Amott test tubes contain fresh (distilled) water for spontaneous imbibition and record oil recovery versus time.

The visual observations of the samples exposed to fresh (distilled) water during spontaneous imbibition showed that several along bedding cracks were induced in Barnett samples. There were also along bedding cracks in the Marcellus Shale samples, although they are not so visible (Figure 4.1). Eagle Ford samples were least sensitive to water salinity with no visible crack development (Figure 4.1). This is attributed to the low abundance of swelling clays in the samples (Figure 4).

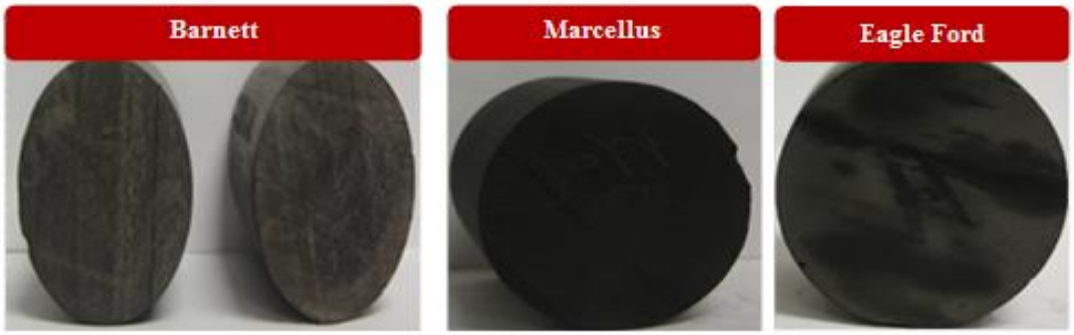

Figure 4.1 Barnett, Marcellus, and Eagle Ford Shale samples after one week of exposure in fresh water

Oil recovery from Mancos, Barnett, Marcellus, and Eagle Ford samples exposed to fresh water and 2 wt% KCl are presented in Figures 4.2 and 4.3. Distilled water gave higher recovery factors compared to 2% KCl, which was attributed to increased clay swelling in water compared to 2 wt% KCl brine that would result in micro-fractures opening (Figure 4.2). Eagle Ford and Barnett recovery factors were 20 and 24% respectively using distilled water, and 12 and 13% using 2 wt% KCl solution. The cracks were induced over time in Barnett samples when exposed to the distilled water and as a result, more oil was recovered. Although no fractures were visually observed in the Eagle Ford sample, the distilled water recovery factor was almost double the 2 wt% KCl solution recovery. It is believed that the induced fractures in the Eagle Ford sample in the micro scale that cannot be seen visually improved the oil recovery. The Marcellus sample showed the lowest recovery of about 2% and with almost no effect on its imbibitions in either solutions.

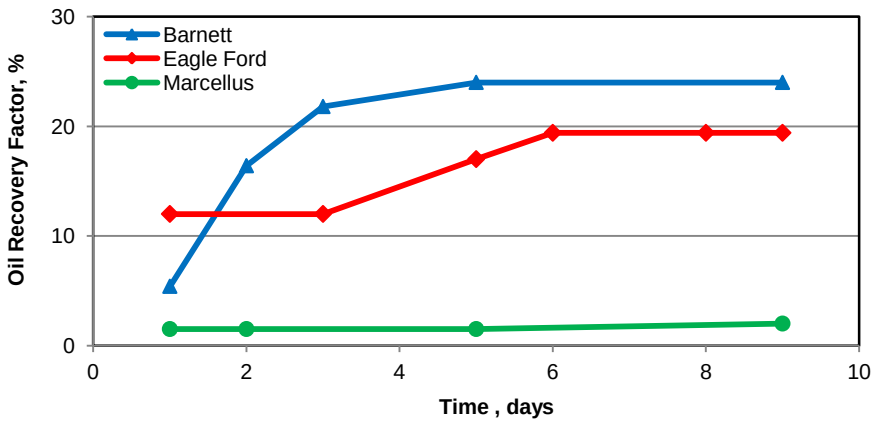

Figure 4.2 Oil recovery factors (RF) in spontaneous imbibition in fresh water From the Barnett, Eagle Ford, Mancos, and Marcellus Shale samples

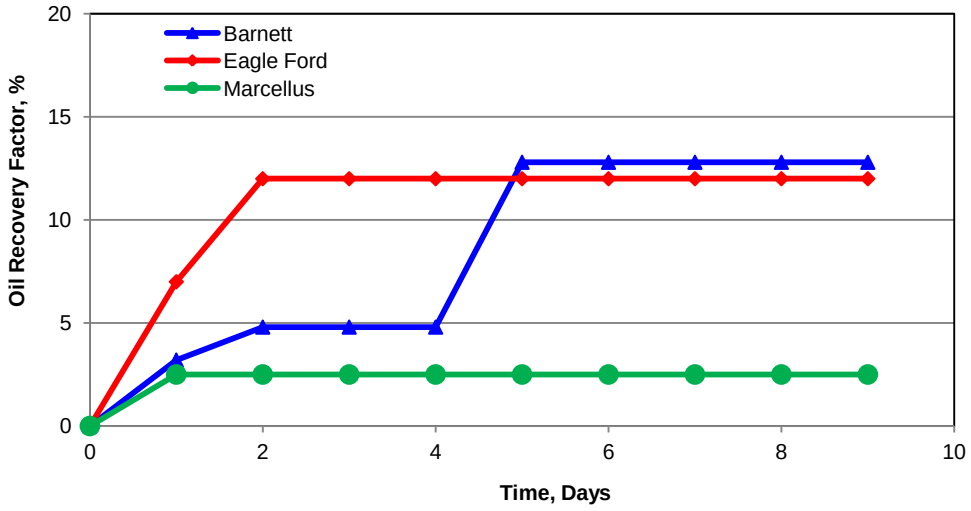

Figure 4.3 Oil recovery factors (R.F) after spontaneous imbibition in 2 wt% KCl From Barnett, Eagle Ford, and Marcellus samples

4.1.2 Effect of Water Salinity on Mancos Shale Stability and recovery

Outcrop samples of Mancos Shale ranging from 2.54 to 3.81 cm in diameter and 0.762 to 5.08 cm in length were used in this study. The experimental procedure was the same as in Section 4.1.1, except the saline solutions used were 5, 10, 15, and 30 wt% of NaCl and KCl.

Mancos samples were most sensitive to distilled water as the samples were severely damaged due to hydration (Figure 4.4 left). The Mancos samples, when exposed to a lower salinity solutions (<15% of NaCl and KCl), showed significant damage after one week of spontaneous imbibition (Figure 4.5 right). Figure 4.5 shows the Mancos shale samples had cracks, and became fragmented to different degrees depending on solution salinity. At 0%, 5% and 10% NaCl, the rock samples were fragmented, although in the 15% solution the sample had fewer visible cracks. When the Mancos samples were exposed to water with 30% of NaCl, they showed very few cracks (Figure 4.5).

Based on the Mancos Shale published data (Sarker and Batzle 2010), the Mancos formation water is very saline with 13.8-21.2%. It indicates that the Mancos Shale samples are stable in the formation water salinity range. The oil recoveries from Mancos samples in different saline water solutions are shown in Figure 4.6. The oil recovery factor was enhanced up to 59% from the samples exposed to the 5% NaCl

solution compared with only 4% from the samples exposed to the 30% NaCl solution. More oil was recovered from the Mancos sample exposed to the 5% NaCl solution than from either of the samples exposed to 10% or 15% NaCl solutions; this correlates with visible degrees of fragmentation (Figures 4.4 & 4.5). The shale samples in KCl solutions were more stable compared to the NaCl solution experiments (Figures 4.4 & 4.5).

Figure 4.4 Mancos samples in distilled water (the left), and in 5%, 10% and 15% NaCl solutions (the right)

Figure 4.5 – Mancos samples in 5%, 15% and 30% NaCl solutions

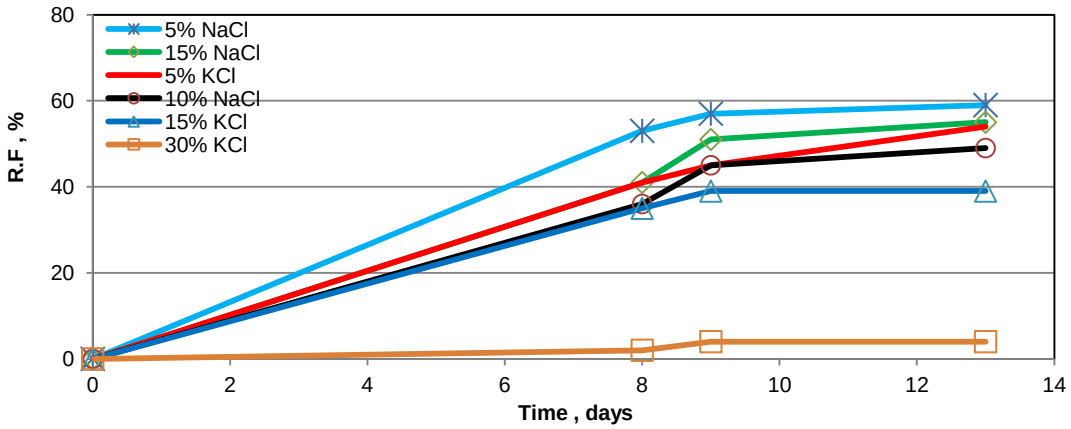

Figure 4.6 – Oil recovery factors of the Mancos Shale samples after spontaneous imbibition in different saline solutions

4.1.3 Effect of Brine Salinity on Bakken Shale Oil Recovery and Rock Surface Wettability

In this experiment, reservoir samples from Bakken Shale formation (Middle Member) were used with reservoir crude oil and synthetic brine formulation. Sample preparation was different as the samples were saturated under confining pressure of 2000 psi for two weeks and then placed in an oven at 200ºF for one week to age the reservoir crude oil. A brine matching of the formation brine salinity (30%) was prepared in the laboratory. A 15% brine, representing a lower salinity for imbibition purposes was also prepared. The 15% and 30% brines were mixed in accordance with methods described in Chapter 3. The objective of this experiment is to study water imbibition in Bakken Shale reservoir samples using high and low brine salinities.

4.1.3.1 Bakken Shale Oil Recovery Factors

The Bakken samples treated with low salinity solutions (15%) have similar responses to other shales in this study. Oil recovery factors were higher in lower salinity solutions (15% in 15wt% salinity brine) compared with 7% from samples exposed to 30 wt% brine solution (Figure 4.7). The Bakken samples that were exposed to 15% brine did not show any cracks suggesting that the mechanism responsible for higher recovery factors was different. The mechanism of oil recovery improvement in Bakken Shale samples using 15% brine solution cannot be explained

by clay swelling alone in a similar way to the cases with the previous experiments where distilled water were used.

Wettability alteration could be a possible mechanism of improving oil recovery of carbonate reservoirs using lower salinity solutions (Ramez *et al.* 2013), as the low salinity solutions may alter rock wettability by changing the electric charge of the oil/brine and rock/brine interfaces. When the electric charge at the interfaces become more negative, the repulsive forces between rock and oil increase resulting in more water-wet conditions after expansion of the electric double layer stabilizes water film surrounding the rock surface. Since Bakken Middle Member Shale has a high calcite content, which is a similar case to carbonate reservoirs. Thus, the improvement in Bakken oil recovery using 15% brine solution could be caused by wettability alteration.

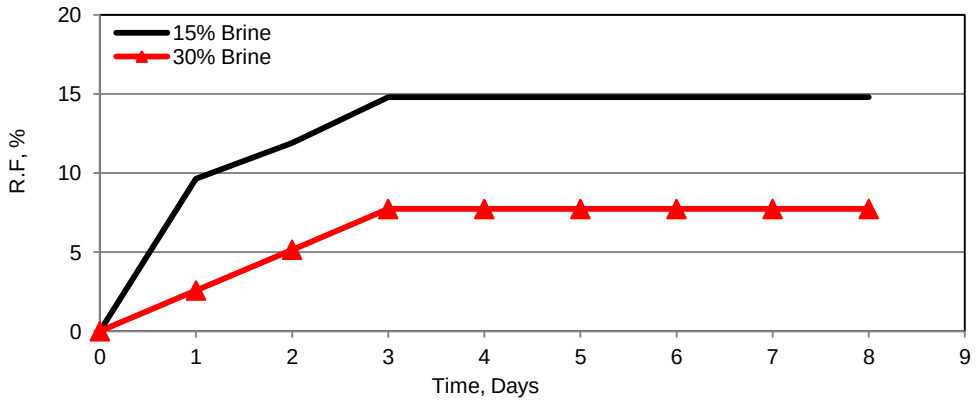

Figure 4.7 Bakken oil recovery factors (R.F) after spontaneous imbibition in 15% and 30% synthetic brines

4.1.3.2 Effect of Water Salinity on Bakken Shale Wettability

There was an improvement in spontaneous imbibition oil recovery from the Bakken Shale samples in different synthetic formation brine solutions and that may be explained by wettability alteration. So to determine the role of wettability alteration on shale recovery using low saline solutions, the present experiments are designed to measure the contact angles of all samples used in the spontaneous imbibition experiments on Bakken samples. The procedure of the contact angle measurement is the same as described in Chapter 2. Studied samples were saturated with Bakken crude oil as described in Section 4.1.3.1. The oil saturated samples were placed in 15% and 30% formation synthetic brine solution for one week before contact angle

measurements in order to stimulate the effect of brine salinity during the spontaneous imbibition process.

Bakken samples in this study have formation brine salinity of 30% (Wang *et al.* 2012), so the measured contact angle in the 30% synthetic formation brine may be considered equivalent to initial Bakken contact angle. The measured contact angles showed the initial contact angles in the 30% brine (81°) were lowered to 74° in the 15% brine showing a shift towards water-wet (Figure 4.8). This improvement of Bakken recovery in low salinity brine solutions (15%) is therefore attributed to wettability alteration. Therefore, Bakken oil recovery may be increased by optimizing injected water to lower the salinity of the formational brine, thereby reducing rock surface wettability.

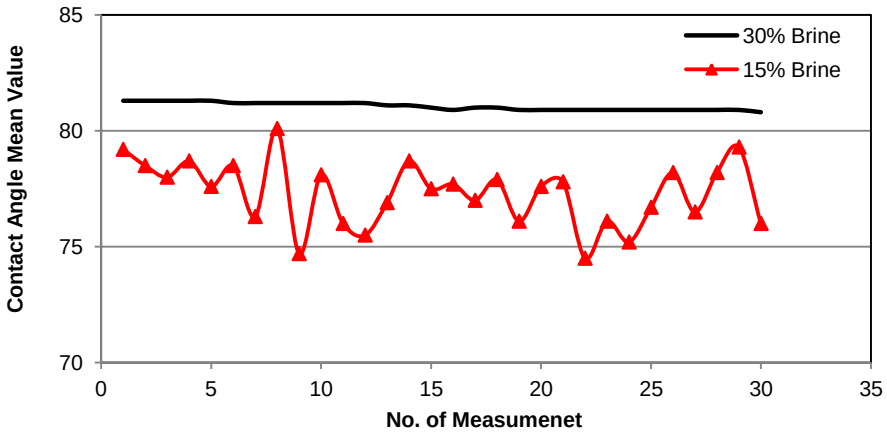

Figure 4.8 Bakken samples contact angles in 15% and 30% synthetic brines

4.2 Potential of Alkaline Flooding in Shale Formations

Use of alkaline solutions (high pH solutions) may also alter shale stability, wettability, and oil recovery. In this section, four different high pH solutions (pH11.7-13) are used to determine their contrasting impact on samples from Eagle Ford, Mancos, Marcellus, and Barnett Shale formations. The pH11.7 solution was prepared with 0.1 wt% NaOH in distilled water, pH11.8 (2 wt% NaOH in distilled water), pH12.43 (2 wt% NaOH in 2 wt% KCl), and pH13 (2 wt% NaOH in 30 wt% KCl). The high pH solutions were used in conjunction with either 2 wt% KCl or 30 wt% KCl neutral fluids to prevent clay swelling during the experiments.

4.2.1 Effect of Alkaline (High pH) Solutions on Shale Stability and Recovery

Outcrop samples from the Barnett, Mancos, and Marcellus, and reservoir samples from Eagle Ford Shale formation were prepared as described in Chapter 2. The samples were CT scanned before and after oil saturation, then placed in labeled Amott test tubes with different alkaline solutions.

The CT scanned images for the samples before and after oil saturation were used to calculate average porosities. The studied samples showed an average porosity value of 8% for Barnett, 1.8% for Eagle Ford, 3.5% for Mancos, and 7.8% from Marcellus Shale samples (Figures 4.9 through 4.12).

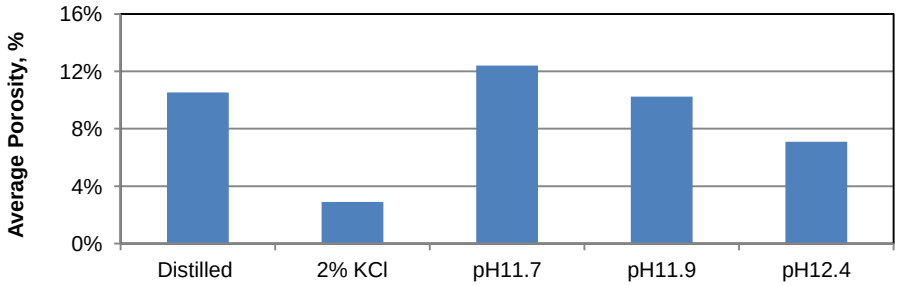

Figure 4.9 CT-scanning porosity values for the studied Barnett Shale samples before imbibition in distilled water, 2% KCl, and different alkaline solutions

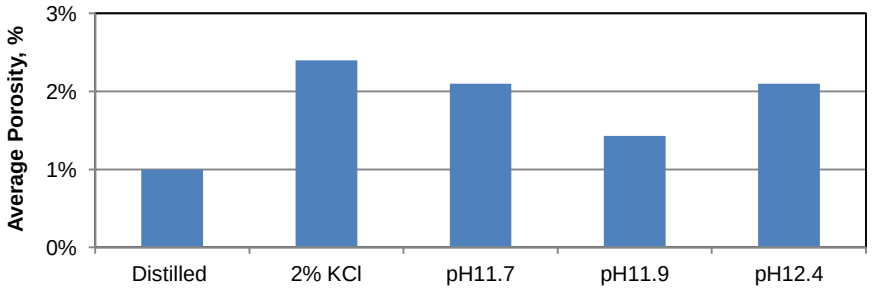

Figure 4.10 CT-scanning porosity values for the studied Eagle Ford Shale samples before imbibition in distilled water, 2% KCl, and different alkaline solutions

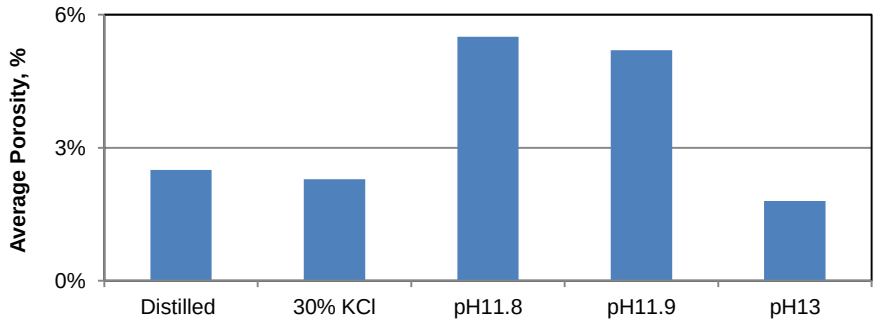

Figure 4.11 CT-scanning porosity values for the studied Mancos Shale samples before imbibition in distilled water, 2% KCl, and different alkaline solutions

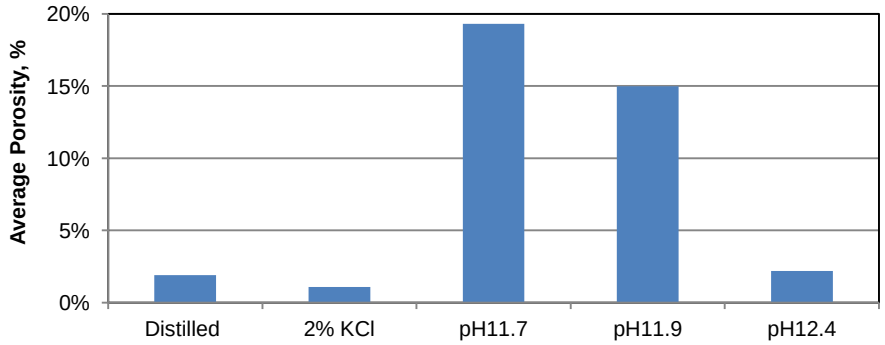

Figure 4.12 CT-scanning porosity values for the studied Marcellus Shale samples before imbibition in distilled water, 2% KCl, and different alkaline solutions

The effect of high pH solutions on the spontaneous imbibition of Mancos Shale samples was examined using pH11.8- pH13 NaOH solutions. The color of the alkaline solutions changed to light red color. This was caused by a reaction between rock minerals and the NaOH solutions (Figure 4.13). The samples showed clear minor visible cracks (Figure 4.14) and became softer when exposed to pH11.9 (2 wt% NaOH in distilled water) and pH13 (2 wt% NaOH in 30% KCl) solutions.

The highest oil recovery factor for the Mancos samples (38%) when the sample exposed to the highest pH solutions (Figure 4.15). The recovery factor increased almost three times compared to the recovery factor achieved using 30 wt% KCl solution alone. The rate of production was also accelerated when the alkaline solution was added to the 30 wt% KCl solution. Oil produced after one hour using a pH 13 solution was almost the same as the total recovery (9.4%) achieved by 30 wt% KCl solution alone. In contrast, high pH solutions resulted in lowered oil recoveries when used with distilled water. The oil recovery achieved using pH 11.8 (0.1 wt%

NaOH in distilled water) and pH 11.9 (2 wt% NaOH in distilled water) was between 31% and 40% compared to 59% when using distilled water alone. The samples exposed to alkaline solutions in distilled water were not damaged as observed with the samples exposed only to distilled water (Figure 4.14). The reduction in the recovery factors observed when using high pH alkaline concentrations in distilled water may be due to the combination of clay swelling and mineral reactivity that might results in some precipitations plugging pore space in the samples. This may also result in greater structural stability for Mancos samples compared to samples exposed to distilled water alone. There was also early acceleration in the first day of oil production from the distilled water experiments compared with the high pH solutions (Figures 4.15).

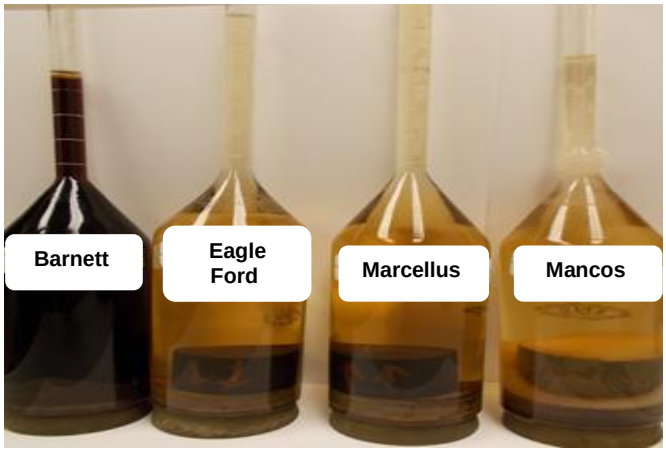

Figure 4.13 Changes in alkaline solutions color after one week of reaction with Barnett, Eagle Ford, Marcellus, and Mancos Shales in pH12.4 (2 wt% of NaOH and 2 wt% of KCl) solutions

Figure 4.14 Mancos (in the left side), Marcellus (in the middle), and Eagle Ford (in the right side) Shale samples after one week in pH12.4 (2 wt% NaOH in 2 wt% KCl) solution

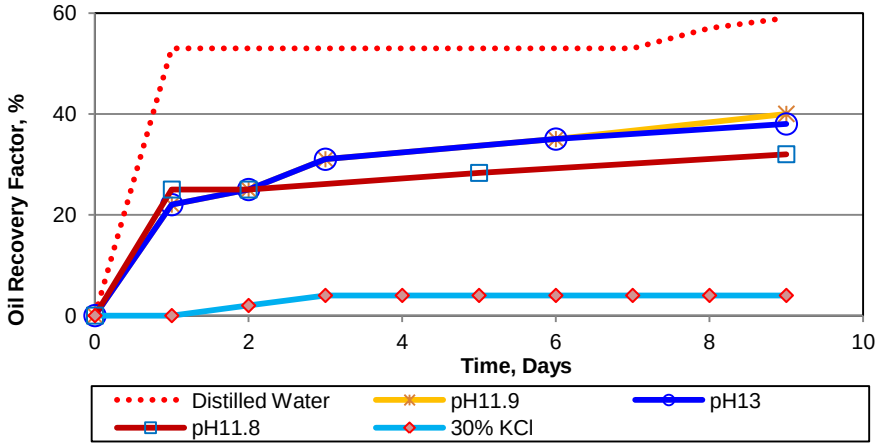

Figure 4.15 Oil recovery factors for Mancos Shale samples using different high pH solutions

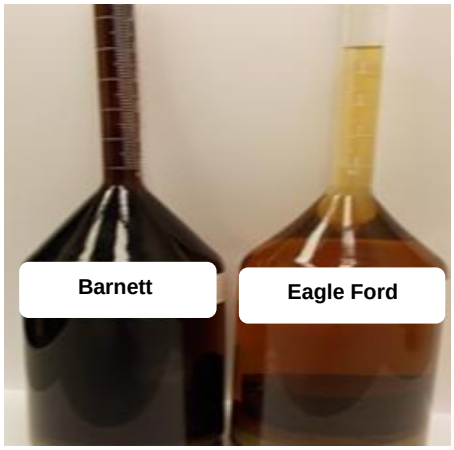

Figure 4.16 Changes in alkaline solutions color after one week of reaction with Barnett and Eagle Ford, Shale samples in pH11.9 (2 wt% of NaOH in fresh water) solution

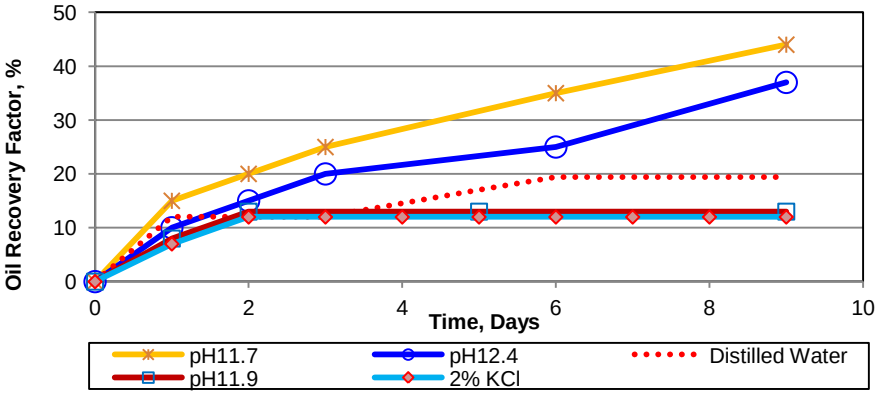

Figure 4.17 Oil recovery factors for the Eagle Ford Shale samples using different high pH solutions

The effect of high pH solutions on the spontaneous imbibitions of the Eagle Ford Shale samples was examined using pH 11.7 and 12.4 NaOH solutions. The color of the solutions changed to light and dark red for all samples due to the reaction of rock minerals with the NaOH solution (Figures 4.13 & 4.16). . The samples did show visible cracks (Figure 4.14), but became softer when exposed to 2 wt% NaOH solution solutions.

The highest oil recovery factor (44%) was from the sample exposed to pH 11.7 (0.1 wt% NaOH in distilled water) (Figure 4.17). There was an increase of 132% in the recovery factor when distilled water with 2 wt% NaOH was used compared with distilled water alone, which is believed to be due to wettability alteration. The rate of production was also accelerated when the alkaline solution was added to distilled water. The oil produced after 1.5 days using pH11.7 was almost the same (19%) as the total recovery achieved by distilled water alone. In contrast, high pH solutions resulted in lowered oil recoveries when used with distilled water. The oil recovery achieved by using pH 11.9 (2 wt% NaOH in distilled water) was about 13% compared with 19% when using distilled water alone. The reduction in the recovery factors achieved when using high alkaline concentrations (2 wt% NaOH) in distilled water, as opposed to brines, maybe due to the combination of clay swelling and mineral dissolution in alkaline solution that may result in pore plugging in some areas in the samples. This observation correlates well with the recovery factor (44%) achieved for low alkaline solutions (0.1 wt% NaOH), which is higher than the recovery factor (13%) achieved by the stronger alkaline solution (2 wt% NaOH). Also, there was early acceleration in the first days of oil production from the low alkaline solutions in distilled water compared with distilled water alone; the oil recovery of the high alkaline solution remained constant after the second day of the experiment.

In contrast to distilled water, high pH solutions (pH12.4 2wt% NaOH in 2wt% KCl) improved oil recovery from the Eagle Ford shale sample to about 37% compared to 12% from 2 wt% KCl base brine alone (Figure 4.17). The improvement in the oil recovery here is believed to be caused by wettability alteration by the alkaline solution, as the 2 wt% KCl base solution acts as a clay swelling inhibitor.

Figure 4.18 Barnett samples after one week of spontaneous imbibition in (a) pH11.9 (0.1 wt% NaOH in Distilled Water) (on the left side), (b) pH11.7 (2 wt% NaOH in Distilled water), and (c) pH12.4 (2 wt% NaOH in 2 wt% KCl) (on the right side)

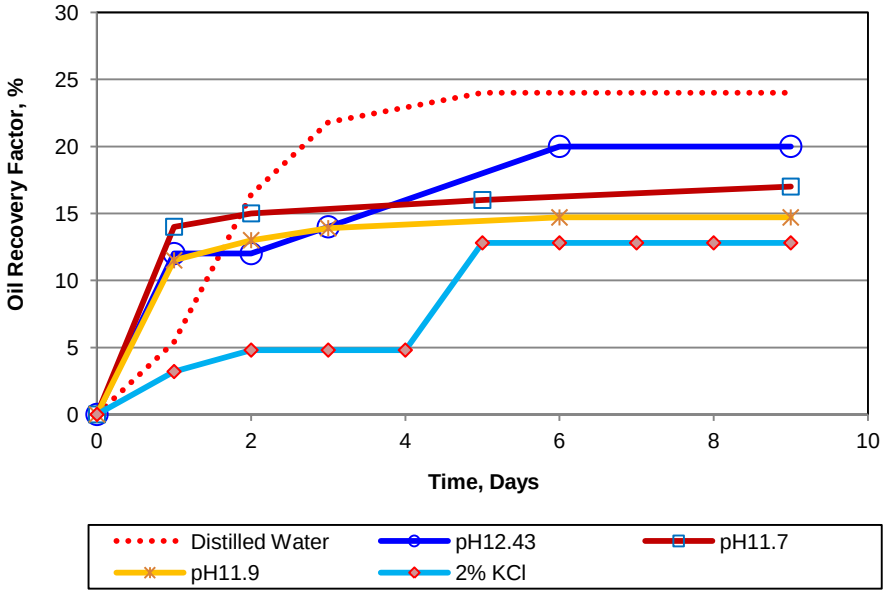

Figure 4.19 Oil recovery factors for the Barnett Shale samples using different high pH solutions

The effect of high pH solutions on the spontaneous imbibitions of the Barnett shale samples has been examined using pH11.7-12.4 NaOH solutions. The Barnett shale samples after one week in different alkaline solutions are shown in Figures 4.13 & 4.18. The color of the alkaline solutions changed to light and dark red for all samples due to the reaction of rock minerals with the NaOH solution. The color of the NaOH solutions for Barnett samples darkened with increasing alkalinity and salinity of solutions. Greater reactivity was observed when Barnett samples were exposed to 2 wt% NaOH solutions, compared to the partial damage in samples exposed to distilled

water or 2% KCl base solutions. The samples had cracks and displayed softness when exposed to 2 wt% NaOH solution with distilled water or with 2 wt% of KCl base solutions (Figure 4.18). While the Barnett samples exposed to 0.1 wt% NaOH solution in distilled water did not show the same damage as observed with 2 wt% NaOH solutions, the samples were still stable with no cracks (Figure 4.18).

The highest oil recovery factor was from the sample exposed to pH 12.4 (2 wt% NaOH in 2 wt% KCl base brine solution). This sample was significantly damaged due to significant mineral dissolution (Figure 4.18). The highest oil recovery using high pH solutions was about 20% (Figure 4.19). There is an increase of 56% in the recovery factor achieved by 2 wt% KCl brine solution when 2 wt% NaOH was added to the solution compared with 2% KCl brine solution alone . The rate of production was also accelerated when the alkaline solution was added to 2 wt% KCl base brine compared with using 2 wt% KCl solution alone. Oil produced after one day using pH 12.4 was almost equal (12%) to the total recovery achieved by 2 wt% KCl brine solution after five days. In contrast, high pH solutions prepared with distilled water resulted in lower oil recoveries. The oil recovery achieved by using pH 11.7 (0.1 wt% NaOH in distilled water) was about 17%, and 14.7% from pH 11.9 (2 wt% NaOH in distilled water), compared with 24% when using distilled water.

The reduction in the recovery factors observed when using alkaline solutions in distilled water may be due to the combination of clay swelling and mineral dissolution in alkaline solution. This observation correlates with observed recovery factors (17%) achieved by low alkaline solution (0.1 wt% NaOH). This is higher than the recovery factor (14.7%) achieved by the higher alkaline solution (2 wt% NaOH). Also, there was early acceleration in the first day recovery from the alkaline solutions in distilled water compared with distilled water alone, but the rate of production thereafter was much steeper and did not increase the same way as was observed with distilled water.

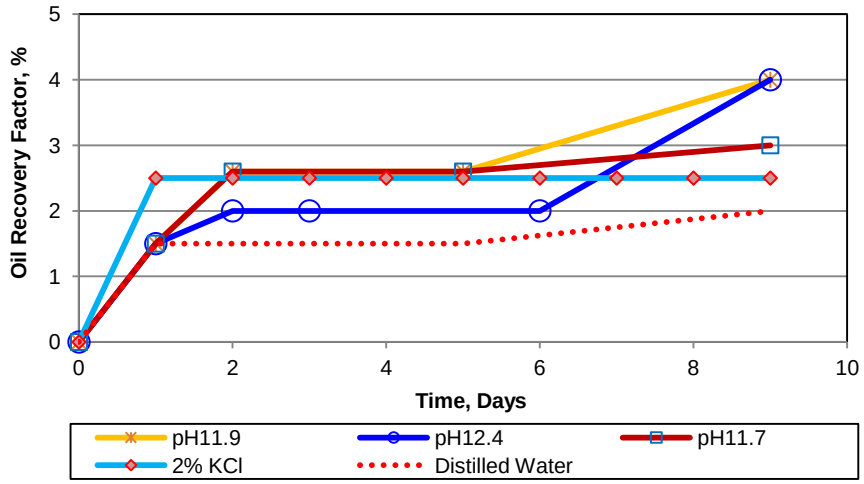

Figure 4.20 Oil recovery factors for Marcellus Shale samples using different high pH solutions

Marcellus Shale samples typically have very poor pore connectivity (Myers 2008), and did not respond well to any of the tested solutions; oil recovery factors achieved by the water spontaneous imbibition were very low. The effect of high pH solutions on the spontaneous imbibition of Marcellus Shale samples has been examined using pH 11.78-12.43 (0.1- 2 wt% NaOH) solutions. The color of the alkaline solutions changed to a light red color for all of the samples due to the reaction of rock minerals with the NaOH solution (Figure 4.13). The samples show cracks and softness when exposed to pH 11.9 (2 wt% NaOH in distilled water) or with pH 12.4 (2 wt% NaOH in 2 wt% of KCl base solution) (Figure 4.14). The oil recoveries of the high pH solutions were almost double the oil recovery achieved by distilled water or 2 wt% KCl solutions alone, but still the oil recovery factors are low (4%) (Figure 4.20). The improvement in the oil recovery might be due to wettability alteration. The rate of production was also accelerated when the alkaline solution was added to 2 wt% KCl base brine compared with using a 2 wt% KCl solution or distilled water. The more alkaline the solutions, the more oil recovered, particularly when the alkaline solution was prepared with distilled water or 2 wt% KCl solutions.

4.2.2 Effect of Alkaline (High pH) Solutions on Shale Rock Wettability

There was an improvement in spontaneous imbibition oil recovery from the tested shales in this study, which was postulated to be caused by wettability alteration when exposed to high pH solutions. To test this hypothesis, experiments to measure

the contact angles of all the samples used in the spontaneous imbibition experiments were designed.

The values of the measured contact angles correlate with the achieved oil recovery factors suggesting that rock wettability was altered by the high pH solutions in this study (Table 4.1). The initial contact angles of the tested shales were 12º from Mancos, 17º from Eagle Ford, 27º from Marcellus Shale samples, which is considered a water-wet rock. The measured values after exposure to the alkaline solutions were lower and may be interpreted as the rock becoming strongly water-wet. The contact angles of the pH 11.8 (0.1 wt% NaOH in distilled water) solution were slightly higher compared with the initial contact angles of the other samples soaked in higher alkaline solutions (2 wt% NaOH). It was also interesting to observe the change in solution pH values after one week of samples soaking (Table 4.1). The initial pH values were measured before samples were soaked, while the final pH values were measured after seven days of soaking. The pH values of most solutions increased after soaking, which is attributed to mineral dissolution.

Table 4.1 Measured contact angles for the used Shale samples soaked in different high pH solutions

Shale	Base Brine	Initial Contact Angle	Soaking Fluid	Initial pH at day 0	Temperature, ºF	Aging time, day	Final pH at day 7	Final Contact Angle
Mancos Shale	30 wt% KCl	12	0.1 wt% NaOH in DI water	11.78	150ºF	7	12.11	16
	30 wt% KCl	12	2 wt% NaOH in DI water	11.91	150ºF	7	12.43	5
	30 wt% KCl	12	2 wt% NaOH in 30 wt% of KCl	13	150ºF	7	12.87	3
Eagle Ford Shale	2wt% KCl	17	0.1 wt% NaOH in DI water	11.78	150F	7	12.11	20.4
	2wt% KCl	17	2 wt% NaOH in DI water	11.9	150F	7	12.43	5
	2wt% KCl	17	2 wt% NaOH in 2 wt% of KCl	12.43	150F	7	12.48	3
Marcellus Shale	2wt% KCl	27	0.1 wt% NaOH in DI water	11.78	150ºF	7	12.11	22
	2wt% KCl	27	2 wt% NaOH in DI water	11.91	150ºF	7	12.43	10
	2wt% KCl	27	2 wt% NaOH in 2 wt% of KCl	12.43	150ºF	7	12.48	5

4.2.3 Effect of Alkaline (High pH) Solutions on Shale Rock Hardness

High pH solutions affect samples hardness in different ways depending on which minerals are dissolved (section 4.3.1). Experiments to measure the hardness of the samples after one week of exposure to same solutions of spontaneous imbibtion experiments were designed. Four values were taken at different locations of each sample and the average hardness was recorded. The test procedure is the same as described in Section 2.8.3.

As seen in Section 4.1.3, the tested shales behave differently when exposed to the high pH solutions. While Eagle Ford and Marcellus only showed softness with no damage, Barnett was significantly damaged, but in contrast, the Mancos became more stable. The initial hardness values of the shales were 44,554 psi for Eagle Ford,

68,842 psi for Marcellus, and 11,405 psi for Mancos samples (Table 4.2). The hardness, as expected, declines when the samples were soaked in high pH solution, with values as low as 875.4 psi for Eagle Ford and 21,781 psi for Marcellus rock samples recorded. Meanwhile the higher pH solutions strengthened the Mancos samples (as seen in Section 4.1.3) with hardness values ranging from 18,628 to 27,667 psi compared with the initial hardness measured after exposure to 30% NaCl solution. The increase in Mancos rock hardness in high pH solutions prepared with 30% NaCl might be correlated to mineral dissolution in NaOH alkaline that could result in more stability conditions to the samples, which resulted in more stability compared with using 30% NaCl only. The values were measured at four locations in each sample to obtain an average value, but there was a higher standard deviation, which might be correlated with the higher heterogeneity degree in these samples.

Table 4.2 Measured hardness for the used shale samples soaked in different high pH solutions

Shale	soaking fluid	Conditions	Avg. BH (psi)
Eagle Ford	2 wt% KCL solution	Initial Conditions	44,553.6
	2 wt% NaOH in 2 wt% of KCl	After soaking	875.4
	2 wt% NaOH in DI water	After soaking	3,0891.1
Mancos	30% KCL solution	Initial Conditions	11,405.6
	0.1 wt% NaOH in DI water	After soaking	27,666.9
	2 wt% NaOH in DI water	After soaking	24,723.3
	2 wt% NaOH in 30 wt% of KCl	After soaking	18,628.7
Marcellus	2 wt% KCL solution	Initial Conditions	68,842.4
	0.1 wt% NaOH in DI water	After soaking	29,061.3
	2 wt% NaOH in DI water	After soaking	33,772.4
	2 wt% NaOH in 2 wt% of KCl	After soaking	21781.3

4.3 Potential of Surfactant Pre-flood to improve Waterflooding Performance in Shale Formations

This section presents a study of an experimental work done on Bakken Shale reservoir samples and crude oil with synthetic formation brine. The objective of the

section is to study the potential of preflood slugs of surfactants to improve waterflooding performance in shale formations by altering rock wettability. Reservoir rock samples from Bakken Shale were used in this experiment along with Bakken crude oil and synthetic brine. A series of experimental procedures were applied to test different surfactant to alter Bakken Shale wettability and improve recovery factors from spontaneous imbibition.

4.3.1 Surfactant Compatibility Test

In this test, synthetic 15%, and 30% brine solutions were used. The 30% brine represents in situ formation brine and 15% brine is used to represent the diluted formation water after waterflooding. Ten surfactants were tested in this screening step to identify the potential surfactants for later experiments. The recipe for synthetic brines is presented in Chapter 3.

After vigorous mixing of the synthetic brines and surfactants, the test tubes were set aside, and allowed to sit. All of the test tubes were placed in an oven held at 190°F. The clarity of each tube was monitored, and notes were taken of the appearance of each solution after sitting static for one week at 190°F. Several developmental and commercial available products were tested (Figure 4.21). One of the formulas, (Stim aid A) surfactant, showed no precipitation in 15% or 30% brine using 0.1 wt% and 0.2 wt% concentrations at 190°F after one week. Therefore, this study presents the results of this promising formula only.

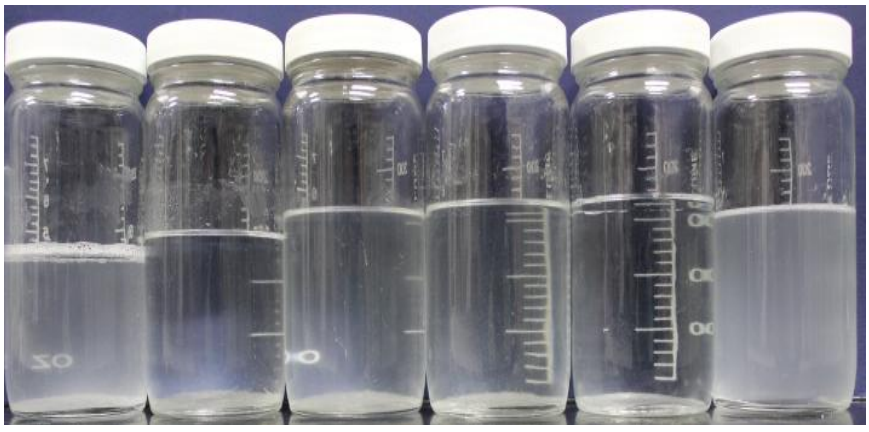

Figure 4.21 Brine compatibility test results for different surfactants after one week in 15% and 30% brines

4.3.2 Contact Angle Measurements

An oil drop (green) surrounded by water (blue) on a water-wet surface (left) forms a bead (Figure 4.22). The contact angle θ is approximately zero. On an oil-wet surface (right), the drop spreads, resulting in a contact angle of about 180°. An intermediate-wet surface (center) also forms a bead, but the contact angle comes from a force balance among the interfacial tension terms, which are γ_{so} and γ_{sw} for the surface-oil and surface-water terms, respectively, and γ_{ow} for the oil-water term.

Using of (Stim aid A) surfactant solutions could alter shale rock wettability, so the contact angles of all samples were measured before and after exposure to surfactant solutions. The contact angles were measured using fully oil-saturated samples in only brine solutions (15% and 30%) as an initial condition. The same samples were treated with 0.2 wt% of (Stim aid A) surfactant in 15% and 30% brine solutions for three hours, after which final contact angles were measured.

The initial measured contact angles for the Bakken samples were about 80º , which in turn means that Bakken Shale has almost equal preference to oil and water (Figures 4.23 and 4.24). After three hours of exposure with 0.2 wt% of (Stim aid A) in either 15% or 30% brine solutions, the shale contact angle was lowered to about 20º, which implies strongly water-wet characteristics (Figure 4.24). The change in shale wettability may enhance the release of oil from the rock as the surface rock preference to water increased and decreased to oil.

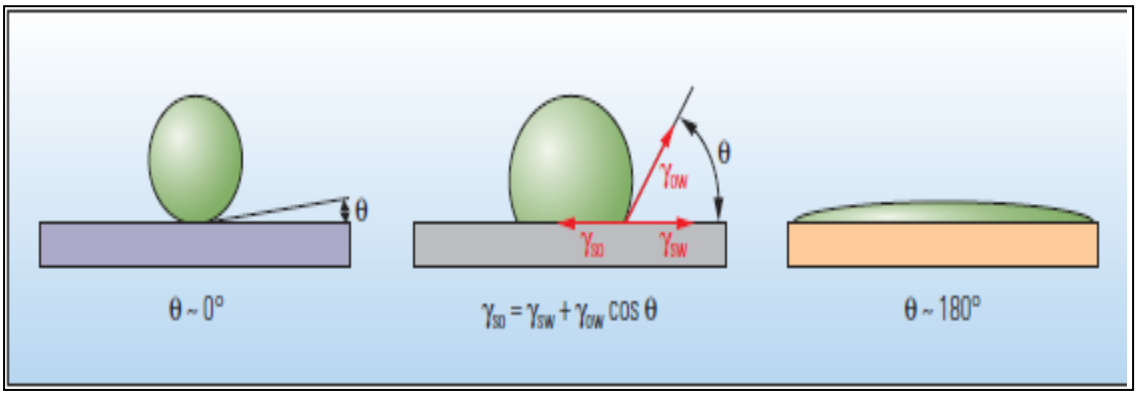

Figure 4.22 Contact angles identification after Abdallah *et al.* 2007

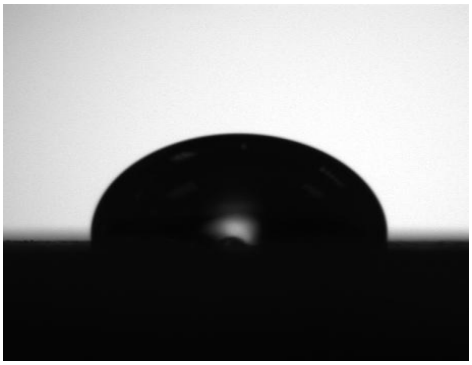

Figure 4.23 Water droplet on Bakken Shale core sample before surfactant treatment (initial contact angle measurement)

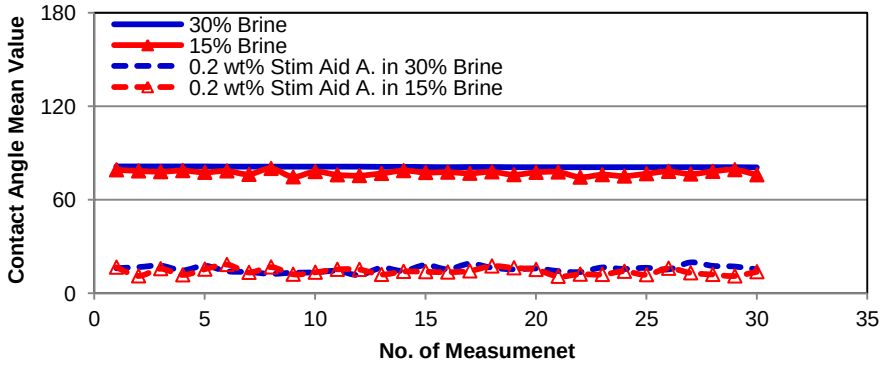

Figure 4.24 Average contact angles values for Bakken Shale cores

4.3.3 Spontaneous Imbibition Experiment

To simulate the effect of preflood surfactant treatment on continued oil production, the test formation material (crude oil and surfactant solutions in the pore systems) were tested. The Bakken reservoir samples were air dried, forced saturated/aged with Bakken crude oil, exposed to surfactant for one week, then air-dried again and forced saturated/aged with Bakken crude oil. Then the samples were placed into the Amott cell with brine only (15% and 30% Brines), no surfactant. Spontaneous water imbibition/oil production was recorded over time at 190°F. The average properties of the samples used in this study is presented in Table 4.3.

Table 4.3 Bakken Shale samples properties			
	Avg. Bulk Density, g/cc	Avg. Porosity, %	Solution of Imbibition
Set 1	2.74	4.93	15% Brine
Set 2	2.75	5.67	30% Brine
Set 3	2.74	6.11	15% Brine -previously treated with 0.1 wt% Stim aid A.
Set 4	2.76	5.63	15% Brine -previously treated with 0.2 wt% Stim aid A.
Set 5	2.75	6.23	30% Brine -previously treated with 0.1 wt% Stim aid A.
Set 6	2.75	6.40	30% Brine -previously treated with 0.2 wt% Stim aid A.

Figures 4.25 and 4.26 indicate additional oil production from cores pre-treated in 0.1 and 0.2 wt% (Stim aid A.) surfactant in 15% and 30% brines (30-32%). The higher recovery was attributed to surfactant adsorption on the rock surface, altering the wetting preference during the pre-treatment of surfactant as supported by the contact angles and visual wettability experiments results.

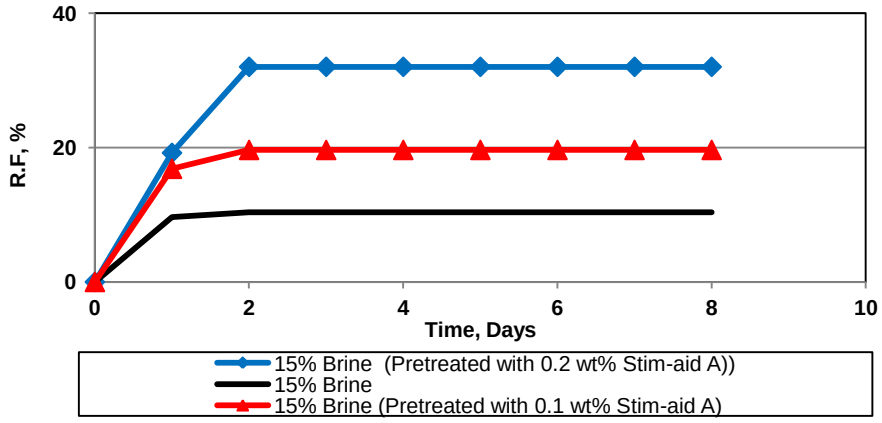

Figure 4.25 Oil recoveries from Bakken Shale Cores in 15% Brine

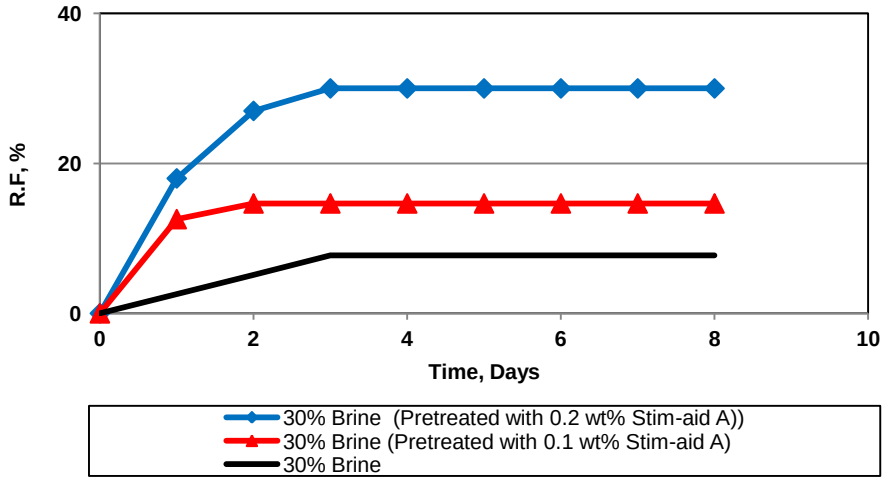

Figure 4.26 Oil recoveries from Bakken Shale cores in 30% Brine

4.4 Conclusions

Waterflooding performance in fractured reservoirs and especially shale formation depends mainly on water imbibition due to the ultra low permeability of such reservoirs. Thus, the objective of this study was to enhance water imbibition oil recovery factors in shale formation using water with different salinities, alkaline concentrations, and surfactant concentrations. The study presented experiments on different shales (Eagle Ford, Mancos, Barnett, Marcellus, and Bakken). The role of each mechanism was examined by studying shale oil recovery, stability, and wettability using different water formulations. The study conclusions may be summarized as follows:

1. Mancos samples were sensitive to distilled water, which resulted in whole sample damage due to clay swelling, while Barnett and Marcellus showed along bedding cracks and Eagle Ford showed no visual cracks.
2. All shale samples exposed to distilled water recovered more oil compared with 2 wt% KCl or 30% KCl due to clay swelling in distilled water.
3. Bakken reservoir samples recovered more oil when exposed to 15% brine solution compared with 30% brine due to wettability alteration.
4. High pH solutions caused the most damage to Barnett samples.
5. Oil recovery of the Barnett shale sample was improved by 56% when 2 wt% NaOH solution was added.

6. High pH solutions did not improve oil recoveries from the Barnett samples when mixed with distilled water possibly due to pore plugging after mineral dissolution and reprecipitation and/or clay swelling.
7. Oil recovery factors from the Eagle Ford Shale were enhanced by mineral dissolution and wettability alteration using high pH solutions.
8. Eagle Ford, Mancos, and Marcellus Shale wettability was altered to strongly water-wet by using high pH alkaline solutions.
9. Eagle Ford Shale samples lost about 93-98% of its hardness when exposed to high pH solutions (2 wt% NaOH in distilled water and in 2 wt% KCl).
10. The rock hardness of Marcellus Shale samples was significantly reduced when using high pH solutions; a 50 to 68% loss in hardness was recorded.
11. Bakken oil recovery was enhanced by wettability alteration when samples were pretreated with 0.2 wt% of (Stim aid A.) surfactant either in 15% or 30% synthetic formation brine solutions.

Chapter 5

Numerical Simulation of Waterflooding in a sector Model in the Eagle Ford Shale Formation

5.1 Model Description

To study the potential of waterflooding in the Eagle Ford Shale formation, a numerical simulation study for a sector model was implemented. The 3D model represents a section between a pair of horizontal oil producer and water injector in the Eagle Ford Shale formation. Both wells are assumed to be stimulated by a set of multi-stage hydraulic fractures, with well spacing of 660 ft (in Y-direction), fracture half-length of 500 ft, and fracture spacing of 300 ft (Figure 5.1).

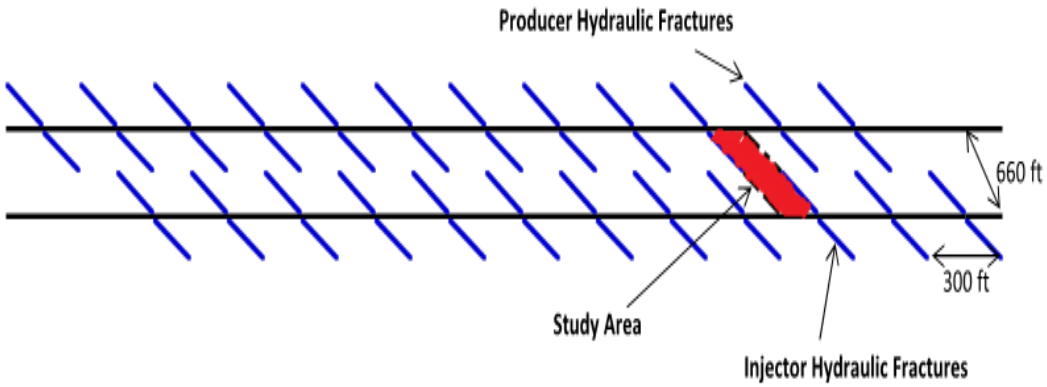

Figure 5.1 Schematic of two multi-stages hydraulically fractures horizontal Wells, showing the study area between the producer fracture and injector fracture

The spacing between the oil producer fracture and the water injector fracture is assumed to be 150 ft (in X-direction). Fracture network created during hydraulic fracturing is modeled using locally refined grids with single porosity approach. These grids are highly permeable and represent main flow path between the injector and producer. Figure 5.1 shows the producer and injector fractures, with locally refined grids, used in all the simulation study. The dimensions and properties of this model

are based on published information on the Eagle Ford Reservoir (Chaudhary *et al.* 2011).

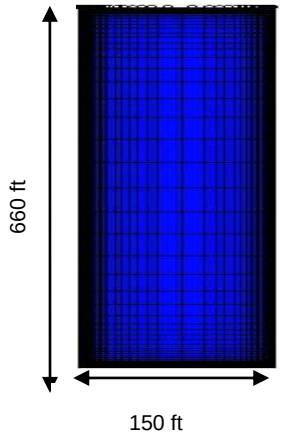

Figure 5.2 Study area base model with one fracture in the horizontal injector and one fracture in the horizontal producer with locally refined grids

The basic model is 49x65x5 with 15,925 grids. The average initial reservoir pressure is 7350 psi and the well produces for 30 years at a minimum pressure constraint of 2500 psi. Reservoir, hydraulic fracture, PVT properties, and relative permeability end points for matrix and fracture are presented in Tables 5.1 through 5.4. The simulation code for the depletion base case is presented in Appendix A.

Table 5.1 Reservoir properties for the Eagle Ford Shale oil formation	
Initial Reservoir Pressure, psi	7350
Porosity in Shale, %	9
Initial Water Saturation, %	30
Compressibility of Shale, psi^{-1}	5.10-6
Permeability of Shale, m.d	0.0013
Reservoir Thickness, ft	290
Depth, ft	10500

Table 5.2 Hydraulic fracture properties for the Eagle Ford Shale oil formation	
Fracture Stages	12
Fracture Spacing, ft	300ft.
Fracture Permeability, md	83.3
Fracture Half-length, ft	500
Fracture width, ft	1

Table 5.3 PVT properties of the Eagle Ford oil	
Reservoir Temperature, °F	320
Bubble Point for Oil, psi	2500
API for Oil	42°
Gas Specific Gravity	0.8

Table 5.4 Relative permeability end points for fracture and matrix		
	Matrix	Fracture
N_o	5	1.5
N_g	2	1
S_{wi}	0.3	0.05
S_{org}	0.3	0.1
S_{gc}	0.05	0
K_{rg} at S_{org}	1	1

In the natural depletion drive case, the two horizontal wells were on production mode for the whole 30 years. While, in the waterflooding case, only one well was producing for 30 years and the other well produced only for five years and then converted to injection mode. The vertical to horizontal permeability for the base case was assumed as 0.1. To better optimize and understand waterflooding in the Eagle Ford Shale formation, different sensitivity cases were implemented towards the basic waterflooding model that is shown in Figure 5.2. The sensitivity cases including the effect of the spacing between the producer and injector fractures, fracture half-length, and vertical to horizontal permeability ratio.

5.2 Base Case Results

Figures 5.3 and 5.4 show the average reservoir pressure variation, over a period of 30 years under natural depletion drive and waterflooding in and around the hydraulic fracture and Figure 5.5 shows the oil saturation after 30 years for the natural depletion drive and waterflooding cases.

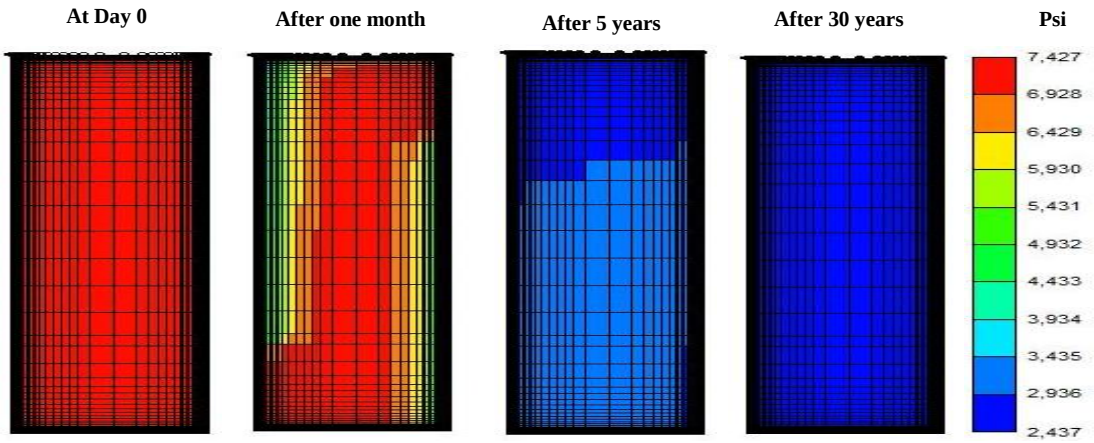

Figure 5.3 Average reservoir pressure profile for the natural depletion drive base case at different times

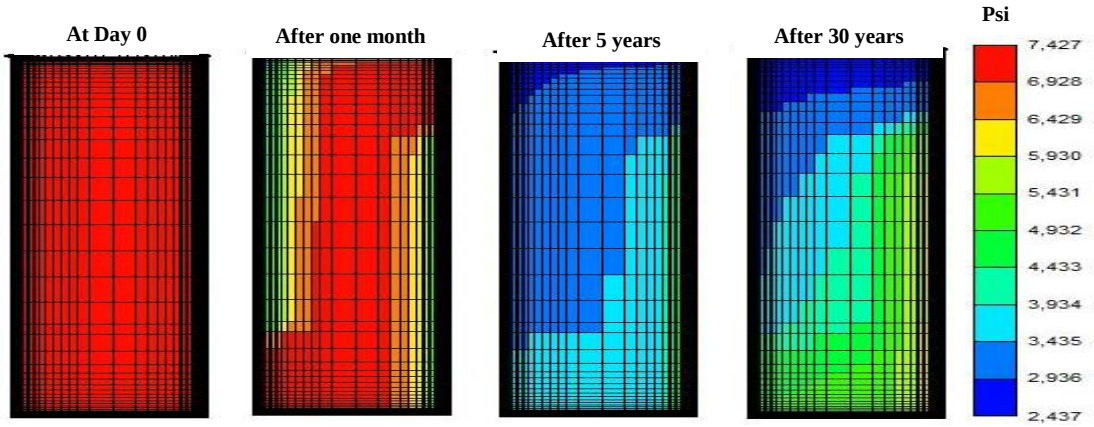

Figure 5.4 Average reservoir pressure profile for the waterflooding base case at different times

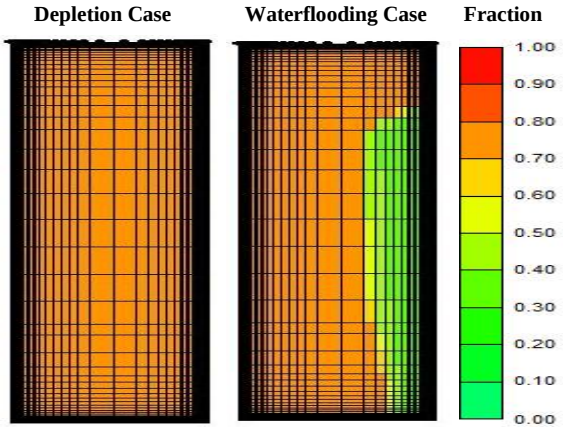

Figure 5.5 Oil saturation profile after 30 years for both natural depletion and waterflooding base cases

The average reservoir pressure in Figure 5.3 declined rapidly as the recovery in this reservoir was mainly produced by depletion drive and some solution gas drive.

The reservoir pressure decreased inside the fracture from an initial pressure of 7350 psi to about 5,000 psi after only one month of production, around 2500 psi after 5 years, and after that the pressure stayed almost constant till the end of 30 years as there was not much production from the reservoir. The pressure was maintained higher in the case of waterflooding, which could reduce the in-situ stress in the formation (Figure 5.4)

The oil saturation (Figure 5.5) did not change after 30 years under the natural depletion drive around the fractures, which confirms that the production was mainly coming from the fractures. For the waterflooding case, the oil saturation changed in and around the hydraulic fracture of the injector indicating that the water did not only move through fractures, but also across the matrix system which when applied to real reservoirs may cause opening of the micro-fractures and improve oil recovery as described by Fakcharoenphol *et al.* (2012).

The overall recovery factor of the simulated section was about 18% for the case of waterflooding and 12% for the case of natural depletion drive (Figure 5.6). Cumulative oil, cumulative gas, and daily oil curves for the natural depletion drive and waterflooding cases are shown in Figures. 5.7 through 5.9. Because of increased reservoir pressure, the oil rate in the producer increased.

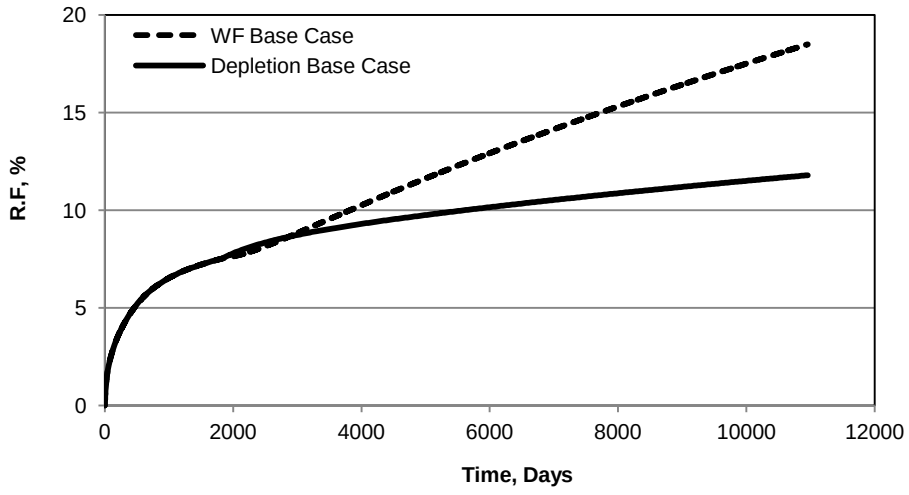

Figure 5.6 Oil recovery factors of the natural depletion and waterflooding (WF) base cases

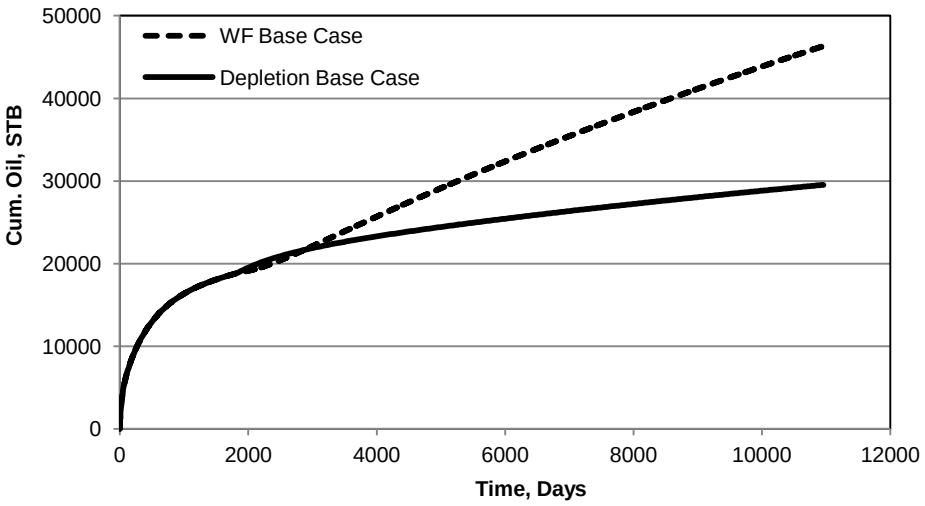

Figure 5.7 Cumulative oil production of the natural depletion and waterflooding (WF) base cases

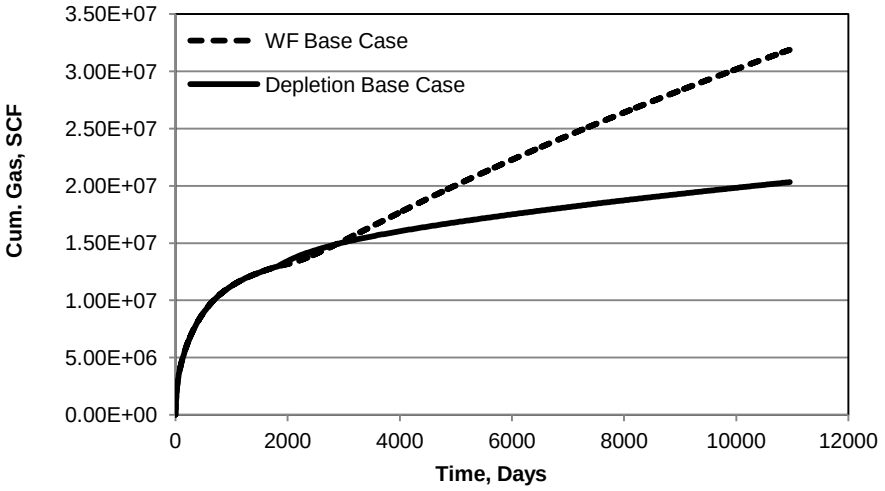

Figure 5.8 Cumulative gas production of the natural depletion and waterflooding (WF) base cases

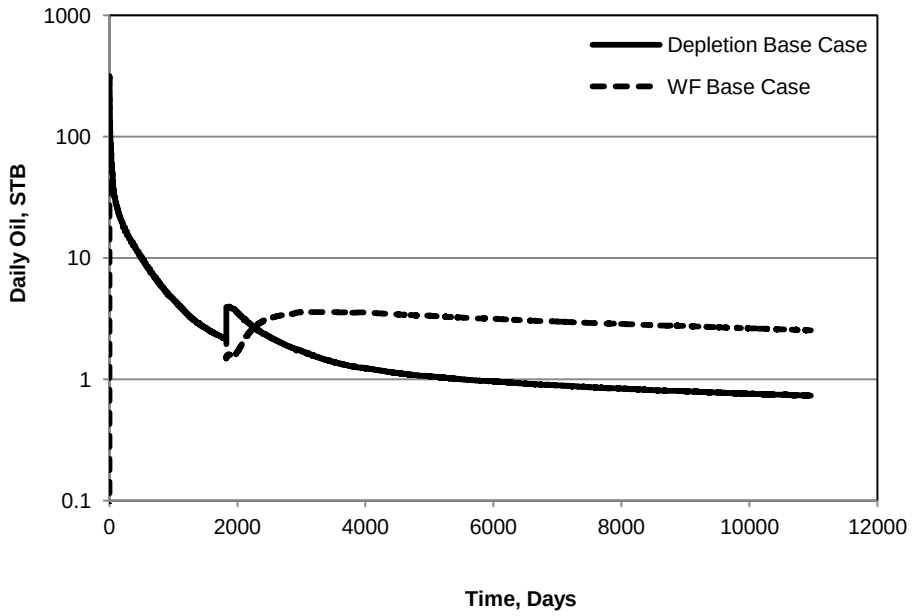

Figure 5.9 Daily oil production of the natural depletion and waterflooding (WF) base cases

5.3 Sensitivity Cases Results

Three main sensitivity cases were examined in this study; fracture half-length, fracture spacing between producer and injector, and vertical to horizontal permeability. Waterflooding performance was significantly affected by fracture half-length, the oil recovery changed from 8% using 200 ft fracture half-length to 12% using 330 ft to 18% using 500 ft (Figure 5.10). The oil recovery increases as fracture half-length increases as both producer and injector fractures get close and that helps the water to better displace oil between fractures.

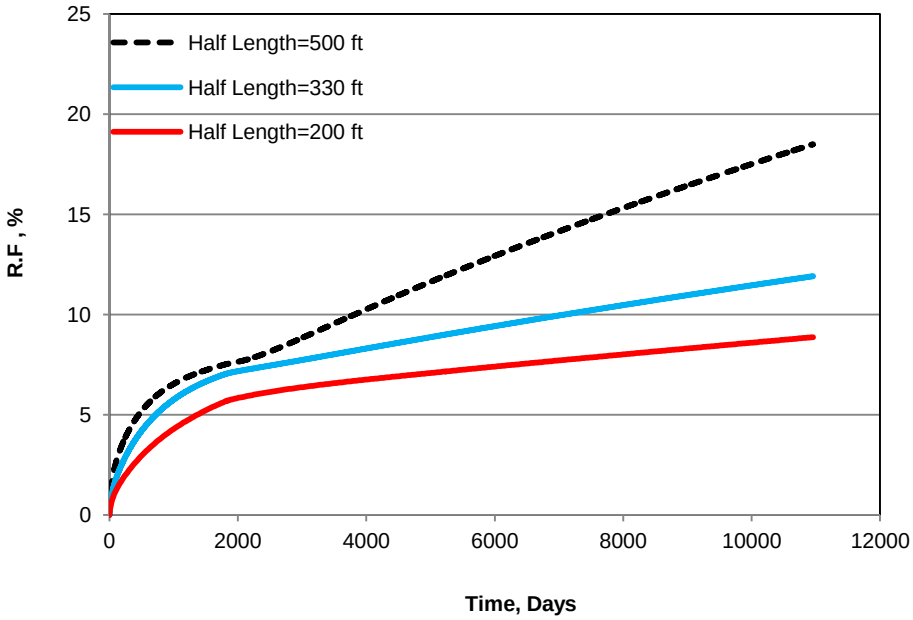

Figure 5.10 Oil recovery factors of the half-fracture length sensitivity cases

The sensitivity of waterflooding performance gets higher for the case of spacing between the producer and injector fractures as the oil recovery was 11% using spacing of 200 ft, 18% using 150ft, and 20% using 50 ft (Figure 5.11). The closer the producer fracture to the injector fracture, the higher the efficiency of the water to displace oil in the area between the fractures.

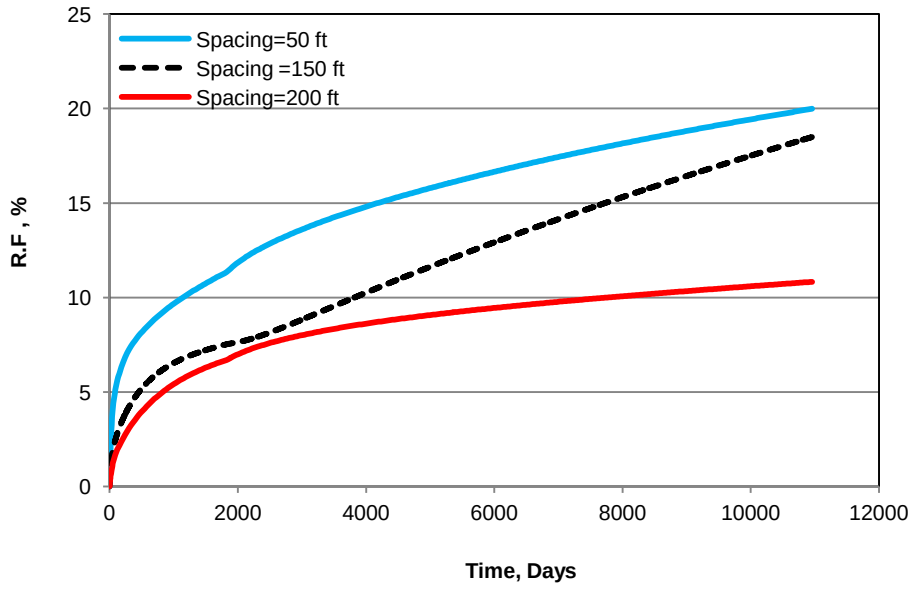

Figure 5.11 Oil recovery factors of the spacing sensitivity cases

The most influential parameter for waterflooding performance in this study was the vertical to horizontal permeability ratio as the oil recovery was 21% when modeled with equal permeability (Kv/Kh=1), 18% when modeled with 0.1 ratio and 13% when 0.01 ratio was used (Figure 5.12). Unfortunately, shale formations are very heterogonous in all directions, but with the existence of natural fractures and the expected extended fracture network resulting from waterflooding, recoveries may be improved.

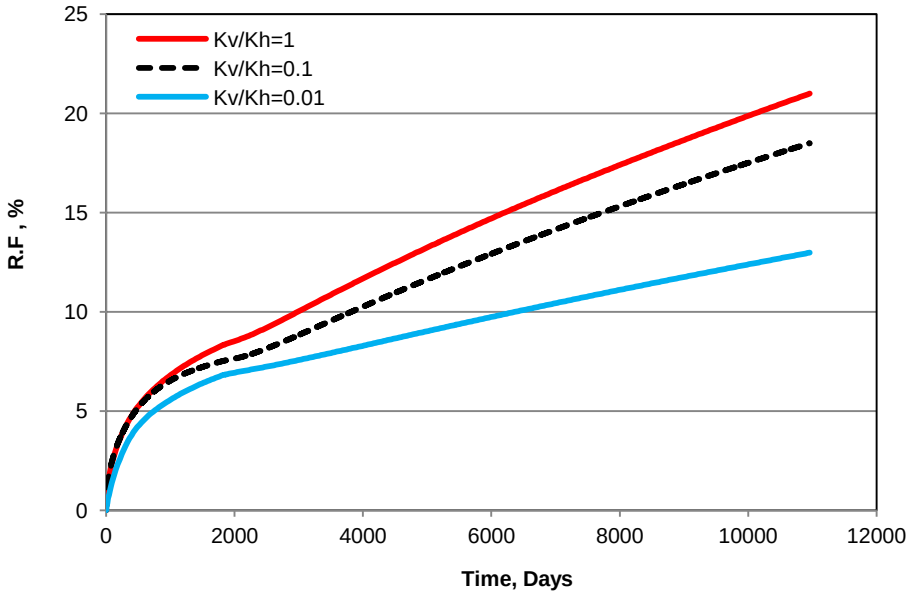

Figure 5.12 Oil recovery factors of the Kv/Kh sensitivity cases

5.4 Conclusions

Chapter 5 presented a simulation study on the Eagle Ford Shale formation to investigate the potential of wateflooding in the field using Eagle Ford reservoir published data. A black-oil simulator owned by Computer Modeling Group Ltd was used in this study to simulate depletion and waterflooding production strategies. 15,925 (49*65*5) grid-cells were used to build the reservoir model. The 3D model represents a section between a pair of horizontal oil producer and water injector in the Eagle Ford Shale formation. In addition, a number of sensitivity cases were modeled to study the effect of fracture half-length, fracture spacing, and permeability anisotropy on waterflooding recovery factors.

The simulation study using Eagle Ford reservoir fluid and rock data and completion data revealed a good potential for waterflooding using closer spacing between the oil producer and the water injector fractures that forced the injected water to invade the hydraulic created fractures, natural fractures, and the reservoir matrix as well, which maximized the oil recovery.

Chapter 6
Conclusions and Recommendations

This dissertation is a study investigating and evaluating the potentials of mechanisms to improve oil production from shale formations. The study covers improved oil recovery for primary and secondary stages of production. The main objective was to assess the viability of different techniques to improving oil recovery from shale formation by improving shale properties and water imbibitions. This chapter contains a summary of this study. Ideas for future work based this dissertation are then presented.

6.1 Summary and Conclusions

Shale is considered as not only a petroleum source, but also a great potential for future oil and gas resources especially in North America where significant exploration activities are underway. Shales could not be so successful without hydraulic fracturing combined with horizontal drilling techniques. However, shale oil and gas wells suffer from rapid production decline compared with conventional wells.

The complex characteristics of shales in terms of mineralogy, geology, and heterogeneity make them unique in their treatment and production performance compared to conventional reservoirs. Primary production of shales is not sustained because of conductivity loss and secondary recovery "waterflooding" is an immature technique. Due to such challenges, this study was designed to help industry improve primary and secondary oil recovery from shale formations.

In order to improve primary oil recovery of shale oil formations, the potential of combining matrix acidizing and propped hydraulic fracturing was investigated. Low acid concentrations (1-3 wt%) were used for matrix acidizing experiments, which is considered lower compared to the concentrations used for conventional reservoirs (typically 15 wt% HCl). Lower HCl concentrations are preferred because shales are ductile compared to sandstone and carbonate reservoirs and excessive softening could result in fine particle migration, which causes formation damage. Matrix acidizing was applied to North America shale rocks (Eagle Ford, Mancos, Barnett, and Marcellus) and evaluated using many techniques. Chapter 2 showed the effects of matrix acidizing on shale porosity, mechanical, wettability,

and primary oil recovery. The lower acid concentrations improved shale samples' average porosity and created new cracks that improved primary oil recovery when exposed to water. Shale wettability also was altered towards strongly water-wet when exposed to HCl solutions. However, lower acid concentrations significantly reduced affected hardness and showed a great reduction in shale compressive strength.

Chapter 3 presented another mechanism to improve primary oil recovery by optimizing surfactant additives in well stimulation fluid. This study was completed on Bakken Shale reservoir samples, crude oil, and synthetic formation water. The study was initiated to enhance primary oil recovery by changing fracture surface wettability. Different surfactants were pre-screened in this study to see if they are compatible with the formation water, oil, and different fracture fluids typically used for Bakken shale. Only one surfactant (Stim aid A.) out of the tested commercial surfactants was fully compatible with Bakken shale and used after for spontaneous imbibition experiments to measure its ability to alter Bakken Shale wettability and improve oil recovery. The study showed a good compatibility between Stim Aid A. surfactant and formation brine, Bakken crude oil, and stimulation fluids. The primary Bakken recoveray factors using different surfactant concentration were improved from about 7% to 30% due to wettability alteration by surfactant from intermediate/mixed wettability towards strongly water-wet.

Chapter 4 presented a detailed study to improve (waterflooding) secondary oil recovery of shale formations using different water formulations. Waterflooding performance in fractured reservoirs and especially shale formation depends mainly on water imbibition due to the ultra low permeability of such reservoirs. Thus, the objective of this study was to enhance water imbibition oil recovery in shale formation using water with different salinities, alkaline concentrations, and surfactant concentrations. The study presented experiments on different shales (Eagle Ford, Mancos, Barnett, Marcellus, and Bakken). The role of each mechanism was examined by studying the shale recovery factor, rock stability, and wettability using different water formulations. The three tested methods were able to improve shale secondary oil recovery by enhancing water imbibition oil recovery through wettability alterations and creation of cracks in different directions due to mineral dissolutions. Water with different salinities greatly affected Mancos Shale recovery as the shale was very sensitive to water salinity as it may only be stable at higher salinity ranges

(<15 wt%), while Barnett and Marcellus were slightly affected using fresh water, and showed cracks along bedding that helped release oil in water imbibition experiments. Eagle Ford samples did not show visible cracks, but its recovery was improved by natural fracture opening when exposed to fresh water. By a different mechanism, alkaline solutions only affects Barnett samples through clay dissolution, while other shales showed a reduction in rock hardness and wettability alteration towards strongly water wet. Surfactant solutions were also able to alter Bakken Shale rock wettability to improve secondary oil recovery.

Chapter 5 presented a simulation study done on Eagle Ford Shale formation to investigate the potential of wateflooding in the field using Eagle Ford reservoir published data. A black-oil simulator owned by Computer Modeling Group Ltd was used in this study to simulate depletion and waterflooding production strategies. 15,925 (49*65*5) grid-cells were used to build the reservoir model. The 3D model represents a section between a pair of horizontal oil producer and water injector in the Eagle Ford Shale formation. In addition, a number of sensitivity cases were developed to study the effect of fracture half length, fracture spacing, and permeability anisotropy on waterflooding recovery factors. The simulation study using Eagle Ford reservoir fluid and rock data with completion data revealed a good potential for waterflooding using closer spacing between the oil producer and the water injector fractures that forced the injected water to invade the hydraulic created fractures, natural fractures, and the reservoir matrix as well, which maximized the oil recovery.

6.2 Recommendations

1. The results of this study recommend using low acid concentrations (up to 2 wt%) slugs deep in shale formations as part of the propped hydraulic fracturing process, and not only around the wellbore.
2. Mud acid needs to be investigated to study its impact on silica-rich shales (such as Mancos, Marcellus, and Barnett).
3. The studied Stim Aid A. surfactant may be used as an enhanced stimulation surfactant to improve primary oil recovery and as a pre-flood surfactant to

improve secondary oil recovery (waterflooding) with an optimum concentration of 0.2 wt%.

4. More analysis is needed to study the effect of water salinity on shale recovery using formation water formulations.
5. Different alkaline solutions need to be studied for their ability to change shale rock wettability and oil recovery as well.
6. Imbibition results are not only important to understand waterflooding performance in shales, but also can help industry to overcome the trapped water stayed behind induced hydraulic fractures though enhancing shale water imbibition.
7. These results are encouraging to consider waterflooding as a secondary recovery method in shale formations especially with the high cost of re-fracking to restore production rates.

Bibliography

Akin S., Schembre J.M., Bhat S.K., ve Kovscek A.R.: "Spontaneous Imbibition Chracteristics of Diatomite" J. Pet. Sci. Eng., (25), 3-4, 149-165, 2000.

Akrad, O., Miskimins, J., and Prasad, M. 2011. The Effects of Fracturing Fluids on Shale Rock Mechanical Properties and Proppant Embedment. Paper SPE 146658 presented at the SPE Annual Technical Conference and Exhibition, Denver, 30 October - 2 November.

Abousleiman, Y.N., Hoang, S.K., Tran, M.H. Mechanical characterization of small shale samples subjected to fluid exposure using the inclined direct shear testing device. International Journal of Rock Mechanics and Mining Sciences 2010, 47, 355–367.

Abdallah W. Buckley J.S. Carnegie A. *et al.* Fundamentals of Wettability. Oilfield Review Summer 2007. 44-61. http://www.ingenieria.unam.mx/~vharana/archivos/cdy/articulos/Art%2006%20Sep%2014%202013%20Fundamentals%20of%20Wettability.pdf

Alexander, T.; Baihly, J.; Boyer, C.; Clark, B.; Waters, G.; Jochen, V.; Le Calvez, G.; Lewis, R..; Thaeler, J.; and Toelle, B.E. Shale Gas Revolution. Oilfield Review Autumn 2011: 23, no. 3, 40-57.

Anderson, D. S., and Harris, N. B. (2006). Integrated Sequence Stratigraphic and Geochemical Resource Characterization of the Lower Mancos Shale, Uinta Basin, Utah (Vol. Open-File Report, pp. 219). Salt Lake City: Utah Geological Survey.

Bennion D.B., Thomas F.B., Bietz R.F., *et al.* 1996. Water and Hydrocarbon Phase Trapping in Porous Media—Diagnosis, Prevention and Treatment. JPT Journal, December 1996, Volume 35, No. 10.

Borstmayer K., Stegent N., Wagner A. *et al.* Approach Optimizes Completion Design. The American Oil and Gas Reporter. August 2011. http://www.halliburton.com/public/pe/contents/Papers_and_Articles/web/A_through_P/Eagle%20Ford%20-%20Approach%20Optimizes%20Completion%20Design.pdf (Accessed March 2013).

Bale A., Smith M. B., and Henry Klein H. H. 2010. Stimulation of Carbonates Combining Acid Fracturing With Proppant (CAPF): A Revolutionary Approach for Enhancement of Final Fracture Conductivity and Effective Fracture Half-Length. SPE- 134307-MS presented at SPE Annual Technical Conference and Exhibition, Florence, Italy, 19-22 September 2010. http://dx.doi.org/10.2118/134307-MS.

B. Wu and C.P. Tan. Effect of Shale Bedding Plane Failure On Wellbore Stability - Example From Analyzing Stuck-Pipe Wells. ARMA-10-350. Presented at the 44th U.S. Rock Mechanics Symposium and 5th U.S.-Canada Rock Mechanics Symposium, 27-30 June 2010, Salt Lake City, Utah.

Bruner K. R. and Smosna R.. 2011. A Comparative Study of the Mississippian Barnett Shale, Fort Worth Basin, and Devonian Marcellus Shale, Appalachian Basin. DOE/NETL-2011/1478. National Energy Technology Laboratory (NETL). U.S. Department of Energy. http://www.netl.doe.gov/technologies/oil-gas/publications/brochures/DOE-NETL-2011-1478%20Marcellus-Barnett.PDF (accessed 02 March 2013).

Bleam, W. F. ReV. Geophys. 1993, 31, 51-73.
Boek, E. S.; Coveney, P. V.; Skipper, N. T. J. Am. Chem. Soc. 1995, 117, 12608-12617.

Boyce, M. L., and Carr, T. R. (2009). Lithostratigraphy andPetrophysics o f the Devonian Marcellus Interval in West Virginia and Southwestern Pennsylvania. Paper presented at the 29th Annual GCSSEPM Foundation Bob F. Perkins Research Conference, Houston, TX, USA. http://search.proquest.com/docview/916837583?accountid=14677.

Chaudhary A. S., Ehlig-Economides C. and, Wattenbarger R. 2011. Shale Oil Production Performance from a Stimulated Reservoir Volume. SPE-147596-MS presented at the SPE Annual Technical Conference and Exhibition, Denver, Colorado, USA, 30 October-2 November 2011. http://dx.doi.org/10.2118/147596-MS.

Chang, F.-R. C.; Skipper, N. T.; Sposito, G. Langmuir 1995, 11, 2734-2741.
Cuiec L., Bourbiaux B., Kalaydjian F.: "Oil Recovery by Imbibition in Low-Permeability Chalk," SPE Formation Evaluation Sept. 1994, 200-208.

Cooke Jr., C.E., Williams, R.E., Kolodzie, P.A., 1974. Oil Recovery by Alkaline Waterflooding. *J. Pet Tech* 26(12): 1365-1374. SPE- 4739-PA. http://www.onepetro.org/mslib/servlet/onepetropreview?id=00004739.

Chang, F.-R. C.; Skipper, N. T.; Refson, K.; Greathouse, J. A.; Sposito, G. In Mineral-Water Interfacial Reactions: Kinetics and Mechanism; Sparks, D. L., Grundl, T. J., Eds.; American Chemical Society: Washington, DC, 1999; pp 88-106.

Ciminelli V.S.T. and Osseo-Asare K., 1995. Kinetics of Pyrite Oxidation in Sodium Hydroxide Solutions. Metallugical and Materials *Trans* B. Volume 26B: 677-685, August 1995. http://link.springer.com/article/10.1007%2FBF02651713?LI=true#page-1 (accessed 20 March 2013).

Cha´vez-Pa´ez, M.; Van Workum, K.; De Pablo, L.; De Pablo, J. J. J. Chem. Phys. 2001, 114, 1405-1413.

C.C Plummer; McGeary; Carlson Physical Geology, 8th Edition; McGraw-Hill Companies: Boston, MA.1999 577 p

Das, P., Achalpurkar, M., and Pal, O. SPE-167787. Impact of Formation Softening and Rock Mechanical Properties on Selection of Shale Stimulation Fluid: Laboratory Evaluation. Presented at SPE/EAGE European Unconventional

Resources Conference and Exhibition, Vienna, Austria. 25-27 February 2014. http://dx.doi:10.2118/167787-MS.

D.H. Gray and R.W. Rex, Clays Clay Miner., 14 (1966) 355.

De Swaan A.: "Theory of Waterflooding in Fractured Reservoirs," SPEJ, 117-122, April 1978.

Dill W. and Smolarchuk P. 1988. Iron Control In Fracturing And Acidizing Operations. J. Cdn. Pet. Tech 27(3). SPE-88-03-08. May-Jun 1988. http://dx.doi.org/10.2118/88-03-08

Delville, A. J. Phys. Chem. 1995, 99, 2033-2037.

D.B. Bennion, D.W. Bennion, F.B. Thomas, and R.F. Bietz. Injection Water Quality-A key Factor to Successful Waterflooding. JCPT June 1998, Vol. 37. No. 6.

Emadi, H., Soliman, M., Samuel, R., Ziaja, M., Moghaddam, R., and Hutchison, S. SPE- 166250. Experimental Study of the Swelling Properties of Unconventional Shale Oil and the Effects of Invasion on Compressive Strength. Presented at SPE Annual Technical Conference and Exhibition, New Orleans, Louisiana, USA, 30 September-2 October, 2013. http://dx.doi:10.2118/166250-MS

Energy Information Administration (EIA). 2011. Annual Energy Outlook Report 2011. http://www.eia.doe.gov/oiaf/aeo/.

EOG Resources Company Annual Report on Form 10-K. December 31th 2009. http://investor.shareholder.com/eogresources/sec.cfm?DocType=andDocTypeExclude=andSortOrder=FilingDate%20DescendingandYear=andPagenum=24andCIK=

EL Shaari N., Minner W.A., and LaFollette R.F. 2011. Is there a "Silver Bullet Technique" to Stimulating California. SPE- 144526-MS presented at SPE Western North American Region Meeting Anchorage, Alaska, USA, 7-11 May 2011. http://dx.doi.org/10.2118/144526-MS.

Foster, M.D. (1955) The relationship between composition and swelling in clays: in Clays and Clay Minerals, Proc. 3rd NatL Conf., Houston, Texas, 1954, W. O. Milligan, ed., NatL Acad. Sci. Natl. Res. Counc. PubL 395, Washington, D.C., 205-220.

F.O. Jones, J. Pet. Technol., 16 (1964) 441.

Final Oil Shale and Tar Sands (OSTS), 2012, Oil Shale Development Background and Technology Overview. Volume 4 -Appendix A.

Fontaine J., Johnson N., and Schoen D. 2008. Design, Execution, and Evaluation of a "Typical" Marcellus Shale Slickwater Stimulation: A Case History. SPE-117772-MS presented at SPE Eastern Regional/AAPG Eastern Section Joint Meeting, Pittsburgh, Pennsylvania, USA, 11-15 October 2008. http://dx.doi.org/10.2118/117772-MS.

Fernø, M. A., Haugen, Å., and Graue, A. 2012. Surfactant Prefloods for Integrated EOR in Fractured, Oil-Wet Carbonate Reservoirs. Paper SPE-159213-MS presented at the SPE Annual Technical Conference and Exhibition, San Antonio, Texas, 8-10 October.

Gomez, S. and He, W. 2012. "Fighting Wellbore Instability: Customizing Drilling Fluids Based on Laboratory Studies of Shale-Fluid Interactions." SPE 155536, IADC/SPE Asia Pacific Drilling Technology Conference, Tianjin, China, 9-11 July. http://dx.doi.org/10.2118/155536-MS.

Grieser B., Wheaton B., Magness B., Blauch M. and Loghry R. 2007. Surface Reactive Fluid's Effect on Shale. SPE- 106815-MS presented at Production and Operations Symposium, Oklahoma City, Oklahoma, U.S.A., 31 March-3 April 2007. http://dx.doi.org/10.2118/106815-MS.

Guo Q., Ji L., Rajabov V., and Friedheim J., Portella C.,and Wu R., 2012. Shale Gas Drilling Experience and Lessons Learned From Eagle Ford. SPE-155542-MS presented at SPE Americas Unconventional Resources Conference, Pittsburgh, Pennsylvania USA. 5-7 June 2012. http://dx.doi.org/10.2118/155542-MS.

Fakcharoenphol P., Charoenwongsa S., Kazemi H., *et al.* 2012. The Effect of Water Induced Stress to Enhance Hydrocarbon Recovery in Shale Reservoirs. Paper SPE 158053-MS presented at the SPE Annual Technical Conference and Exhibition, San Antonio, Texas, USA, 8-10 October 2012. http://dx.doi.org/10.2118/158053-MS.

Haszeldine R.S., Quinn O., England G. *et al.* 2005. Natural Geochemical Analogues for Carbon Dioxide Storage in Deep Geological Porous Reservoirs, a United Kingdom Perspective. Oil and Gas Science and Technology – Rev. IFP, Vol. 60: 33-49. http://webpages.fc.ul.pt/~fbarriga/ZeroEm/Bibliografia_files/Haszeldine+al_2005_Oil+GasSci+Tech.pdf (accessed 20 May 2013).

Hensen, E. J. M.; Tambach, T. J.; Bliek, A.; Smit, B. J. Chem. Phys. 2001, 115, 3322-3329.

Hendricks, S. B.. 1945, Base exchange of crystalline silicates: Ind. Eng. Chem., V. 37, pp, 625-630.

Holt, R. M., Fjaer, E., Nes, O. M., and Alassi, H. T. (2011, January 1). A Shaly Look At Brittleness. American Rock Mechanics Association (Arma). ARMA-11-366, presented at 45th U.S. Rock Mechanics / Geomechanics Symposium, San Francisco, California, 26-29 June, 2011. https://www.onepetro.org/conference-paper/ARMA-11-366.

Iwere F.O., Heim R. N. and Cherian B. V. 2012. Numerical Simulation of Enhanced Oil Recovery in the Middle Bakken and Upper Three Forks Tight Oil Reservoirs of the Williston Basin. SPE-154937-MS presented at SPE Americas Unconventional Resources Conference, Pittsburgh, Pennsylvania USA. 5-7 June 2012. http://dx.doi.org/10.2118/154937-MS .

Ji, L. and Geehan, T., SPE- SPE 167155 Shale Failure around Hydraulic Fractures in Water Fracturing of Shale Gas. Presented at SPE Unconventional Resources Conference. Calgary, Alberta, Canada, 5-7 November, 2013. http://dx.doi.org/10.2118/167155-MS.

K.C. Khilar, Ph.D. Dissertation, University of Michigan, MI

Lever A.and R.A. Dawe, J. Pet. Geol., 7 (1984) 97.

Myers, R. Marcellus shale update. Independent Oil and Gas Association of West Virginia. 2008.

McCurdy R. February 24-25, 2011. EPA Hydraulic Fracturing Workshop 1. High Rate Hydraulic Fracturing Additives in NonMarcellus Unconventional Shales.

Morsy S. S., Soliman M., and Sheng, J. Improving Hydraulic Fracturing of Shale Formations by Acidizing. SPE-165688-MS presented at SPE Eastern Regional Meeting, Pittsburgh, Pennsylvania, USA, 20-22 August 2013. http://dx.doi.org/10.2118/165688-MS.

N. Mungan, J. Pet. Technol., 17 (1965) 1449.

Kantzas A., Pow M., and Allsopp, K., "Co-current and Counter-current Imbibition Analysis for Tight Fractured Carbonate Gas Reservoirs", CIM paper 97-181, presented at the 7th Saskatchewan Petroleum Conference, held in Regina Saskatchewan, October 20-22, 1997.

Killen J. C., and Biglarbigi K. Sep-2012. Oil Shale Research in the United States-Profiles of Oil Shale Research and Development Activities in Universities: National Laboratories, and Public Agencies. U.S. Department of Energy, Office of Petroleum Reserves, and Office of Naval Petroleum and Oil Shale Reserves. http://www.unconventionalfuels.org/publications/reports/Research_Project_Profiles_Book2011.pdf (accessed 20 Mar 2013).

Kumar V., Sondergeld C. H., and Rai C. S. 2012. Nano to Macro Mechanical Characterization of Shale. SPE- 159804-MS presented at SPE Annual Technical Conference and Exhibition, San Antonio, Texas, USA, 8-10 October 2012. http://dx.doi.org/10.2118/159804-MS.

K. K. Mohan, R. N. Vaidyab, M. G. Reed and H. S. Fogler. Water sensitivity of sandstones containing swelling and non-swelling clays. Colloids and Surfaces A: Physicochemical and Engineering Aspects. 73 (1993) 231-254 Elsevier Science Publishers B.V., Amsterdam.

Karaborni, S.; Smit, B.; Heidug, W.; Urai, J.; Van Oort, E. Science 1996, 271, 1102-1104.

L. Fan, R. Martin, J. Thompson, K. Atwood, J. Robinson, and G. Lindsay. 2011. An Integrated Approach for Understanding Oil and Gas Reserves Potential in Eagle

Ford Shale Formation. SPE- 148751-MS presented at Canadian Unconventional Resources Conference, Alberta, Canada, 15-17 November 2011. http://dx.doi.org/10.2118/148751-MS.

Makhanov K., Dehghanpour H., and Kuru E. 2012. An Experimental Study of Spontaneous Imbibition in Horn River Shales. SPE-162650-MS presented at SPE Canadian Unconventional Resources Conference, Calgary, Alberta, Canada, 30 October-1 November 2012. http://dx.doi.org/10.2118/162650-MS.

Morsy S., Hetherington C., and Sheng J., Effect of Low-Concentration HCl on the Mineralogical, Mechanical, and Physical Properties of Shale Rocks. SPE **Error! Reference source not found.** presented at SPE Eastern Regional Meeting, Pittsburgh, Pennsylvania, USA, 20 August -22 August 2013. http://dx.doi.org/10.2118/165689-MS.

Morsy S., Sheng J.J., and Ezewu R. O. Potential of Waterflooding in Shale Formations. SPE-167510-MS. Presented at SPE Nigeria Annual International Conference and Exhibition, 5-7 August, Lagos, Nigeria.

Mokhtari M., Alqahtani A. A., and Tutuncu, A. N. 2013. Impacts of Stress, Natural and Induced Fractures on Mechanical Properties of Organic-Rich Shales. SPE-168901-MS presented at the Unconventional Resources Technology Conference, Denver, Colorado, USA, 12-14 August 2013. doi:10.1190/URTEC2013-058

Patton B.J., Pitts F., Goeres T., Hertfelder G. 2003. Matrix Acidizing Case Studies for the Point Arguello Field. SPE- 83490-MS presented at SPE Western Regional/AAPG Pacific Section Joint Meeting, Long Beach, California, 19-24 May 2003. http://dx.doi.org/10.2118/83490-MS.

Penny G., Pursley J.T., and Holcomb D. 2005. The Application of Microemulsion Additives in Drilling and Stimulation Results in Enhanced Gas Production. Paper SPE- 94274-MS presented at the SPE Production Operations Symposium, Oklahoma City, Oklahoma, 16-19 April. http://dx.doi.org/10.2118/94274-MS.

Paktinat, J., Pinkhouse, J.A., Johnson, N., Williams, C., Lash, G.G., Penny, G.S., and Goff, D.A., 2006. Case Studies: Optimizing Hydraulic Fracturing Performance in Northeastern Fractured Shale Formations. Paper SPE-104306-MS presented at the SPE Eastern Regional Meeting, Canton, Ohio, 11-13 October.

R.M. Bustin, A. Bustin, D. Ross, G. Chalmers, V. Murthy, C. Laxmi, and X. Cui, "Shale Gas Opportunities and Challenges," Search and Discovery Articles, No. 40382, 2009.
http://www.searchanddiscovery.com/documents/2009/40382bustin/ndx_bustin.pdf
Rickman R., Mullen M., Petre E., Grieser B. and Kundert D. 2009. Petrophysics Key In Stimulating Shales. The American Oil and Gas Reporter. March 2009. http://shale-consortium.com/docs/Singh_VI_Ingepet_Manuscript.pdf.

Ridgley J. 2002. Sequence Stratigraphic Analysis and Facies Architecture of the Cretaceous Mancos Shale on and Near the Jicarilla Apache Indian Reservation,

New Mexico- their relation to Sites of Oil Accumulation. Combined Final Technical Report on Mancos Shale Phase 1 and Phase 2, NETL, USA, March 31, 2000. http://www.netl.doe.gov/KMD/cds/disk37/B%20-%20Native%20American%20Program/15026R11.PDF

Runtuwene M., Fasa M., *et al.* 2010. Crosslinked Acid as an Effective Diversion Agent in Matrix Acidizing. SPE- 133926-MS presented at IADC/SPE Asia Pacific Drilling Technology Conference and Exhibition, Ho Chi Minh City, Vietnam, 1-3 November 2010. http://dx.doi.org/10.2118/133926-MS.

R.N. Vaidya, Ph.D. Dissertation, University of Michigan, MI. 1991.

R. Nolen-Hoeksema. Elements of Hydraulic Fracturing. Oilfield Review Summer 2013: 25, no. 2. 51-52.

SF. Kia, H.S. Fogler, M.G. Reed and R.N. Vaidya, SPE Prod. Eng., 2 (1987) 277.

Sahimi M. "Flow and Transport in Porous Media and Fractured Rock: From Classical Methods to Modern Approaches ", VCH, Weinheim, Germany, 1995, 482 pp.

Sarker R., Batzle M. 2010. Anisotropic Elastic Moduli of the Mancos B Shale- An Experimental Study. SPE- 2010-2600 presented at 2010 SEG Annual Meeting, Denver, Colorado, USA, October 17 - 22, 2010. http://dx.doi.org/10.2118/2010-2600

Shuler P., Tang H., Lu Z. *et al.* 2010. Chemical Process for Improved Oil Recovery From Bakken Shale. SPE- 147531-MS presented at Canadian Unconventional Resources Conference, Alberta, Canada, 15-17 November 2011. http://dx.doi.org/10.2118/147531-MS.

Scheuerman R.F. and Bergersen B. M., 1990. Injection-Water Salinity, Formation Pretreatment, and Well-Operations Fluid-Selection Guidelines. *J. Pet Tech* 42(7): 836-845. SPE-18461-PA. http://dx.doi.org/10.2118/18461-PA.

Skipper, N. T.; Chang, F.-R. C.; Sposito, G. Clays Clay Miner. 1995, 43, 285-293.

Taylor R., Fyten G. C., and McNeil F. 2012. Acidizing-Lessons from the Past and New Opportunities. SPE-162238-MS presented at SPE Canadian Unconventional Resources Conference, Calgary, Alberta, Canada. 30 October-1 November 2012. http://dx.doi.org/10.2118/162238-MS.

T. Alexander, J. Baihly, Chuck Boyer, Bill Clark, George Waters, Valerie Jochen, Joel Le Calvez, Rick Lewis, John Thaeler, and Brain E. Toelle. Shale Gas Revolution. Oilfield Review Autumn 2011: 23, no. 3.40-57

Torsæter M., Vullum P. E.,. Nes O. M. *et al.* 2012. Nanostructure vs. Macroscopic Properties of Mancos Shale. SPE- 162737-MS presented at SPE Canadian Unconventional Resources Conference, Calgary, Alberta, Canada, 30 October-1 November 2012. http://dx.doi.org/10.2118/162737-MS

Thornton, S.D. 1988. Role of Silicate and Aluminate Ions in the Reaction of Sodium Hydroxide With Reservoir Minerals. *SPE Res Eng* 3(4): 1153-1160. SPE-16277-PA. http://dx.doi.org/10.2118/16277-PA.

Takahashi S. and Kovscek A. R. 2009. Spontaneous Counter Current Imbibition and Forced Displacement Characteristics of Low Permeability, Siliceous Rocks. SPE-121354-MS presented at SPE Western Regional Meeting, San Jose, California, 24-26 March 2009. http://dx.doi.org/10.2118/121354-MS.

van Oort, E. (1994). A novel technique for the investigation of drilling fluid induced borehole instability in shales. Paper SPE/ ISRM 28064 presented at the SPE/ISRM Conference on Rock Mechanics in Petroleum Engineering, Delft, Aug. 29–31.

van Oort, E.; Ripley, D.; Ward, I.; Chapman, J.W.; Williamson, R. and Aston, M. (1999). Silicate-based drilling fluids: competent, cost-effective and benign solutions to wellbore stability problems. SPE paper 35059, SPE/IADC Drilling Conference, New Orleans (LA), March 12-15.

van Oort, E. (2003). On the physical and chemical stability of shales. J. Petr. Sci. Eng., 38, 213–235

van Oort, E., Hale, A.H., Mody, F. K. and Sanjit R. (1996a) "Transport in Shales and the Design of Improved Water-Based Shale Drilling Fluids." SPE Drilling and Completion, vol. 11, no. 3 (September) 137-146. http://dx.doi.org/10.2118/28309-PA.

V. Oort, E.; Hale, A.H., van Oort, E.; Ripley, D.; Ward, I.; Chapman, J.W.; Wiliamson, R. and Aston, M. (1996b). Silicate-based drilling fluids: competent, cost-effective and benign solutions to wellbore stability problems. Paper SPE 35059 presented at the IADC/SPE Drilling Conference, New Orleans, LA, March 12– 15.

Wood T. and Milne B. 2011. Waterflood potential could unlock billions of barrels: Crescent Point Energy.
http://www.investorvillage.com/uploads/44821/files/CPGdundee.pdf (accessed 20 Mar 2013).

Wang D., Butler R., Liu H. *et al.* 2010. Flow Rate Behavior in Shale Rock. Paper SPE 138521-MS presented at the North American Unconventional Gas Conference and Exhibition, The Woodlands, Texas, USA, 14-16 June 2011. http://dx.doi.org/10.2118/138521-MS.

Wang D., Butler R., Liu H. *et al.* 2011. Surfactant Formulation Study For Bakken Shale Imbibition. SPE- 145510-MS presented at SPE Annual Technical Conference and Exhibition, Denver, Colorado, USA, 30 October-2 November 2011. http://dx.doi.org/10.2118/145510-MS.

Xu, L. and Fu, Q. 2012. Ensuring Better Well Stimulation in Unconventional Oil and Gas Formations by Optimizing Surfactant Additives. Paper SPE-154242-MS presented at the SPE Western Regional Meeting, Bakersfield, California, 21-23 March.

Xu, L. and Fu, Q. 2012. Proper Selection of Surfactant Additive Ensures Better Well Stimulation in Unconventional Oil and Gas Formations. Paper SPE- 153265-MS presented at the SPE Middle East Unconventional Gas Conference and Exhibition, Abu Dhabi, UAE, 23-25 January. http://dx.doi.org/10.2118/153265-MS.

Young, D. A.; Smith, D. E. J. Phys. Chem. B 2000, 104, 9163- 9170.1981.

Zhang X., Morrow N.R., and Ma S.: "Experimental Verification of a Modified Scaling Group for Spontaneous Imbibition," SPERE, Nov. 1996, 280-285.

Appendix: Base Case Simulation CMG Input File

```
RESULTS SIMULATOR IMEX 200900
INTERRUPT RESTART-STOP
INUNIT FIELD
WSRF WELL 1
WSRF GRID TIME
WSRF SECTOR TIME
OUTSRF WELL LAYER NONE
OUTSRF RES ALL
OUTSRF GRID BPP KRG KRO KRW PRES SG SO SSPRES SW VISG VISO
WINFLUX
WPRN GRID 0
OUTPRN GRID NONE
OUTPRN RES NONE
**$  Distance units: ft
RESULTS XOFFSET         0.0000
RESULTS YOFFSET         0.0000
RESULTS ROTATION         0.0000  **$  (DEGREES)
RESULTS AXES-DIRECTIONS 1.0 -1.0 1.0
**********************************************************************
**$ Definition of fundamental cartesian grid
**********************************************************************
GRID VARI 47 65 5
KDIR DOWN
DI IVAR
 2       0.2115277      0.2562716      0.3104801      0.3761553
   0.4557225    0.5521204      0.6689092      0.810402
   0.9818244    1.189507       1.441121       1.745958
   2.115277     2.562716       3.104801       3.761553
   4.557225     5.521204       6.689092       8.10402
9.7841128       11.8     12       11.8     9.7841128
   8.10402      6.689092       5.521204       4.557225       3.761553
   3.104801     2.562716       2.115277       1.745958       1.441121
```

```
  1.189507    0.9818244    0.810402     0.6689092    0.5521204
  0.4557225   0.3761553    0.3104801    0.2562716    0.2115277    2
DJ JVAR
 1 0.2115277 0.2562716 0.3087 0.3761553 0.4557225 0.5521204 0.6689092
0.810402 0.9818244 1.189507 1.441121 1.745958 2.115277 2.562716
3.104801 3.761553 4.557225 5.521204 6.689092 8.10402 8.79895035
10 11 15 17 20 21 34 35 40 45 52 52 45 40 18 30 25 15 11 10 8.79895035
8.1 6.69 5.52 4.5 4 3.5 3 2.562716 2.115277 1.745958 1.441121
1.189507 0.9818244 0.810402 0.6689092 0.5521204 0.4557225
0.3761553 0.3104801 0.2562716 0.2115277 1
DK ALL
15275*58
DTOP
3055*10500
**$  0 = null block, 1 = active block
*NULL *CON 1
*POR  *CON 0.09
*PERMI   *CON 0.0013
PERMJ EQUALSI
PERMK EQUALSI * 0.1
*PERMI *IJK
1 1:37 1:5 41.65
47 29:65 1:5 41.65
**$ Property: Pinchout Array Max: 1 Min: 1
**$ 0 = pinched block, 1 = active block
**$ 0 = pinched block, 1 = active block
PINCHOUTARRAY *CON 1
PRPOR  7350
CPOR  5e-6
MODEL BLACKOIL
TRES 320
PVT EG 1
**$ p Rs Bo Eg viso visg
14.696 4.68138 1.09917 4.10159 0.902644 0.0136014
```

173.583 32.1923 1.11173 49.1225 0.803844 0.0137243

332.47 65.2796 1.12711 95.3676 0.719427 0.0139054

491.357 101.621 1.1443 142.801 0.651788 0.0141273

650.244 140.36 1.16295 191.364 0.59727 0.014385

809.131 181.027 1.18287 240.971 0.552597 0.0146766

968.018 223.32 1.20393 291.506 0.515357 0.0150009

1126.9 267.027 1.22604 342.824 0.483819 0.0153574

1285.79 311.989 1.24913 394.75 0.45674 0.0157453

1444.68 358.084 1.27314 447.084 0.433209 0.0161637

1603.57 405.212 1.29803 499.604 0.412545 0.0166117

1762.45 453.293 1.32376 552.077 0.394234 0.0170877

1921.34 502.257 1.3503 604.264 0.377877 0.0175899

2080.23 552.048 1.3776 655.935 0.363163 0.0181162

2239.11 602.616 1.40566 706.874 0.349843 0.0186643

2398 653.915 1.43443 756.888 0.337718 0.0192317

3218.4 929.142 1.59372 995.379 0.288941 0.0223706

4038.8 1219.15 1.76935 1195.74 0.255067 0.0256431

4859.2 1521.47 1.95964 1360.49 0.229917 0.0288538

5679.6 1834.43 2.16332 1496.29 0.21036 0.0319135

6500 2193.142554 2.37939 1609.67 0.19463 0.0347948

GRAVITY GAS 0.8

REFPW 14.696

DENSITY WATER 59.1613

BWI 1.06212

CW 3.72431e-006

VWI 0.23268

CVW 0.0

**$ Property: PVT Type Max: 1 Min: 1

PTYPE *CON 1

DENSITY OIL 50.863

CO 1e-5

ROCKFLUID

RPT 1

**$ Sw krw krow

SWT

0.3 0 1

0.325 9.53674e-007 0.724196

0.35 3.05176e-005 0.512909

0.375 0.000231743 0.354093

0.4 0.000976562 0.237305

0.425 0.00298023 0.15359

0.45 0.00741577 0.0953674

0.475 0.0160284 0.0563135

0.5 0.03125 0.03125

0.525 0.0563135 0.0160284

0.55 0.0953674 0.00741577

0.575 0.15359 0.00298023

0.6 0.237305 0.000976563

0.625 0.354093 0.000231743

0.65 0.512909 3.05176e-005

0.675 0.724196 9.53674e-007

0.7 1 0

**$ Sl krg krog

SLT

0.6 1 0

0.621875 0.878906 9.53674e-007

0.64375 0.765625 3.05176e-005

0.665625 0.660156 0.000231743

0.6875 0.5625 0.000976563

0.709375 0.472656 0.00298023

0.73125 0.390625 0.00741577

0.753125 0.316406 0.0160284

0.775 0.25 0.03125

0.796875 0.191406 0.0563135

0.81875 0.140625 0.0953674

0.840625 0.0976562 0.15359

0.8625 0.0625 0.237305

0.884375 0.0351562 0.354093

0.90625 0.015625 0.512909

0.928125 0.00390625 0.724196

0.95 0 1

RPT 2

**$ Sw krw krow

SWT

0.05 0 1

0.103125 0.015625 0.90773

0.15625 0.0441942 0.818488

0.209375 0.0811899 0.732378

0.2625 0.125 0.649519

0.315625 0.174693 0.570045

0.36875 0.22964 0.494106

0.421875 0.289379 0.421875

0.475 0.353553 0.353553

0.528125 0.421875 0.289379

0.58125 0.494106 0.22964

0.634375 0.570045 0.174693

0.6875 0.649519 0.125

0.740625 0.732378 0.0811899

0.79375 0.818488 0.0441942

0.846875 0.90773 0.015625

0.9 1 0

**$ Sl krg krog

SLT

0.15 1 0

0.203125 0.9375 0.015625

0.25625 0.875 0.0441942

0.309375 0.8125 0.0811899

0.3625 0.75 0.125

0.415625 0.6875 0.174693

0.46875 0.625 0.22964

0.521875 0.5625 0.289379

0.575 0.5 0.353553

```
0.628125 0.4375 0.421875
0.68125 0.375 0.494106
0.734375 0.3125 0.570045
0.7875 0.25 0.649519
0.840625 0.1875 0.732378
0.89375 0.125 0.818488
0.946875 0.0625 0.90773
1 0 1
RTYPE   *CON 1
RTYPE  *IJK
1 1:37 1:5 2
47 29:65 1:5 2
**$ Property: Rel Perm Set Num Max: 2 Min: 1
INITIAL
VERTICAL DEPTH_AVE WATER_OIL EQUIL
REFDEPTH 10500
REFPRES 7350
DWOC 10790
**$ Property: Bubble Point Pressure (psi) Max: 2398 Min: 2398
PB  *CON 2500
NUMERICAL
DTMIN 1e-9
NORTH 40
ITERMAX 100
RUN
DATE 2010 1 1
DTWELL 1e-008
**$
WELL '1'
PRODUCER '1'
OPERATE MIN BHP 2500. CONT
**$ UBA ff Status Connection
**$ rad geofac wfrac skin
**$ UBA ff Status Connection
```

```
**$ UBA            ff  Status  Connection
**$ UBA           ff  Status  Connection
**$ UBA     ff  Status  Connection
**$         rad  geofac  wfrac  skin
GEOMETRY  J  0.25  0.37  1.  0.
PERF  GEOA  '1'
**$ UBA    ff  Status  Connection
   1 1 1  1.  OPEN    FLOW-TO  'SURFACE'
**$
WELL  'Well-2'
PRODUCER 'Well-2'
OPERATE  MIN  BHP  2500.  CONT
**$ UBA            ff  Status  Connection
**$ UBA     ff  Status  Connection
**$         rad  geofac  wfrac  skin
GEOMETRY  K  0.25  0.37  1.  0.
PERF  GEOA  'Well-2'
**$ UBA      ff  Status  Connection
   47 65 3  1.  OPEN    FLOW-TO  'SURFACE'
**$ Property: Implicit flag Max: 1 Min: 1
AIMSET *CON 1
DATE 2010 1 1.04167
DATE 2010 1 1.08333
DATE 2010 1 1.12500
DATE 2010 1 1.16667
DATE 2010 1 1.20833
DATE 2010 1 1.25000
DATE 2010 1 1.29167
DATE 2010 1 1.33333
DATE 2010 1 1.37500
DATE 2010 1 1.41667
DATE 2010 1 1.45833
DATE 2010 1 1.50000
DATE 2010 1 1.54167
```

DATE 2010 1 1.58333
DATE 2010 1 1.62500
DATE 2010 1 1.66667
DATE 2010 1 1.70833
DATE 2010 1 1.75000
DATE 2010 1 1.79167
DATE 2010 1 1.83333
DATE 2010 1 1.87500
DATE 2010 1 1.91667
DATE 2010 1 1.95833
DATE 2010 1 2.00000
DATE 2010 1 2.08333
DATE 2010 1 2.16667
DATE 2010 1 2.25000
DATE 2010 1 2.33333
DATE 2010 1 2.41667
DATE 2010 1 2.50000
DATE 2010 1 2.58333
DATE 2010 1 2.66667
DATE 2010 1 2.75000
DATE 2010 1 2.83333
DATE 2010 1 2.91667
DATE 2010 1 3.00000
DATE 2010 1 3.12500
DATE 2010 1 3.25000
DATE 2010 1 3.37500
DATE 2010 1 3.50000
DATE 2010 1 3.62500
DATE 2010 1 3.75000
DATE 2010 1 3.87500
DATE 2010 1 4.00000
DATE 2010 1 5.00000
DATE 2010 1 6.00000
DATE 2010 1 7.00000

DATE 2010 1 8.00000
DATE 2010 1 9.00000
DATE 2010 1 10.00000
DATE 2010 1 11.00000
DATE 2010 1 12.00000
DATE 2010 1 13.00000
DATE 2010 1 14.00000
DATE 2010 1 15.00000
DATE 2010 1 16.00000
DATE 2010 1 17.00000
DATE 2010 1 18.00000
DATE 2010 1 19.00000
DATE 2010 1 20.00000
DATE 2010 1 21.00000
DATE 2010 1 22.00000
DATE 2010 1 23.00000
DATE 2010 1 24.00000
DATE 2010 1 25.00000
DATE 2010 1 26.00000
DATE 2010 1 27.00000
DATE 2010 1 28.00000
DATE 2010 1 29.00000
DATE 2010 1 30.00000
DATE 2010 1 31.00000
DATE 2010 2 1.00000
DATE 2010 3 1.00000
DATE 2010 4 1.00000
DATE 2010 5 1.00000
DATE 2010 6 1.00000
DATE 2010 7 1.00000
DATE 2010 8 1.00000
DATE 2010 9 1.00000
DATE 2010 10 1.00000
DATE 2010 11 1.00000

DATE 2010 12 1.00000
DATE 2011 1 1.00000
DATE 2011 2 1.00000
DATE 2011 3 1.00000
DATE 2011 4 1.00000
DATE 2011 5 1.00000
DATE 2011 6 1.00000
DATE 2011 7 1.00000
DATE 2011 8 1.00000
DATE 2011 9 1.00000
DATE 2011 10 1.00000
DATE 2011 11 1.00000
DATE 2011 12 1.00000
DATE 2012 1 1.00000
DATE 2012 2 1.00000
DATE 2012 3 1.00000
DATE 2012 4 1.00000
DATE 2012 5 1.00000
DATE 2012 6 1.00000
DATE 2012 7 1.00000
DATE 2012 8 1.00000
DATE 2012 9 1.00000
DATE 2012 10 1.00000
DATE 2012 11 1.00000
DATE 2012 12 1.00000
DATE 2013 1 1.00000
DATE 2013 2 1.00000
DATE 2013 3 1.00000
DATE 2013 4 1.00000
DATE 2013 5 1.00000
DATE 2013 6 1.00000
DATE 2013 7 1.00000
DATE 2013 8 1.00000
DATE 2013 9 1.00000

DATE 2013 10 1.00000
DATE 2013 11 1.00000
DATE 2013 12 1.00000
DATE 2014 1 1.00000
DATE 2014 2 1.00000
DATE 2014 3 1.00000
DATE 2014 4 1.00000
DATE 2014 5 1.00000
DATE 2014 6 1.00000
DATE 2014 7 1.00000
DATE 2014 8 1.00000
DATE 2014 9 1.00000
DATE 2014 10 1.00000
DATE 2014 11 1.00000
DATE 2014 12 1.00000
DATE 2015 1 1.00000

DATE 2015 2 1.00000
DATE 2015 3 1.00000
DATE 2015 4 1.00000
DATE 2015 5 1.00000
DATE 2015 6 1.00000
DATE 2015 7 1.00000
DATE 2015 8 1.00000
DATE 2015 9 1.00000
DATE 2015 10 1.00000
DATE 2015 11 1.00000
DATE 2015 12 1.00000
DATE 2016 1 1.00000
DATE 2016 2 1.00000
DATE 2016 3 1.00000
DATE 2016 4 1.00000
DATE 2016 5 1.00000

DATE 2016 6 1.00000
DATE 2016 7 1.00000
DATE 2016 8 1.00000
DATE 2016 9 1.00000
DATE 2016 10 1.00000
DATE 2016 11 1.00000
DATE 2016 12 1.00000
DATE 2017 1 1.00000
DATE 2017 2 1.00000
DATE 2017 3 1.00000
DATE 2017 4 1.00000
DATE 2017 5 1.00000
DATE 2017 6 1.00000
DATE 2017 7 1.00000
DATE 2017 8 1.00000
DATE 2017 9 1.00000
DATE 2017 10 1.00000
DATE 2017 11 1.00000
DATE 2017 12 1.00000
DATE 2018 1 1.00000
DATE 2018 2 1.00000
DATE 2018 3 1.00000
DATE 2018 4 1.00000
DATE 2018 5 1.00000
DATE 2018 6 1.00000
DATE 2018 7 1.00000
DATE 2018 8 1.00000
DATE 2018 9 1.00000
DATE 2018 10 1.00000
DATE 2018 11 1.00000
DATE 2018 12 1.00000
DATE 2019 1 1.00000
DATE 2019 2 1.00000
DATE 2019 3 1.00000

DATE 2019 4 1.00000
DATE 2019 5 1.00000
DATE 2019 6 1.00000
DATE 2019 7 1.00000
DATE 2019 8 1.00000
DATE 2019 9 1.00000
DATE 2019 10 1.00000
DATE 2019 11 1.00000
DATE 2019 12 1.00000
DATE 2020 1 1.00000
DATE 2020 2 1.00000
DATE 2020 3 1.00000
DATE 2020 4 1.00000
DATE 2020 5 1.00000
DATE 2020 6 1.00000
DATE 2020 7 1.00000
DATE 2020 8 1.00000
DATE 2020 9 1.00000
DATE 2020 10 1.00000
DATE 2020 11 1.00000
DATE 2020 12 1.00000
DATE 2021 1 1.00000
DATE 2021 2 1.00000
DATE 2021 3 1.00000
DATE 2021 4 1.00000
DATE 2021 5 1.00000
DATE 2021 6 1.00000
DATE 2021 7 1.00000
DATE 2021 8 1.00000
DATE 2021 9 1.00000
DATE 2021 10 1.00000
DATE 2021 11 1.00000
DATE 2021 12 1.00000
DATE 2022 1 1.00000

DATE 2022 2 1.00000
DATE 2022 3 1.00000
DATE 2022 4 1.00000
DATE 2022 5 1.00000
DATE 2022 6 1.00000
DATE 2022 7 1.00000
DATE 2022 8 1.00000
DATE 2022 9 1.00000
DATE 2022 10 1.00000
DATE 2022 11 1.00000
DATE 2022 12 1.00000
DATE 2023 1 1.00000
DATE 2023 2 1.00000
DATE 2023 3 1.00000
DATE 2023 4 1.00000
DATE 2023 5 1.00000
DATE 2023 6 1.00000
DATE 2023 7 1.00000
DATE 2023 8 1.00000
DATE 2023 9 1.00000
DATE 2023 10 1.00000
DATE 2023 11 1.00000
DATE 2023 12 1.00000
DATE 2024 1 1.00000
DATE 2024 2 1.00000
DATE 2024 3 1.00000
DATE 2024 4 1.00000
DATE 2024 5 1.00000
DATE 2024 6 1.00000
DATE 2024 7 1.00000
DATE 2024 8 1.00000
DATE 2024 9 1.00000
DATE 2024 10 1.00000
DATE 2024 11 1.00000

DATE 2024 12 1.00000
DATE 2025 1 1.00000
DATE 2025 2 1.00000
DATE 2025 3 1.00000
DATE 2025 4 1.00000
DATE 2025 5 1.00000
DATE 2025 6 1.00000
DATE 2025 7 1.00000
DATE 2025 8 1.00000
DATE 2025 9 1.00000
DATE 2025 10 1.00000
DATE 2025 11 1.00000
DATE 2025 12 1.00000
DATE 2026 1 1.00000
DATE 2026 2 1.00000
DATE 2026 3 1.00000
DATE 2026 4 1.00000
DATE 2026 5 1.00000
DATE 2026 6 1.00000
DATE 2026 7 1.00000
DATE 2026 8 1.00000
DATE 2026 9 1.00000
DATE 2026 10 1.00000
DATE 2026 11 1.00000
DATE 2026 12 1.00000
DATE 2027 1 1.00000
DATE 2027 2 1.00000
DATE 2027 3 1.00000
DATE 2027 4 1.00000
DATE 2027 5 1.00000
DATE 2027 6 1.00000
DATE 2027 7 1.00000
DATE 2027 8 1.00000
DATE 2027 9 1.00000

DATE 2027 10 1.00000
DATE 2027 11 1.00000
DATE 2027 12 1.00000
DATE 2028 1 1.00000
DATE 2028 2 1.00000
DATE 2028 3 1.00000
DATE 2028 4 1.00000
DATE 2028 5 1.00000
DATE 2028 6 1.00000
DATE 2028 7 1.00000
DATE 2028 8 1.00000
DATE 2028 9 1.00000
DATE 2028 10 1.00000
DATE 2028 11 1.00000
DATE 2028 12 1.00000
DATE 2029 1 1.00000
DATE 2029 2 1.00000
DATE 2029 3 1.00000
DATE 2029 4 1.00000
DATE 2029 5 1.00000
DATE 2029 6 1.00000
DATE 2029 7 1.00000
DATE 2029 8 1.00000
DATE 2029 9 1.00000
DATE 2029 10 1.00000
DATE 2029 11 1.00000
DATE 2029 12 1.00000
DATE 2030 1 1.00000
DATE 2030 2 1.00000
DATE 2030 3 1.00000
DATE 2030 4 1.00000
DATE 2030 5 1.00000
DATE 2030 6 1.00000
DATE 2030 7 1.00000

DATE 2030 8 1.00000

DATE 2030 9 1.00000

DATE 2030 10 1.00000

DATE 2030 11 1.00000

DATE 2030 12 1.00000

DATE 2031 1 1.00000

DATE 2031 2 1.00000

DATE 2031 3 1.00000

DATE 2031 4 1.00000

DATE 2031 5 1.00000

DATE 2031 6 1.00000

DATE 2031 7 1.00000

DATE 2031 8 1.00000

DATE 2031 9 1.00000

DATE 2031 10 1.00000

DATE 2031 11 1.00000

DATE 2031 12 1.00000

DATE 2032 1 1.00000

DATE 2032 2 1.00000

DATE 2032 3 1.00000

DATE 2032 4 1.00000

DATE 2032 5 1.00000

DATE 2032 6 1.00000

DATE 2032 7 1.00000

DATE 2032 8 1.00000

DATE 2032 9 1.00000

DATE 2032 10 1.00000

DATE 2032 11 1.00000

DATE 2032 12 1.00000

DATE 2033 1 1.00000

DATE 2033 2 1.00000

DATE 2033 3 1.00000

DATE 2033 4 1.00000

DATE 2033 5 1.00000

DATE 2033 6 1.00000
DATE 2033 7 1.00000
DATE 2033 8 1.00000
DATE 2033 9 1.00000
DATE 2033 10 1.00000
DATE 2033 11 1.00000
DATE 2033 12 1.00000
DATE 2034 1 1.00000
DATE 2034 2 1.00000
DATE 2034 3 1.00000
DATE 2034 4 1.00000
DATE 2034 5 1.00000
DATE 2034 6 1.00000
DATE 2034 7 1.00000
DATE 2034 8 1.00000
DATE 2034 9 1.00000
DATE 2034 10 1.00000
DATE 2034 11 1.00000
DATE 2034 12 1.00000
DATE 2035 1 1.00000
DATE 2035 2 1.00000
DATE 2035 3 1.00000
DATE 2035 4 1.00000
DATE 2035 5 1.00000
DATE 2035 6 1.00000
DATE 2035 7 1.00000
DATE 2035 8 1.00000
DATE 2035 9 1.00000
DATE 2035 10 1.00000
DATE 2035 11 1.00000
DATE 2035 12 1.00000
DATE 2036 1 1.00000
DATE 2036 2 1.00000
DATE 2036 3 1.00000

DATE 2036 4 1.00000
DATE 2036 5 1.00000
DATE 2036 6 1.00000
DATE 2036 7 1.00000
DATE 2036 8 1.00000
DATE 2036 9 1.00000
DATE 2036 10 1.00000
DATE 2036 11 1.00000
DATE 2036 12 1.00000
DATE 2037 1 1.00000
DATE 2037 2 1.00000
DATE 2037 3 1.00000
DATE 2037 4 1.00000
DATE 2037 5 1.00000
DATE 2037 6 1.00000
DATE 2037 7 1.00000
DATE 2037 8 1.00000
DATE 2037 9 1.00000
DATE 2037 10 1.00000
DATE 2037 11 1.00000
DATE 2037 12 1.00000
DATE 2038 1 1.00000
DATE 2038 2 1.00000
DATE 2038 3 1.00000
DATE 2038 4 1.00000
DATE 2038 5 1.00000
DATE 2038 6 1.00000
DATE 2038 7 1.00000
DATE 2038 8 1.00000
DATE 2038 9 1.00000
DATE 2038 10 1.00000
DATE 2038 11 1.00000
DATE 2038 12 1.00000
DATE 2039 1 1.00000

DATE 2039 2 1.00000

DATE 2039 3 1.00000

DATE 2039 4 1.00000

DATE 2039 5 1.00000

DATE 2039 6 1.00000

DATE 2039 7 1.00000

DATE 2039 8 1.00000

DATE 2039 9 1.00000

DATE 2039 10 1.00000

DATE 2039 11 1.00000

DATE 2039 12 1.00000

DATE 2040 1 1.00000

STOP

RESULTS SPEC 'Permeability J'

RESULTS SPEC SPECNOTCALCVAL -99999

RESULTS SPEC REGION 'All Layers (Whole Grid)'

RESULTS SPEC REGIONTYPE 'REGION_WHOLEGRID'

RESULTS SPEC LAYERNUMB 0

RESULTS SPEC PORTYPE 1

RESULTS SPEC EQUALSI 0 1

RESULTS SPEC SPECKEEPMOD 'YES'

RESULTS SPEC STOP

RESULTS SPEC 'Permeability K'

RESULTS SPEC SPECNOTCALCVAL -99999

RESULTS SPEC REGION 'All Layers (Whole Grid)'

RESULTS SPEC REGIONTYPE 'REGION_WHOLEGRID'

RESULTS SPEC LAYERNUMB 0

RESULTS SPEC PORTYPE 1

RESULTS SPEC EQUALSI 1 0.1

RESULTS SPEC SPECKEEPMOD 'YES'

RESULTS SPEC STOP